



Model-independent search for the presence of new physics in events including $H \rightarrow \gamma\gamma$ with $\sqrt{s} = 13$ TeV pp data recorded by the ATLAS detector at the LHC

The ATLAS Collaboration

A model-independent search for new physics leading to final states containing a Higgs boson, with a mass of 125.09 GeV, decaying to a pair of photons is performed with 139 fb⁻¹ of $\sqrt{s} = 13$ TeV pp collision data recorded by the ATLAS detector at the Large Hadron Collider at CERN. This search examines 22 final states categorized by the objects that are produced in association with the Higgs boson. These objects include isolated electrons or muons, hadronically decaying τ -leptons, additional photons, missing transverse momentum, and hadronic jets, as well as jets that are tagged as containing a b -hadron. No significant excesses above Standard Model expectations are observed and limits on the production cross section at 95% confidence level are set. Detector efficiencies are reported for all 22 signal regions, which can be used to convert detector-level cross-section limits reported in this paper to particle-level cross-section constraints.

Contents

1	Introduction	2
2	ATLAS detector	4
3	Data and Monte Carlo samples	5
3.1	Data sample	5
3.2	Monte Carlo samples	5
4	Object and event selection	8
4.1	Object definitions	8
4.2	Event preselection	9
5	Signal regions	10
6	Signal and background modelling	11
6.1	Modelling of BSM and SM Higgs boson production	12
6.2	Continuum background modelling	13
6.3	Modelling of the background in the multilepton signal region	13
7	Systematic uncertainties	14
7.1	Systematic uncertainties in modelling $m_{\gamma\gamma}$ for SM and BSM Higgs boson production	14
7.2	Uncertainty in the continuum background modelling	14
7.3	Uncertainties in resonant background yields	14
8	Results	15
8.1	Upper limits on BSM production cross sections	19
8.2	Interpretation with particle-level simulation	20
9	Conclusions	23

1 Introduction

The discovery of the Higgs boson by the ATLAS and CMS experiments at the CERN Large Hadron Collider (LHC) [1, 2] opened up new avenues to search for physics beyond the Standard Model (BSM physics). The properties of the Higgs boson, including its inclusive production cross sections and decay rates, as well as its differential cross sections, may be altered by the presence of new interactions and new particles beyond the SM. In addition, the Higgs boson may also be produced in BSM processes as a decay product of unknown new particles, which could give rise to deviations of Higgs boson production rates from SM predictions in exclusive final states. For example, the Higgs boson can be produced in the decays of supersymmetric particles predicted by weak-scale supersymmetry (SUSY) models [3–8], in exotic decays of top quarks in models such as those having flavour-changing neutral currents (FCNCs) [9–13], or in the decay of the partner of the top quark or bottom quark as predicted by models of vector-like quarks [14, 15]. So far, observations of Higgs boson production and decay properties at the LHC are consistent with SM predictions [16, 17], and direct searches targeting the aforementioned BSM models also reported no

significant deviations from the SM expectation. Most of these analyses are designed with certain model assumptions, either targeting a specific SM Higgs boson production mode or optimized for a given BSM process involving the production of the Higgs boson.

This paper reports the results of a model-independent search for excesses in the production rate of the Higgs boson with a mass of 125.09 GeV in many distinct signal regions with the ATLAS detector at the LHC. The regions are defined by the presence and kinematic properties of objects produced in association with the Higgs boson. While a large fraction of such signals may populate signal regions probed by SM Higgs boson measurements, such as measurements of ‘simplified template cross sections’ [18, 19] and fiducial and differential cross-section measurements [20], unknown BSM production of the Higgs boson could result in events that do not enter signal regions optimized for existing SM measurements. The signal regions in this search are chosen to cover a wide range of signatures defined by particles accompanying the production of the Higgs boson, and they are defined with simple and mostly inclusive selections in order to minimize model dependence.

In this search the Higgs boson is reconstructed via its diphoton decay channel, which has a predicted branching ratio of $(0.227 \pm 0.007)\%$ [18] in the SM. While the rate of $H \rightarrow \gamma\gamma$ decay is much lower than that of several other Higgs boson decay channels, the sensitivity of an analysis targeting this channel can be competitive with that of analyses targeting higher-rate channels. This is primarily because the diphoton background to the Higgs boson signal is relatively small and because of better experimental resolution for the reconstructed resonance mass, especially in comparison with hadronic decay modes of the Higgs boson. Another advantage of performing this model-independent search in the $H \rightarrow \gamma\gamma$ channel is that the same background modelling strategy can be applied to most signal regions; the signal and background can be determined by fitting analytic functions to the diphoton invariant mass ($m_{\gamma\gamma}$) distribution in data. This fit-based background estimation method breaks down only when the signal region does not have a sufficient number of events to constrain the analytic background function.

If data in the signal regions are found to be consistent with the SM expectations, including contributions from resonant Higgs boson production, limits are set on the BSM production cross section of the Higgs boson in detector-level signal regions. To enable the use of these detector-level cross-section limits in constraining BSM physics models, the detector efficiencies for different signal regions are evaluated. These efficiencies depend on the kinematics of the final-state particles and therefore vary between different BSM models. As a result, this paper reports a range of efficiency values for each signal region, evaluated from Monte Carlo simulation of several benchmark BSM models. Correlations in the observed limits between signal regions with a large number of events are also reported.

This paper is organized as follows. Section 2 gives a brief description of the ATLAS detector. Section 3 presents the simulated SM samples used to describe the backgrounds, and also the new-physics models used to determine the expected sensitivity of the search in each signal region. Section 4 describes the reconstructed data objects and subsequent selections used in the analysis. Section 5 discusses in detail the signal regions defined for the search. Section 6 describes the modelling of signal and background in each search region. Section 7 addresses systematic uncertainties related to the search. Section 8 presents the results of this search. Finally, Section 9 summarizes the conclusions of the paper.

2 ATLAS detector

The ATLAS detector [21] at the LHC covers nearly the entire solid angle around the collision point.¹ It consists of an inner tracking detector surrounded by a thin superconducting solenoid, electromagnetic and hadronic calorimeters, and a muon spectrometer incorporating three large superconducting toroidal magnet systems. The inner-detector system is immersed in a 2 T axial magnetic field and provides charged-particle tracking in the range $|\eta| < 2.5$.

The fine-granularity silicon pixel detector covers the vertex region and typically provides four measurements per track, the first hit normally being in the insertable B-layer installed before Run 2 [22, 23]. The pixel detector is followed by the silicon microstrip tracker, which usually provides eight measurements per track. These silicon detectors are complemented by the transition radiation tracker (TRT), which enables radially extended track reconstruction up to $|\eta| = 2.0$. The TRT also provides electron identification information based on the fraction of hits (typically 30 hits in total) above a higher energy-deposit threshold corresponding to transition radiation.

The calorimeter system covers the pseudorapidity range $|\eta| < 4.9$. Within the region $|\eta| < 3.2$, electromagnetic (EM) calorimetry is provided by barrel and endcap lead/liquid-argon (LAr) calorimeters, with an additional thin LAr presampler covering $|\eta| < 1.8$ to correct for energy loss in material upstream of the calorimeters. Hadronic calorimetry is provided by a steel/scintillator-tile calorimeter, segmented into three barrel structures within $|\eta| < 1.7$, and two copper/LAr hadronic endcap calorimeters. The solid angle coverage is completed with forward copper/LAr and tungsten/LAr calorimeter modules optimized for electromagnetic and hadronic measurements, respectively.

The muon spectrometer comprises separate trigger and high-precision tracking chambers measuring the deflection of muons in a magnetic field generated by the superconducting air-core toroids. The field integral of the toroids ranges between 2.0 and 6.0 T m across most of the detector. A set of precision chambers covers the region $|\eta| < 2.7$ with three layers of monitored drift tubes, complemented by cathode-strip chambers in the forward region, where the background is highest. The muon trigger system covers the range $|\eta| < 2.4$ with resistive-plate chambers in the barrel, and thin-gap chambers in the endcap regions.

Interesting events are selected to be recorded by the first-level trigger system implemented in custom hardware, followed by selections made by algorithms implemented in software in the high-level trigger [24]. The first-level trigger accepts events from the 40 MHz bunch crossings at a rate below 100 kHz, which the high-level trigger reduces in order to record events to disk at about 1 kHz. An extensive software suite [25] is used in data simulation, in the reconstruction and analysis of real and simulated data, in detector operations, and in the trigger and data acquisition systems of the experiment.

¹ ATLAS uses a right-handed coordinate system with its origin at the nominal interaction point (IP) in the centre of the detector and the z -axis along the beam pipe. The x -axis points from the IP to the centre of the LHC ring, and the y -axis points upwards. Cylindrical coordinates (r, ϕ) are used in the transverse plane, ϕ being the azimuthal angle around the z -axis. The pseudorapidity is defined in terms of the polar angle θ as $\eta = -\ln \tan(\theta/2)$. Angular distance is measured in units of $\Delta R \equiv \sqrt{(\Delta\eta)^2 + (\Delta\phi)^2}$.

3 Data and Monte Carlo samples

3.1 Data sample

This study uses the full Run-2 data set of $\sqrt{s} = 13$ TeV proton–proton collisions recorded by the ATLAS detector during 2015–2018. After data quality requirements [26] are applied to ensure the good working condition of all detector components, the data set amounts to an integrated luminosity of $139.0 \pm 2.4 \text{ fb}^{-1}$ [27, 28]. The mean number of interactions per bunch crossing was $\langle \mu \rangle = 33.7$ on average during Run 2.

The data sample was selected using a combination of diphoton and single-photon triggers. The transverse energy thresholds of the diphoton trigger were 35 GeV and 25 GeV for the leading and subleading photon candidates, respectively [29]. The diphoton trigger applies photon identification selections based on calorimeter shower shape variables. In 2015–2016, a loose photon identification requirement was used, and in 2017–2018, this requirement was tightened to cope with higher instantaneous luminosity. The single-photon trigger had a transverse energy threshold of 120 GeV for the leading photon in data collected between 2015 and 2017, and the threshold was increased to 140 GeV for data collected in 2018. The photon candidate used in the trigger decision is required to satisfy the loose photon identification criteria. The use of the single-photon trigger is found to improve the trigger efficiency for high- p_T Higgs boson candidates. Typically, the trigger efficiency is greater than 98% for events that pass the diphoton event selection described below.

3.2 Monte Carlo samples

Monte Carlo (MC) simulation samples are used to determine the SM Higgs boson event yield, test the continuum background modelling, and estimate detector efficiencies for various signal regions. These simulated samples include three categories of processes: SM Higgs boson production, SM diphoton continuum production, and BSM production of the Higgs boson with a mass of 125.09 GeV.

Table 1: Configuration of MC simulation of SM Higgs boson production and the predicted cross sections at $\sqrt{s} = 13$ TeV. The generator set-up includes the software programs used for the matrix element (ME) calculation and parton showering (PS). The parton distribution function (PDF) is given separately for the ME calculation and the parton showering, along with the set of tuned parameters (Tune) used in modelling the underlying event (UE).

Process	Generator (ME+PS)	PDF (ME)	PDF, Tune (PS, UE)	Cross section [pb] ($\sqrt{s} = 13$ TeV)
ggF	POWHEG NNLOPS + PYTHIA 8	PDF4LHC15	CTEQ6, AZNLO	48.5
VBF	POWHEG BOX + PYTHIA 8	PDF4LHC15	CTEQ6, AZNLO	3.78
WH	POWHEG BOX + PYTHIA 8	PDF4LHC15	CTEQ6, AZNLO	1.37
$q\bar{q} \rightarrow ZH$	POWHEG BOX + PYTHIA 8	PDF4LHC15	CTEQ6, AZNLO	0.76
$gg \rightarrow ZH$	POWHEG BOX + PYTHIA 8	PDF4LHC15	CTEQ6, AZNLO	0.12
$t\bar{t}H$	POWHEG BOX + PYTHIA 8	PDF4LHC15	NNPDF2.3, A14	0.51
$b\bar{b}H$	POWHEG BOX + PYTHIA 8	PDF4LHC15	NNPDF2.3, A14	0.49
$tHbj$	aMC@NLO + PYTHIA 8	NNPDF3.0	NNPDF2.3, A14	0.074
tWH	aMC@NLO + PYTHIA 8	NNPDF3.0	NNPDF2.3, A14	0.015

MC samples generated for SM Higgs boson production are summarized in Table 1. The gluon–gluon fusion (ggF), vector-boson fusion (VBF), and VH production modes were generated using POWHEG NNLOPS or POWHEG BOX [30–38], with the PDF4LHC15 PDF set [39], and interfaced to PYTHIA 8 [40, 41] for simulation of parton showering, hadronization and the underlying event, using a set of data-tuned parameters

called the AZNLO tune [42]. The ggF simulation achieves NNLO accuracy for arbitrary inclusive $gg \rightarrow H$ observables by reweighting the Higgs boson rapidity spectrum in HJ-MiNLO [36, 43, 44] to that of HNNLO [45]. The transverse momentum spectrum of the Higgs boson obtained with this sample is found to be compatible with the fixed-order HNNLO calculation and the HRES 2.3 calculation [46, 47] performing resummation at next-to-next-to-leading-logarithm accuracy matched to a NNLO fixed-order calculation (NNLL+NNLO). The VBF production mode was simulated at next-to-leading-order (NLO) accuracy in QCD. The simulation of WH and $q\bar{q} \rightarrow ZH$ production is accurate to NLO in QCD with up to one extra jet in the event, while the simulation of the $gg \rightarrow ZH$ process was performed at leading order in QCD. The $t\bar{t}H$ and $b\bar{b}H$ processes were modelled using the POWHEG BOX v2 [31–33, 38, 48] generator, which provides matrix elements at NLO in the strong coupling constant α_s in the five-flavour scheme with the NNPDF2.3LO [49] PDF set. For the $t\bar{t}H$ sample, the functional form of the renormalization and factorization scale was set to $\sqrt[3]{m_T(t) \cdot m_T(\bar{t}) \cdot m_T(H)^2}$ [18]. The generator was interfaced to PYTHIA 8.230 [41], which used the A14 tune [50] and the NNPDF2.3LO [49] PDF set. The decays of bottom and charm hadrons were simulated using the EVTGEN 1.6.0 program [51]. All the SM Higgs boson samples are normalized to cross-section values recommended by Ref. [18], which are shown in Table 1.

To study the modelling of continuum background, diphoton production event samples were simulated. Besides inclusive diphoton production, specific diphoton processes were also generated for signal regions where electroweak or top-associated production is enhanced. Inclusive diphoton production and diphoton production in association with a vector boson ($V\gamma\gamma$) were simulated with the SHERPA 2.2.4 [52] generator. Matrix elements (MEs) for up to three additional partons were calculated at LO accuracy. For the inclusive diphoton sample, NLO accuracy is reached for MEs including up to one additional parton. The Comix [53] and OPENLOOPS [54–56] libraries were used in these calculations, which were matched with the SHERPA parton shower [57] using the MEPS@NLO prescription [58–61] with a dynamic merging cut [62] of 10 GeV. A smooth-cone isolation requirement [63] was applied in the event generation. Samples were generated using the NNPDF3.0NNLO PDF set [49], along with the dedicated set of tuned parton-shower parameters developed by the SHERPA authors. Diphoton production in association with a top-quark pair ($t\bar{t}\gamma\gamma$) was modelled by the MADGRAPH5_AMC@NLO 2.3.3 generator at LO with the NNPDF2.3LO [64] PDF set, and the events were interfaced with PYTHIA 8.212 for parton-shower and underlying-event simulation.

Several BSM processes were simulated to demonstrate the coverage of the signal regions and estimate the model dependence of the efficiency of the fiducial selections. These samples are summarized in Table 2 and are described as follows.

1. BSM Higgs boson production characterized by the presence of additional charged or neutral leptons:
 - $\tilde{\chi}_1^\pm \tilde{\chi}_2^0 \rightarrow W/Z/H$: the production of a neutralino–chargino pair that decays to final states involving W , Z and Higgs bosons.
 - $\tilde{\chi}_1^\pm \tilde{\chi}_1^\mp \rightarrow H\ell^\pm H\ell^\mp$: the production of a chargino pair that decays to final states involving Higgs bosons and leptons through an R -parity-violating interaction.
2. BSM Higgs boson production characterized by the presence of additional heavy-flavour jets are represented by

² m_T denotes the transverse mass of a particle, defined as $m_T = \sqrt{m^2 + p_T^2}$ where m and p_T are its mass and transverse momentum, respectively.

- $\tilde{t}\tilde{t}, \tilde{b}\tilde{b}$: stop-pair production and sbottom-pair production processes. In the subsequent decays of the stop or sbottom particles, the Higgs boson could be produced in the decays of next-to-lightest supersymmetric particles.
3. BSM Higgs boson production characterized by the presence of an additional top quark is represented by
 - $t\bar{t}, (t \rightarrow u/c + H) + \text{c.c.}$: pair-produced top quarks that decay into final states involving Higgs bosons, through a FCNC interaction.
 4. BSM Higgs boson production characterized by the presence of an additional photon is represented by
 - $pp \rightarrow \chi \rightarrow H\gamma$: a massive neutral boson (χ) decaying into a photon and a Higgs boson, a process predicted by extensions of the Higgs sector or gauge sectors [65–67].

These BSM processes are studied in various dedicated ATLAS searches that may use Higgs boson decay channels other than $H \rightarrow \gamma\gamma$. The specific process, model parameters, expected cross section, and a reference to the dedicated search, are summarized in Table 2. These BSM MC samples were generated with the same set-up as used in the dedicated searches, except that the Higgs boson is configured to decay into a pair of photons.

The SUSY events were generated with up to two additional partons in the matrix element using MADGRAPH5_AMC@NLO 2.6.2 at LO in QCD with the NNPDF3.0LO PDF set and CKKW-L merging scheme. Parton showering and hadronization were handled by PYTHIA 8.230 with the A14 tune, using the NNPDF2.3LO PDF set.

MC samples were generated for the BSM process where a massive neutral resonance is produced and decays into a Higgs boson and a photon ($pp \rightarrow \chi \rightarrow H\gamma$). This process could result in a final state with at least three photons. The event generation used the same set-up as for the SUSY samples, except that PYTHIA 8.235 was used to model the parton shower and underlying event.

A $t\bar{t}$ sample with FCNC-induced top-quark decays is also considered. In this process, one top quark decays into a Higgs boson and an up-type quark through a FCNC interaction, while the other top quark decays into a b -quark and a W boson. These FCNC samples were simulated using MADGRAPH5_AMC@NLO 2.4.3 [68] interfaced to PYTHIA 8.212 [40] with the A14 tune for the modelling of parton showers, hadronization and the underlying event. The FCNC samples were generated separately for the up-quark and charm-quark final states.

The effect of multiple interactions in the same and neighbouring bunch crossings (pile-up) was modelled by overlaying each simulated hard-scattering event with inelastic proton–proton (pp) events generated by PYTHIA 8.186 using the NNPDF2.3LO set of PDFs and the A3 tune [75]. The generated Higgs boson events from Table 1 were passed through a GEANT4 [76] simulation of the ATLAS detector [77]. The remaining QCD diphoton events and BSM samples are passed through a fast simulation of the ATLAS detector to reduce the amount of CPU time needed to process the large numbers of generated events. All simulated events are reconstructed with the same software as used for the data [25].

Table 2: Summary of processes, model parameters, and cross sections for the BSM samples used in this paper. A reference to their dedicated ATLAS search is also included. The cross sections quoted include the SM branching ratio for $H \rightarrow \gamma\gamma$. The $pp \rightarrow \chi \rightarrow H\gamma$ process is expected in multiple BSM models, so no particular model is used for the cross-section calculation.

Process with $H \rightarrow \gamma\gamma$	Signal mass	Cross section [pb]	Ref.
$\tilde{\chi}_1^\pm \tilde{\chi}_2^0 \rightarrow W/Z/H$	$m(\tilde{\chi}_1^\pm/\tilde{\chi}_2^0), m(\tilde{\chi}_1^0) = 150, 0.5$ GeV	5.18	[69]
$\tilde{\chi}_1^\pm \tilde{\chi}_2^0 \rightarrow W/Z/H$	$m(\tilde{\chi}_1^\pm/\tilde{\chi}_2^0), m(\tilde{\chi}_1^0) = 300, 0.5$ GeV	0.39	[69]
$\tilde{\chi}_1^\pm \tilde{\chi}_1^\mp \rightarrow H\ell^\pm H\ell^\mp$	$m(\tilde{\chi}_1^\pm) = 150$ GeV	2.61	[70]
$\tilde{\chi}_1^\pm \tilde{\chi}_1^\mp \rightarrow H\ell^\pm H\ell^\mp$	$m(\tilde{\chi}_1^\pm) = 300$ GeV	0.19	[70]
$\tilde{\chi}_1^\pm \tilde{\chi}_1^0, \tilde{\chi}_1^\mp \rightarrow H\ell^\pm, \tilde{\chi}_1^0 \rightarrow W\ell/Z\nu/H\nu$	$m(\tilde{\chi}_1^\pm/\tilde{\chi}_1^0) = 200$ GeV	1.81	[70]
$\tilde{\chi}_1^\pm \tilde{\chi}_1^0, \tilde{\chi}_1^\mp \rightarrow H\ell^\pm, \tilde{\chi}_1^0 \rightarrow W\ell/Z\nu/H\nu$	$m(\tilde{\chi}_1^\pm/\tilde{\chi}_1^0) = 400$ GeV	0.12	[70]
$\tilde{t}_2 \tilde{t}_2, \tilde{t}_2 \rightarrow \tilde{t}_1 H, \tilde{t}_1 \rightarrow \tilde{\chi}_1^0 b q \bar{q} / b \ell \nu$	$m(\tilde{t}_2), m(\tilde{t}_1), m(\tilde{\chi}_2^0) = 500, 340, 300$ GeV	0.61	[71]
$\tilde{b} \tilde{b}, \tilde{b} \rightarrow \tilde{\chi}_2^0 b, \tilde{\chi}_2^0 \rightarrow \tilde{\chi}_1^0 H$	$m(\tilde{b}), m(\tilde{\chi}_2^0), m(\tilde{\chi}_1^0) = 500, 180, 50$ GeV	0.61	[72]
$\tilde{b} \tilde{b}, \tilde{b} \rightarrow \tilde{\chi}_2^0 b, \tilde{\chi}_2^0 \rightarrow \tilde{\chi}_1^0 H$	$m(\tilde{b}), m(\tilde{\chi}_2^0), m(\tilde{\chi}_1^0) = 1000, 205, 60$ GeV	0.0068	[72]
$\tilde{b} \tilde{b}, \tilde{b} \rightarrow \tilde{\chi}_2^0 b, \tilde{\chi}_2^0 \rightarrow \tilde{\chi}_1^0 H$	$m(\tilde{b}), m(\tilde{\chi}_2^0), m(\tilde{\chi}_1^0) = 1200, 205, 60$ GeV	0.0017	[72]
$pp \rightarrow \chi \rightarrow H\gamma$	$m(\chi) = 200$ GeV	-	[73]
$pp \rightarrow \chi \rightarrow H\gamma$	$m(\chi) = 500$ GeV	-	[73]
$t\bar{t}, (t \rightarrow u/c + H) + \text{c.c.}$	-	0.00123	[74]

4 Object and event selection

4.1 Object definitions

Events in this analysis are selected using the following procedure. First, reconstructed photon candidates are required to satisfy a set of preselection criteria. The two highest- p_T preselected photons along with the reconstructed vertex information in the event, are used as inputs to a neural-network algorithm trained on simulated events to determine the correct primary vertex, which is named the ‘diphoton vertex’ [78]. The selected primary vertex is used to compute the properties of objects in the event. Finally, to be selected the photons are required to satisfy isolation and additional identification criteria. In addition to photons, jets (including b -jets), muons, electrons, and the amount of missing transverse momentum, E_T^{miss} , are used in the analysis to define model-independent signal regions. The specific requirements for objects used in this analysis are as follows.

Photons must satisfy $p_T > 22$ GeV and $|\eta| < 2.37$, excluding the transition region $1.37 < |\eta| < 1.52$ between the barrel and endcap EM calorimeters. Photon candidates are separated from jet backgrounds using a *tight* identification criterion based on calorimeter shower shape variables [79]. The identification efficiency for reconstructed photons ranges from 84% at $p_T = 25$ GeV to 94% at $p_T > 100$ GeV. The final selection of photons includes both calorimeter- and track-based isolation requirements to further suppress jets misidentified as photons. The calorimeter isolation variable is defined as the energy in the EM calorimeter within a cone of size $\Delta R = 0.2$ around the photon candidate, excluding the energy in a fixed-size window that contains the photon shower; a correction is made for photon energy leakage from this window [79]. Contributions from pile-up and the underlying event are subtracted [79–83]. The calorimeter-based isolation must be less than 6.5% of each photon candidate’s transverse energy. The track-based isolation variable is defined as the scalar sum of the transverse momenta of tracks within a $\Delta R = 0.2$ cone around the photon candidate. The tracks used in the isolation variable are restricted to those with $p_T > 1$ GeV that are associated with the selected diphoton vertex and not with a photon conversion vertex [79]. The track isolation must be less than 5% of each photon candidate’s transverse energy.

Electron candidates must have $p_T > 10$ GeV and $|\eta| < 2.47$, excluding the EM calorimeter transition

region of $1.37 < |\eta| < 1.52$, and must satisfy a *medium* selection based on a likelihood discriminant using calorimeter shower shapes and track parameters [79]. Isolation criteria based on calorimeter- and track-based information are applied to electrons. The reconstructed track matched to the electron candidate must be consistent with the diphoton vertex by requiring its longitudinal impact parameter z_0 relative to the vertex to satisfy $|z_0 \sin \theta| < 0.5$ mm. In addition, the electron’s transverse impact parameter d_0 with respect to the beam-spot must satisfy $|d_0|/\sigma_{d_0} < 5$, where σ_{d_0} is the uncertainty in d_0 .

Muon candidates are required to have $p_T > 10$ GeV and $|\eta| < 2.7$, and must satisfy the *medium* identification requirements [84]. Muons are required to satisfy calorimeter- and track-based isolation requirements that are 95%–97% efficient for muons with $p_T \in [10, 60]$ GeV and 99% efficient for $p_T > 60$ GeV. Muon tracks must satisfy $|z_0 \sin \theta| < 0.5$ mm and $|d_0|/\sigma_{d_0} < 3$.

Jets are reconstructed using a particle-flow algorithm [85]. It improves the energy resolution by applying the anti- k_t algorithm [86, 87] with radius parameter $R = 0.4$ to noise-suppressed positive-energy topological clusters [88] in the calorimeter after removing energy deposits associated with primary-vertex-matched tracks, and including the track momenta in the clustering instead. Jets must have $p_T > 25$ GeV and $|y| < 4.4$. To suppress jets from pile-up, a jet-vertex-tagger (JVT) multivariate discriminant [89] is applied to jets with $p_T < 60$ GeV and $|\eta| < 2.4$; in the range $|\eta| > 2.5$, a ‘forward’ version of the JVT [90] is applied to jets with $p_T < 120$ GeV.³ Jets with $|\eta| < 2.5$ containing b -hadrons are identified using the DL1r b -tagging algorithm and its 60%, 70%, 77% and 85% efficiency working points, with the outputs combined into a pseudo-continuous b -tagging score [91].

Hadronically decaying τ -leptons are used in this search. They are required to have $p_T > 20$ GeV and $|\eta| < 2.7$. Furthermore, they must have either one or three charged tracks (‘prongs’) with a charge sum of ± 1 in units of the elementary charge, and must satisfy the *medium* working point [92].

An overlap removal procedure is performed in order to avoid double-counting of objects. First, electrons overlapping with any of the two selected photons ($\Delta R < 0.4$) are removed. Jets overlapping with the selected photons ($\Delta R < 0.4$) and electrons ($\Delta R < 0.2$) are removed. Electrons overlapping with the remaining jets ($\Delta R < 0.4$) are removed to match the requirements imposed when measuring isolated-electron efficiencies. Finally, muons overlapping with photons or jets ($\Delta R < 0.4$) are removed.

The missing transverse momentum is defined as the negative vector sum of the transverse momenta of the selected photons, electrons, muons, and jets, as well as the transverse momenta of remaining low- p_T particles, estimated using tracks associated with the diphoton vertex but not with any selected object [93].

4.2 Event preselection

The two highest- p_T preselected photon candidates are required to satisfy the *tight* identification criteria and the isolation selection described above. Finally, the leading and subleading photon candidates are required to satisfy $p_T^{\gamma 1} > 35$ GeV, $p_T^{\gamma 1}/m_{\gamma\gamma} > 0.35$, and $p_T^{\gamma 2} > 25$ GeV, $p_T^{\gamma 2}/m_{\gamma\gamma} > 0.25$, respectively. Events that fail the *tight* identification or the isolation selection but pass the loose identification are used as a control sample for background estimation and modelling purposes.

The trigger, object, and event selection described above are used to define the events that are selected for further analysis. In total, about 1.2 million events are selected in this data set with a diphoton invariant mass between 105 and 160 GeV.

³ η is used to select jets when applying the JVT and the b -tagging requirements, as the way these selections are defined is based on the jet position in the detector.

5 Signal regions

Preselected events are assigned to signal regions defined by the presence of additional reconstructed objects. These signal regions are designed with simple, inclusive selections, and the specific selections were not optimized for any particular BSM processes. Since the selection criteria are not designed to be orthogonal, selected events can be assigned to multiple signal regions. The overlap and correlations of these signal regions are discussed in Section 8. Based on the requirement of there being additional objects in the event, the signal regions can be broadly classified to six groups: events with heavy-flavour jets; events with high jet multiplicity or a large scalar sum of jet transverse momenta (H_T); events with large E_T^{miss} ; events with leptons; events with additional photons; and events with top quarks. As is discussed in Section 8, each signal region, defined through selection criteria for detector-level objects, has a counterpart defined through equivalent criteria at the particle level, which enables the interpretation of the search results with particle-level simulation samples. These signal regions and their definitions are summarized in Table 3 and described as follows.

Two ‘heavy-flavour’ signal regions are defined. One requires the presence of at least three b -jets tagged at the 85% efficiency working point (WP), and the other requires the presence of at least four b -jets tagged at the same working point.

Six high-jet-activity signal regions are defined. Three of them are defined with inclusive jet-multiplicity requirements, using central jets with $|\eta| < 2.5$. The thresholds for the number of jets are four, six, and eight for these regions. Another three regions are defined by the H_T . The inclusive H_T thresholds for these three regions are 500 GeV, 1000 GeV, and 1500 GeV.

Three high- E_T^{miss} signal regions are defined using E_T^{miss} thresholds of 100 GeV, 200 GeV, and 300 GeV.

Six leptonic signal regions are defined. The inclusive leptonic signal region ($\geq 1\ell$) requires the presence of at least one electron or muon in the event. Three dilepton signal regions are defined with electrons and muons: the inclusive dilepton signal region (2ℓ) requires the presence of exactly two leptons; the dilepton Z -veto ($2\ell-Z$) region is a subset of the 2ℓ region, and it explicitly rejects events where the two leptons have the same flavour and their invariant mass is within 10 GeV of the PDG value of the Z boson mass; the same-sign dilepton ($SS-2\ell$) region is also a subset of the 2ℓ region and requires the electric charges of the two leptons to be the same; The multilepton signal region ($\geq 3\ell$) requires the presence of at least three leptons. The τ -lepton signal region requires the presence of at least two τ -lepton candidates.

Two triphoton signal regions are defined. Both require the presence of at least one additional photon in the preselected diphoton events. In the first photon signal region, the diphoton system that is considered as the Higgs boson candidate is built from the two leading photons in p_T . The second photon region assumes the subleading and third-leading photons come from the Higgs boson decay. While the two photon signal regions mostly have the same definitions of the event selection criteria, the $m_{\gamma\gamma}$ observable is constructed differently. The $1\gamma-m_{\gamma\gamma}^{12}$ region targets exotic processes where the Higgs boson is accompanied by a photon with moderate p_T , while the $1\gamma-m_{\gamma\gamma}^{23}$ region targets exotic processes in which a new state that is much more massive than the Higgs boson decays into a photon and a Higgs boson.

Three ‘top’ signal regions are introduced. One inclusive top signal region (ℓb) requires the presence of at least one electron or one muon and at least one b -jet tagged at the 70% efficiency working point. One exclusive semileptonic top-quark signal region (t_{lep}) requires the presence of exactly one lepton, and one b -jet tagged at the 70% efficiency working point. One exclusive hadronic top-quark signal region (t_{had}) requires the presence of exactly three jets, one of which must be a b -jet tagged at the 70% efficiency

working point. The hadronic top-quark signal region also vetoes events with at least one electron or one muon. To further suppress diphoton-plus-multijet background, a boosted decision tree (BDT) is used in top-quark reconstruction [94] performed with the three jets in the event, and the resulting BDT score is required to be greater than 0.9.

Table 3: Signal region definitions at the detector level and particle level. Particle-level object definitions are detailed in Section 8.2. The H_T variable is defined as the scalar sum of the transverse momenta of jets that have $|\eta| < 2.5$. WP stands for efficiency working point. At the detector level, the τ -lepton identification is optimized for hadronically decaying τ -leptons. The symbols γ_1, γ_2 , and γ_3 denote the leading, subleading, and third-leading photons ordered in p_T , respectively. The BDT_{top} variable is a boosted decision tree (BDT) score used to identify triplets of jets consistent with the hadronic-decay final states of top quarks, which was used in Ref. [19].

Target	Region	Detector level	Particle level
Heavy flavour	$\geq 3b$	$n_{b\text{-jet}} \geq 3$, 85% WP	$n_{b\text{-jet}} \geq 3$
	$\geq 4b$	$n_{b\text{-jet}} \geq 4$, 85% WP	$n_{b\text{-jet}} \geq 4$
High jet activity	$\geq 4j$	$n_{\text{jet}} \geq 4$, $ \eta_{\text{jet}} < 2.5$	$n_{\text{jet}} \geq 4$, $ \eta_{\text{jet}} < 2.5$
	$\geq 6j$	$n_{\text{jet}} \geq 6$, $ \eta_{\text{jet}} < 2.5$	$n_{\text{jet}} \geq 6$, $ \eta_{\text{jet}} < 2.5$
	$\geq 8j$	$n_{\text{jet}} \geq 8$, $ \eta_{\text{jet}} < 2.5$	$n_{\text{jet}} \geq 8$, $ \eta_{\text{jet}} < 2.5$
	$H_T > 500$ GeV	$H_T > 500$ GeV	$H_T > 500$ GeV
	$H_T > 1000$ GeV	$H_T > 1000$ GeV	$H_T > 1000$ GeV
	$H_T > 1500$ GeV	$H_T > 1500$ GeV	$H_T > 1500$ GeV
E_T^{miss}	$E_T^{\text{miss}} > 100$ GeV	$E_T^{\text{miss}} > 100$ GeV	$E_T^{\text{miss,tru}} > 100$ GeV
	$E_T^{\text{miss}} > 200$ GeV	$E_T^{\text{miss}} > 200$ GeV	$E_T^{\text{miss,tru}} > 200$ GeV
	$E_T^{\text{miss}} > 300$ GeV	$E_T^{\text{miss}} > 300$ GeV	$E_T^{\text{miss,tru}} > 300$ GeV
Top	ℓb	$n_{\ell=e,\mu} \geq 1$, $n_{b\text{-jet}} \geq 1$, 70% WP	$n_{\ell=e,\mu} \geq 1$, $n_{b\text{-jet}} \geq 1$
	t_{lep}	$n_{\ell=e,\mu} = 1$, $n_{\text{jet}} = n_{b\text{-jet}} = 1$, 70% WP	$n_{\ell=e,\mu} = 1$, $n_{\text{jet}} = n_{b\text{-jet}} = 1$
	t_{had}	$n_{\ell=e,\mu} = 0$, $n_{\text{jet}} = 3$, $n_{b\text{-jet}} = 1$, 70% WP, $\text{BDT}_{\text{top}} > 0.9$	$n_{\ell=e,\mu} = 0$, $n_{\text{jet}} = 3$, $n_{b\text{-jet}} = 1$
Lepton	$\geq 1\ell$	$n_{\ell=e,\mu} \geq 1$	$n_{\ell=e,\mu} \geq 1$
	2ℓ	$ee, \mu\mu$, or $e\mu$	$ee, \mu\mu$, or $e\mu$
	$2\ell\text{-}\cancel{Z}$	$ee, \mu\mu, e\mu$; $ m_{\ell\ell} - m_Z > 10$ GeV for same-flavour leptons	$ee, \mu\mu, e\mu$; $ m_{\ell\ell} - m_Z > 10$ GeV for same-flavour leptons
	$\text{SS-}2\ell$	$ee, \mu\mu$, or $e\mu$ with same charge	$ee, \mu\mu$, or $e\mu$ with same charge
	$\geq 3\ell$	$n_{\ell=e,\mu} \geq 3$	$n_{\ell=e,\mu} \geq 3$
	$\geq 2\tau$	$n_{\tau,\text{had}} \geq 2$	$n_{\tau} \geq 2$
Photon	$1\gamma\text{-}m_{\gamma\gamma}^{12}$	$n_{\gamma} \geq 3$, $m_{\gamma\gamma}$ defined with γ_1, γ_2	$n_{\gamma} \geq 3$, $m_{\gamma\gamma}$ defined with γ_1, γ_2
	$1\gamma\text{-}m_{\gamma\gamma}^{23}$	$n_{\gamma} \geq 3$, $m_{\gamma\gamma}$ defined with γ_2, γ_3	$n_{\gamma} \geq 3$, $m_{\gamma\gamma}$ defined with γ_2, γ_3

6 Signal and background modelling

This search uses the invariant mass of the diphoton system ($m_{\gamma\gamma}$) as the discriminating variable. The potential BSM signal is a narrow resonance in $m_{\gamma\gamma}$, and the background consists of a resonant component and a continuum component. The resonant component arises from the SM Higgs boson production

processes, which include gluon–gluon fusion (ggF) and vector-boson fusion (VBF), and VH , $t\bar{t}H$, tH , and $b\bar{b}H$ production.

The continuum component arises from the production of two initial- or final-state photons, or from the misidentification of jets as either one or both of the photons selected at the detector level. In signal regions where lepton and/or b -jet requirements are applied, these three types of continuum background processes also involve the production of electroweak bosons or top quarks.

The $m_{\gamma\gamma}$ distribution in each signal region is described by a probability density function (pdf) where the signal and background components are modelled by analytic functions of $m_{\gamma\gamma}$ and are normalized to their expected yields. As in previous ATLAS $H \rightarrow \gamma\gamma$ measurements [19, 95], the analytic functions are defined in the range of $105 \text{ GeV} < m_{\gamma\gamma} < 160 \text{ GeV}$. In the statistical interpretation of the search results, the $m_{\gamma\gamma}$ pdfs corresponding to the signal-plus-background and background-only hypotheses are used to fit the observed $m_{\gamma\gamma}$ distributions.

The event yield in the multilepton signal region is not sufficient for performing a fit to the $m_{\gamma\gamma}$ distribution. In this case, an event-count analysis is performed, as is described in Section 6.3.

6.1 Modelling of BSM and SM Higgs boson production

The modelling of the $m_{\gamma\gamma}$ distribution and its associated systematic uncertainties is done in a consistent way for the BSM and SM Higgs boson production processes. Their $m_{\gamma\gamma}$ distributions are both described by the same double-sided Crystal Ball (DSCB) function [96, 97], consisting of a Gaussian distribution in the region around the peak position, continued by power-law tails at lower and higher $m_{\gamma\gamma}$ values. The potential bias in the estimated signal yield due to an intrinsic shape difference between the DSCB function and signal $m_{\gamma\gamma}$ distribution is found to be much smaller than the MC statistical uncertainty of the signal yield and therefore is negligible [98]. The parameters of the DSCB function in each signal region are obtained by a fit to a mixture of the ggF, VBF, VH , $t\bar{t}H$, tH , and $b\bar{b}H$ samples described in Section 3, which are normalized according to their SM cross sections. A shift of 0.09 GeV is applied to the position of the signal peak to account for the difference between the reference Higgs boson mass used in this analysis ($m_H = 125.09 \text{ GeV}$) [99] and the mass for which the samples were generated ($m_H = 125 \text{ GeV}$). The uncertainty in the $m_{\gamma\gamma}$ modelling is discussed in Section 7.1. There is a modest variation in the DSCB shape parameters between various SM and BSM Higgs boson production samples. However, the impact of this variation on the fitted number of signal events is much smaller than the statistical uncertainty of the fitted signal yield.

SM Higgs boson production is the resonant background to signals arising from BSM production. The cross sections of the resonant backgrounds are assumed to be the same as the theoretical predictions, and their contributions to various signal regions are evaluated using the MC samples described in Section 3. The recent Higgs boson measurements from the ATLAS and CMS experiments have shown that the data are consistent with the theory predictions within statistical and systematic uncertainties, which justifies the fixing of expected resonant background yields to their SM predictions. Potential interference effects between the SM and BSM Higgs boson production processes are not considered in the MC simulation. If the interference effect results in a significant deviation in the production rate from the SM prediction, this search would detect it as a signal.

6.2 Continuum background modelling

The $m_{\gamma\gamma}$ distribution of the continuum background is fully determined from a fit to data. The only systematic uncertainty associated with this method arises from the intrinsic difference between the true continuum background $m_{\gamma\gamma}$ shape and the shape of the chosen analytic pdf.

The modelling of the continuum background follows the same process used in Ref. [98], which involves two main steps: first, a background $m_{\gamma\gamma}$ template is constructed from either the MC diphoton continuum background or a data control sample where at least one of the two leading photons fails the photon identification or isolation requirement. Between these two samples, the one with a higher number of events is selected to construct the $m_{\gamma\gamma}$ template. Second, a background function is selected from a number of candidate functions, using a procedure known as the *spurious-signal test* [98], with the goal of identifying an analytic function that is flexible enough to fit the $m_{\gamma\gamma}$ distribution in data and which results in a small potential bias compared to the background statistical uncertainty.

Several families of analytic functions are tested as candidates to model the $m_{\gamma\gamma}$ distribution for each signal region. They include power-law functions, Bernstein polynomials, and exponential functions of a polynomial. These functional forms can include up to five free parameters. The selected functional forms are mostly power-law and exponential functions with one free parameter. The coefficients of background functions are considered independent across signal regions, regardless of the functions chosen. In all cases, they are treated as free parameters in the fit to data.

6.3 Modelling of the background in the multilepton signal region

The expected continuum background event yield in the multilepton ($\geq 3\ell$) signal region is so small that the $m_{\gamma\gamma}$ distribution may not be fitted with an analytic function. In this case, the event count in the $m_{\gamma\gamma}$ range from 123 GeV to 127 GeV is used for statistical interpretation. The expected background yield in this mass range is extrapolated from a control region in two steps. This control region is referred to as the *non-tight-isolated* region and is defined in the same way as the multilepton signal region, except that at least one of the two leading photons must fail to meet the photon quality criteria detailed in Section 4. The expected background yield in the diphoton mass sidebands of the multilepton signal region is scaled from the event yield in the non-tight-isolated diphoton mass sidebands. The ratio of the event yield in the non-tight-isolated control region to that in the tight-isolated signal region is checked in the other leptonic signal regions and is found to be consistent, which indicates that the scale factor derived from other leptonic signal regions can be applied to the multilepton signal region. The variations in the scale factor between various leptonic signal regions are considered as systematic uncertainties of the scale factor. Similarly, the expected background yield in the mass window of $123 \text{ GeV} < m_{\gamma\gamma} < 127 \text{ GeV}$ is computed from the expected background yield in the diphoton mass sidebands, using scale factors evaluated in the non-tight-isolated control regions defined for various leptonic signal regions. These scale factors are consistent and their variations are considered as systematic uncertainties of the extrapolation. The expected continuum background yield in the multilepton signal region is found to be $0.25^{+0.59}_{-0.25}$ events, where the lower bound of the uncertainty is truncated so that the yield remains positive. The expected resonant background yield in this region is predicted by the MC simulation.

7 Systematic uncertainties

Systematic uncertainties considered in this analysis can be grouped into three categories: uncertainties in the modelling of the $m_{\gamma\gamma}$ distribution for the BSM and SM Higgs boson production processes, uncertainties in the modelling of the continuum background $m_{\gamma\gamma}$ distribution, and uncertainties in the expected resonant background yields in each signal region arising from either experimental or theoretical sources. These systematic uncertainties are incorporated into the analysis likelihood models as nuisance parameters.

7.1 Systematic uncertainties in modelling $m_{\gamma\gamma}$ for SM and BSM Higgs boson production

In general, the $m_{\gamma\gamma}$ modelling systematic uncertainties for a given region depend on the BSM signal considered. However, the signal shape variations associated with the properties of a specific BSM model are negligible relative to those associated with the experimental effects, and only the latter are therefore considered and estimated from the SM Higgs production processes. The extraction of a potential signal component from the data $m_{\gamma\gamma}$ distribution is subject to systematic uncertainties in the diphoton mass resolution and scale. While the diphoton mass resolution and scale uncertainties are also model-dependent, their variations are typically limited. The likelihood model considers only signal systematic uncertainties related to the diphoton mass scale and resolution, and does not include any systematic uncertainty for the signal yield, which is the parameter of interest in the search.

The diphoton mass scale uncertainty includes a contribution from the photon energy scale uncertainty, which is typically less than 1% of the diphoton mass, and also a systematic component of 240 MeV, corresponding to the measurement uncertainty of the Higgs boson mass from the combination of the ATLAS and CMS data [99]. The diphoton mass resolution uncertainty arises from the uncertainty of the photon energy resolution and is about 3%–15% relative to the reconstructed width of the diphoton resonance. The estimation and implementation of the photon energy scale and resolution uncertainties follow the procedure outlined in Ref. [79].

7.2 Uncertainty in the continuum background modelling

The uncertainty in the modelling arises from an intrinsic shape difference between the continuum background $m_{\gamma\gamma}$ distribution and the chosen analytic function. The size of this uncertainty is estimated using the *spurious-signal* test mentioned in Section 6.2 and is always smaller than 20% of the statistical uncertainty of the continuum background.

7.3 Uncertainties in resonant background yields

The definition of the signal regions includes selections based on photons, leptons, jets (b -jets), and missing transverse momentum. As such, the expected resonant background yield is subject to experimental systematic uncertainties in the reconstruction and identification efficiencies of these objects. The typical level of systematic uncertainty for object reconstruction and identification is less than 1% for photons [79], 1%–4% for electrons [79] and muons [100], 2%–16% for jets [101] and b -jets [91], and 2% for τ -leptons [102]. Uncertainties in the theoretical modelling of SM Higgs boson production processes are estimated by varying the scale of QCD renormalization and factorization, by changing the choice of

parton distribution function set, and by comparing the predicted events from different parton showering implementations for a given Higgs boson production process. The theoretical systematic uncertainties typically range from 10% to 35% [18]. The uncertainty in the integrated luminosity of the data sample is 1.7% [27], obtained using the LUCID-2 detector [28] for the primary luminosity measurements. Other uncertainties in background event yields, such as the impact of pile-up on selection efficiencies [103], contribute $< 1\%$.

8 Results

Figures 1–6 show the diphoton mass $m_{\gamma\gamma}$ distributions for all the signal regions considered in this paper, except the multilepton ($\geq 3\ell$) signal region. The result of a signal-plus-background fit as described in Section 6 is shown for each signal region. The expected and observed event yields are determined from the signal-plus-background fit in each signal region and are summarized in Table 4. Also included in this table are the expected and observed event counts in the multilepton signal region. No event is found in the multilepton signal region, while the sum of the continuum and resonant background expectations is $0.27^{+0.59}_{-0.27}$ events. A p_0 -value was evaluated for each of these signal regions, and the largest excess is in the $H_T > 1000$ GeV region and is less than two standard deviations above the expectation. The observed significance [104] is also given in Table 4.

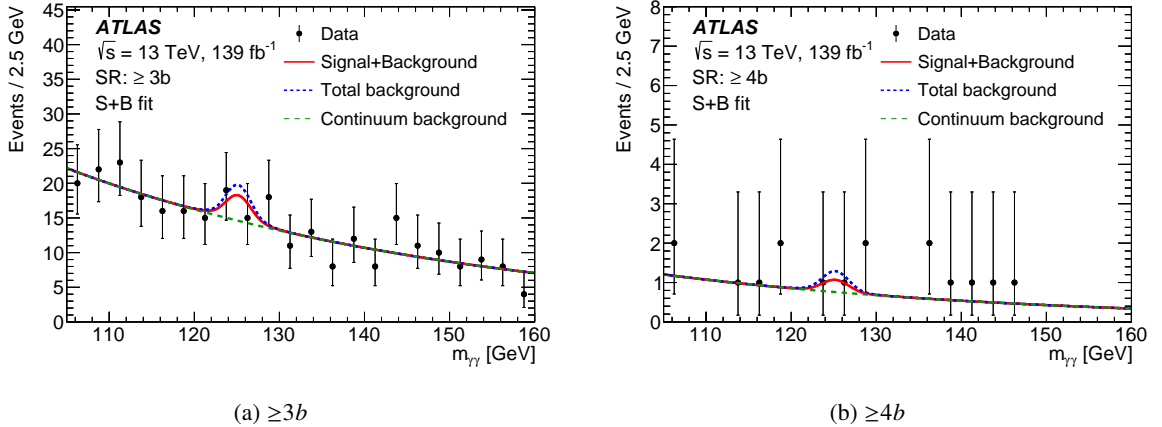


Figure 1: Diphoton mass distributions for heavy-flavour signal regions. Data are shown together with the signal-plus-background fit. The overall fitted signal-plus-background pdf is shown as a solid red curve, the contributions from the resonant Higgs boson and continuum backgrounds are shown as a dashed blue curve, while the contributions only from the continuum backgrounds are shown as a dashed green curve. The difference between the solid red and the dashed blue curves indicates the fitted deviation from the SM expectation.

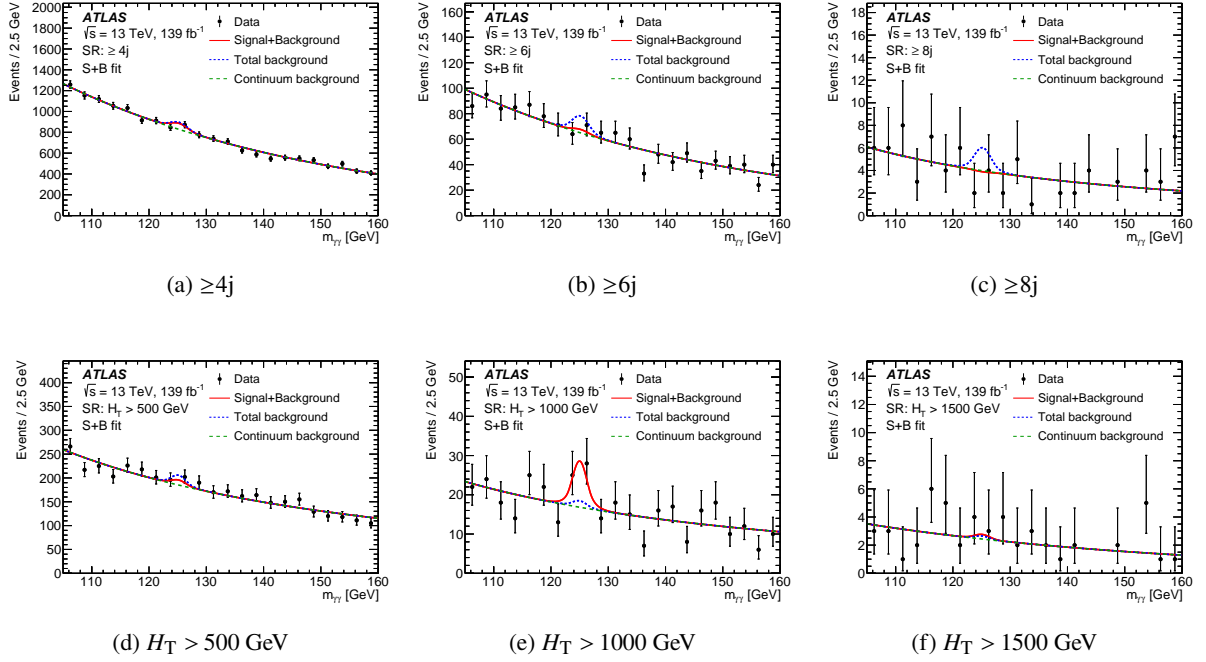


Figure 2: Diphoton mass distributions for high-jet-activity signal regions. Data are shown together with the signal-plus-background fit. The overall fitted signal-plus-background pdf is shown as a solid red curve, the contributions from the resonant Higgs boson and continuum backgrounds are shown as a dashed blue curve, while the contributions only from the continuum backgrounds are shown as a dashed green curve. The difference between the solid red and the dashed blue curves indicates the fitted deviation from the SM expectation.

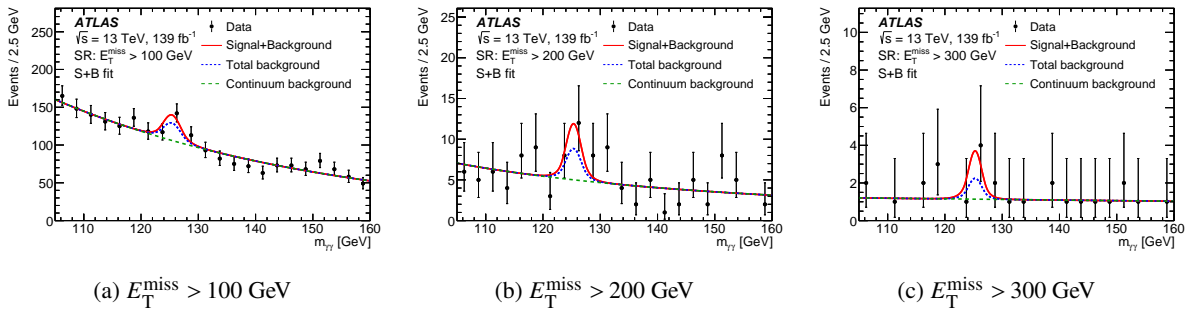


Figure 3: Diphoton mass distributions for E_T^{miss} signal regions. Data are shown together with the signal-plus-background fit. The overall fitted signal-plus-background pdf is shown as a solid red curve, the contributions from the resonant Higgs boson and continuum backgrounds are shown as a dashed blue curve, while the contributions only from the continuum backgrounds are shown as a dashed green curve. The difference between the solid red and the dashed blue curves indicates the fitted deviation from the SM expectation.

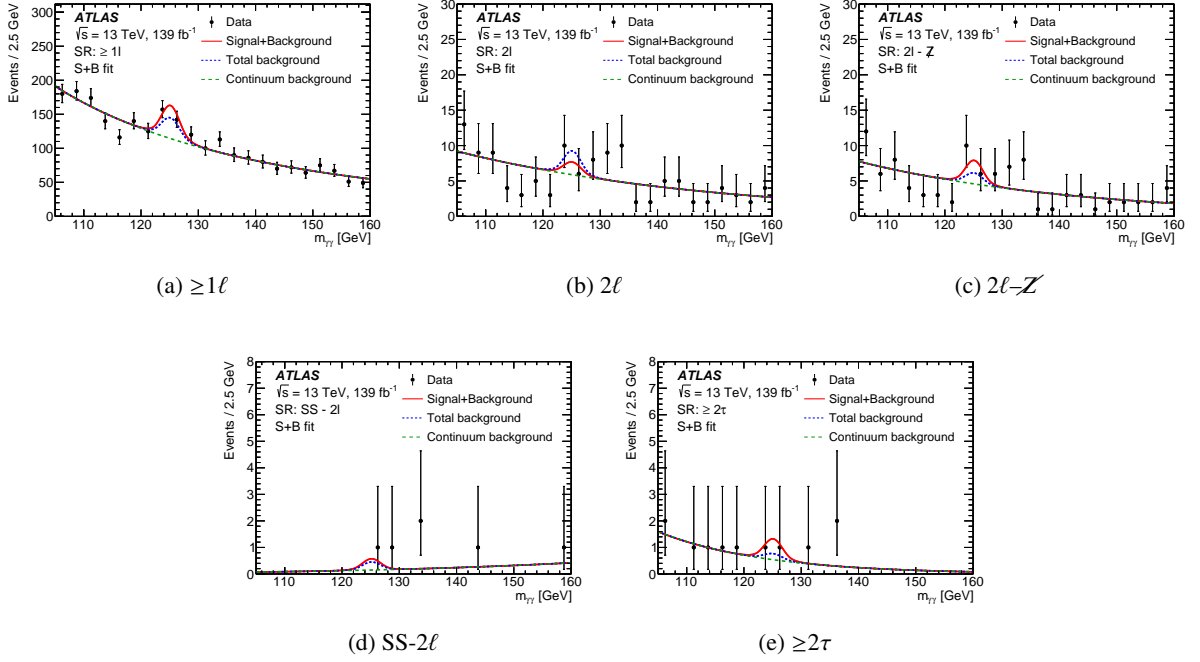


Figure 4: Diphoton mass distributions for lepton signal regions. Data are shown together with the signal-plus-background fit. The overall fitted signal-plus-background pdf is shown as a solid red curve, the contributions from the resonant Higgs boson and continuum backgrounds are shown as a dashed blue curve, while the contributions only from the continuum backgrounds are shown as a dashed green curve. The difference between the solid red and the dashed blue curves indicates the fitted deviation from the SM expectation.

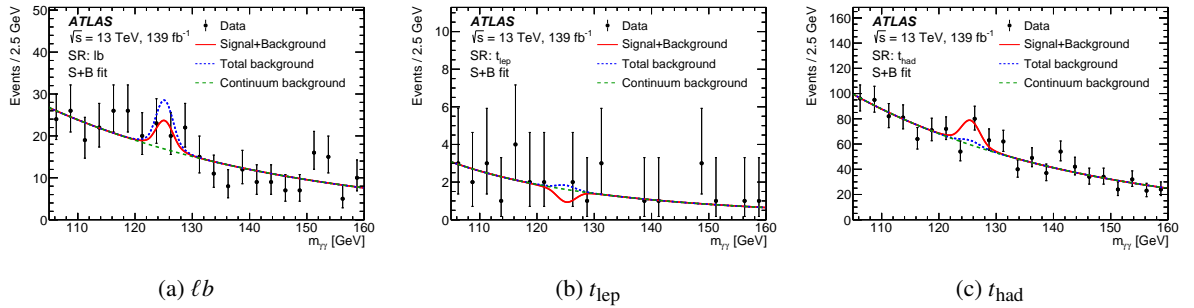


Figure 5: Diphoton mass distributions for top-quark signal regions. Data are shown together with the signal-plus-background fit. The overall fitted signal-plus-background pdf is shown as a solid red curve, the contributions from the resonant Higgs boson and continuum backgrounds are shown as a dashed blue curve, while the contributions only from the continuum backgrounds are shown as a dashed green curve. The difference between the solid red and the dashed blue curves indicates the fitted deviation from the SM expectation.

Table 4: Expected background and observed event yields in the diphoton mass range $123 \text{ GeV} < m_{\gamma\gamma} < 127 \text{ GeV}$. The resonant Higgs boson production and continuum backgrounds are shown separately. The observed significance is also shown for all signal regions except the $\geq 3\ell$ region, where less than one background event is expected and the observed number of events is zero. Note that the significance is calculated using the full mass spectrum of $105 \text{ GeV} < m_{\gamma\gamma} < 160 \text{ GeV}$, which may not be reproduced using yields reported in this table.

SR	Expected Background			Observed Yield	Observed Excess Significance [σ]
	Resonant Higgs	Continuum	Total Background		
Heavy flavour					
$\geq 3b$	6.47	23.4	29.9	30	-0.3
$\geq 4b$	0.69	1.22	1.91	1	-0.2
High jet activity					
$\geq 4j$	85.2	1330	1420	1404	-0.3
$\geq 6j$	16.4	104	121	105	-1.3
$\geq 8j$	2.44	6.37	8.81	6	-0.9
$H_T > 500 \text{ GeV}$	23.9	297	321	310	-0.6
$H_T > 1000 \text{ GeV}$	1.85	27	28.8	39	1.8
$H_T > 1500 \text{ GeV}$	0.264	3.9	4.17	4	0.1
E_T^{miss}					
$E_T^{\text{miss}} > 100 \text{ GeV}$	29	171	200	212	0.8
$E_T^{\text{miss}} > 200 \text{ GeV}$	4.51	8.06	12.6	16	0.9
$E_T^{\text{miss}} > 300 \text{ GeV}$	1.15	1.85	3	5	0.8
Top quark					
ℓb	14.9	27	41.9	34	-0.6
t_{lep}	0.281	2.58	2.86	1	-0.7
t_{had}	4.44	96.3	101	111	1.7
Lepton					
$\geq 1\ell$	38.8	183	222	237	1.4
2ℓ	4.24	9.42	13.7	10	-0.5
$2\ell - \mathcal{Z}$	1.95	7.35	9.3	10	0.7
$SS - 2\ell$	0.431	0.224	0.655	1	0.2
$\geq 3\ell$	0.02	0.25	0.27	0	-
$\geq 2\tau$	0.256	0.875	1.13	2	0.6
Photon					
$1\gamma - m_{\gamma\gamma}^{12}$	2.33	119	121	132	0.7
$1\gamma - m_{\gamma\gamma}^{23}$	0.436	32.8	33.2	42	1.1

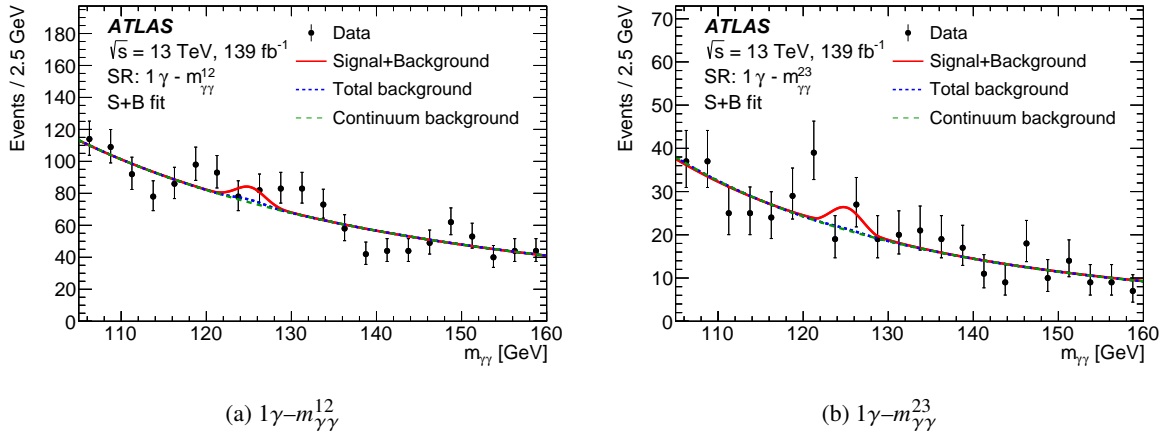


Figure 6: Diphoton mass distributions for photon signal regions. Data are shown together with the signal-plus-background fit. The overall fitted signal-plus-background pdf is shown as a solid red curve, the contributions from the resonant Higgs boson and continuum backgrounds are shown as a dashed blue curve, while the contributions only from the continuum backgrounds are shown as a dashed green curve. The difference between the solid red and the dashed blue curves indicates the fitted deviation from the SM expectation.

8.1 Upper limits on BSM production cross sections

Since no significant excess beyond the SM expectation was observed, the $m_{\gamma\gamma}$ distributions in the signal regions, as well as the event count in the multilepton ($\geq 3\ell$) region, are used to set limits on the visible cross section of BSM production of the Higgs boson with a mass of 125.09 GeV in these regions. The 95% CL limits were derived using the modified frequentist CL_s method [105]. The limits are shown in Table 5 and graphically in Figure 7. The observed 95% CL limit on the visible cross section ranges from 0.05 fb ($\geq 3\ell$) to 0.7 fb ($\geq 4j$).

The observed limits reported here are correlated since the signal regions overlap. To enable the use of limits from multiple signal regions to constrain BSM processes, the correlation between the observed limits from any pair of signal regions considered in this paper is estimated using a pseudo-experiment-based bootstrapping procedure [106]. Readers of this paper could derive a combined limit on the cross section of a BSM signal using the observed limits in individual signal regions and their correlations. Only regions with at least 50 events in the $m_{\gamma\gamma}$ range from 105 GeV to 160 GeV were checked using this procedure. Correlations larger than 5% are observed for a few regions and are reported in Table 6.

Table 5: Observed and expected 95% CL upper limits on the visible cross section of BSM Higgs boson production in each signal region. The $\pm 1\sigma$ and $\pm 2\sigma$ variations of the expected limit are also shown.

SR	Observed	95% CL limit [fb]				
		Median	+1 σ	-1 σ	+2 σ	-2 σ
Heavy flavour						
$\geq 3b$	0.12	0.13	0.18	0.093	0.25	0.069
$\geq 4b$	0.037	0.037	0.054	0.026	0.081	0.02
High jet activity						
$\geq 4j$	0.73	0.81	1.1	0.58	1.5	0.43
$\geq 6j$	0.15	0.22	0.31	0.16	0.42	0.12
$\geq 8j$	0.047	0.065	0.094	0.047	0.13	0.035
$H_T > 500$ GeV	0.28	0.34	0.47	0.24	0.64	0.18
$H_T > 1000$ GeV	0.21	0.11	0.16	0.079	0.22	0.059
$H_T > 1500$ GeV	0.052	0.048	0.07	0.034	0.1	0.026
E_T^{miss}						
$E_T^{\text{miss}} > 100$ GeV	0.4	0.3	0.42	0.22	0.57	0.16
$E_T^{\text{miss}} > 200$ GeV	0.11	0.075	0.11	0.054	0.15	0.04
$E_T^{\text{miss}} > 300$ GeV	0.053	0.04	0.059	0.029	0.088	0.022
Top						
ℓb	0.14	0.16	0.22	0.11	0.29	0.085
t_{lep}	0.034	0.043	0.062	0.031	0.092	0.023
t_{had}	0.39	0.23	0.32	0.17	0.44	0.12
Lepton						
$\geq 1\ell$	0.5	0.32	0.45	0.23	0.61	0.17
2ℓ	0.069	0.08	0.11	0.057	0.16	0.043
$2\ell\text{-}\cancel{Z}$	0.089	0.068	0.098	0.049	0.14	0.037
$SS\text{-}2\ell$	0.028	0.026	0.04	0.019	0.061	0.014
$\geq 3\ell$	0.022	0.022	0.028	0.022	0.046	0.022
$\geq 2\tau$	0.036	0.031	0.046	0.022	0.07	0.016
Photon						
$1\gamma\text{-}m_{\gamma\gamma}^{12}$	0.44	0.35	0.49	0.25	0.66	0.19
$1\gamma\text{-}m_{\gamma\gamma}^{23}$	0.4	0.28	0.4	0.2	0.55	0.15

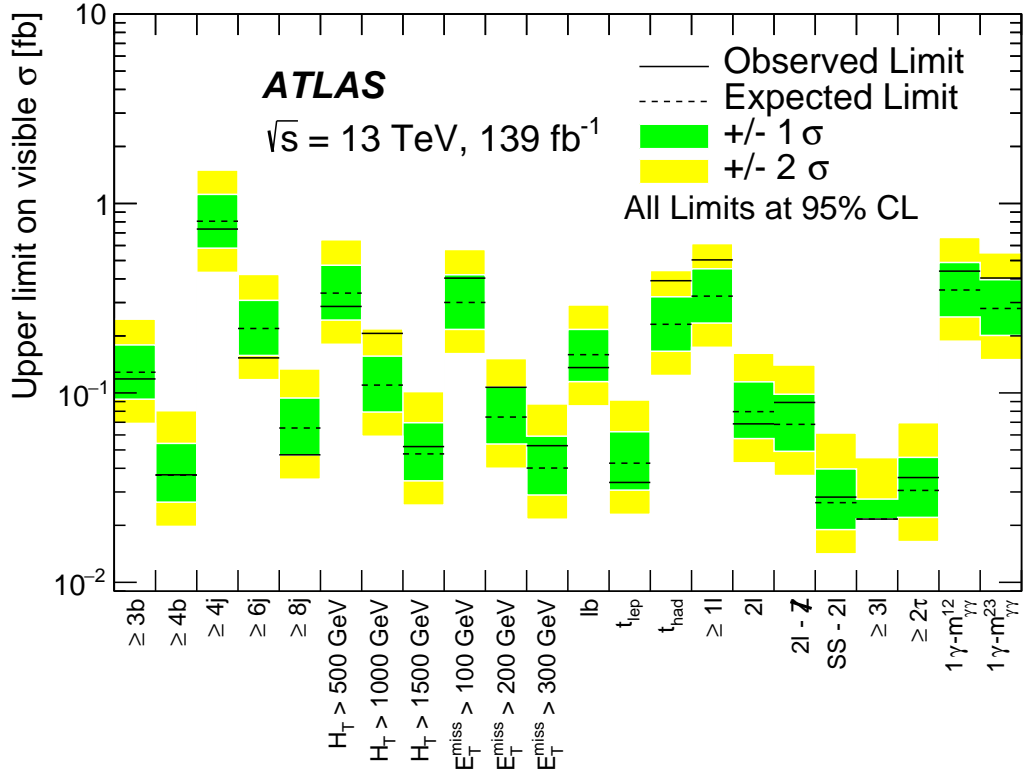


Figure 7: Observed and expected 95% CL limits on the visible cross section of BSM Higgs boson production in each signal region. The 1σ and 2σ variations of the expected limit are also shown as green and yellow bands, respectively.

Table 6: Correlations between observed 95% CL limits for pairs of signal regions. Only regions with a correlation greater than 5% are reported. Pairs of regions that appear in previous rows are not repeated.

Region	Region (Correlation)
$\geq 4j$	$\geq 6j$ (29%), $H_T > 500$ GeV (28%)
$\geq 6j$	$\geq 8j$ (25%), $H_T > 500$ GeV (26%), $H_T > 1000$ GeV (8%)
$H_T > 500$ GeV	$H_T > 1000$ GeV (32%)
$E_T^{\text{miss}} > 200$ GeV	$E_T^{\text{miss}} > 100$ GeV (29%)
1ℓ	2ℓ (26%), ℓb (36%)
2ℓ	$2\ell-Z$ (97%)

8.2 Interpretation with particle-level simulation

This paper aims to present results that can be used without detailed knowledge of the ATLAS detector to derive constraints on the BSM processes of interest. For a specific BSM process, its particle-level cross section, σ_{tru} , in a given region can be derived from MC simulation with particle-level requirements as given in Table 3. To determine if the BSM process is excluded or not, σ_{tru} should be compared with a

particle-level 95% CL limit, σ_{tru}^{95} , for the same region. Since this paper only reports a 95% CL limit on the visible cross section at the detector level, σ_{det}^{95} , for any of the signal regions, a signal-region-specific detector efficiency, ϵ , must be provided to convert σ_{det}^{95} to σ_{tru}^{95} . More specifically, one has $\sigma_{\text{tru}}^{95} = \sigma_{\text{det}}^{95}/\epsilon$.

The region-specific detector efficiency ϵ is defined as the ratio of the event yield in a signal region at the detector level to that in a signal region defined at the particle level. As such, for each signal region considered in this paper, a particle-level definition must be specified. Table 7 summarizes the particle-level object definitions. Particle-level jets are built from all MC generator-level ‘truth’ particles, removing the contributions from muons and stable particles such as neutrinos and lightest supersymmetric particles, using the anti- k_r algorithm with a radius parameter of 0.4. The particle-level objects are required to be isolated by implementing the following overlap removal procedure: electrons, muons, photons, and τ -leptons are removed if there is another object of the same type within $\Delta R < 0.1$. Then any muon, jet or electron is removed if it is within $\Delta R = 0.4$ of any photon, any jet within $\Delta R = 0.2$ of any electron is removed, and finally any muon or electron within $\Delta R = 0.4$ of any jet is removed. In this paper, a particle-level b -jet is defined as a jet that is within $\Delta R = 0.4$ of a b -quark, and the b -quark should pass the requirements of $p_T > 25$ GeV and $|\eta| < 2.5$. This requirement is not fully efficient due to the kinematic requirements on the b -quark. Depending on the specific signal process, the requirement has an efficiency of matching a particle-level jet to a b -quark at the level of 70% to 80%, for a b -quark with $p_T > 25$ GeV and $|\eta| < 2.5$. Then, the particle-level signal regions can be defined with the particle-level objects, and the definitions are detailed in Table 3.

Table 7: Particle-level object definitions and event preselection.

Object	Requirements
Photon	$p_T > 22$ GeV, $ \eta < 2.5$
Electron	$p_T > 10$ GeV, $ \eta < 2.5$
Muon	$p_T > 10$ GeV, $ \eta < 2.7$
Jet	$p_T > 25$ GeV, $ \eta < 4.4$
b -jet	$p_T > 25$ GeV, $ \eta < 2.5$, $\Delta R(b\text{-quark, jet}) < 0.4$
τ -lepton	$p_T > 20$ GeV, $ \eta < 2.5$
Preselection	
$p_T^{\gamma 1} > 35$ GeV, $p_T^{\gamma 2} > 25$ GeV, $p_T^{\gamma 1}/m_{\gamma\gamma} > 0.35$, $p_T^{\gamma 2}/m_{\gamma\gamma} > 0.25$	

The detector efficiency, ϵ , is evaluated for all signal regions considered in this paper and is summarized in Table 8. For each signal region, the value of ϵ is calculated for a few SM and BSM Higgs boson production processes, and the range of ϵ values is reported. Since the final-state object multiplicity and kinematics can differ between processes, variations in ϵ are expected. The reported ϵ values are subject to a small statistical uncertainty, which is much smaller than the variation in ϵ between different physics processes. In general, the detector-level selection is always less efficient than the particle-level selection, except for the following two situations. First, when selecting a particle-level b -jet, the ΔR matching procedure may be less efficient than the detector-level b -tagging, for which a b -jet is defined as a jet containing a b -hadron. The adoption of the ΔR matching procedure is motivated by the convenience of implementation at the particle level. Second, when a signal region is defined by placing a cut at a value in the tail of a variable’s distribution, such as for H_T or the number of jets, detector-level effects could lead to event migration and hence a higher detector-level selection efficiency. However, when all the detector effects are combined, as

shown in Table 8, ϵ is always less than 1. The value of ϵ is very small for the 2τ signal region because the particle-level τ -leptons include all τ -leptons regardless of their decay modes. This choice is also motivated by the convenience of selection implementation at the particle level.

As an example, an electroweak SUSY production model, corresponding to the one shown in the first row of Table 2 is used to demonstrate how information reported in this section can be used to derive a constraint on a given BSM model. In this SUSY process, a chargino and neutralino pair ($\tilde{\chi}_1^\pm \tilde{\chi}_2^0$) is produced in the pp collision, which results in a final state of a W boson, a Higgs boson, and two light neutralinos, $\tilde{\chi}_1^0$. The light neutralinos are undetectable, giving rise to large values of E_T^{miss} . The masses of the pair-produced chargino and neutralino are 150 GeV, and the light neutralino's mass is 0.5 GeV. For this model, a targeted search has already been carried out by the ATLAS Collaboration [69], which reported a 95% CL upper limit of 2 pb for the cross section at this specific signal point.

The $E_T^{\text{miss}} > 100$ GeV signal region can be used to probe the same SUSY process, which predicts a particle-level cross section, σ_{tru} , of 1.05 fb for this $E_T^{\text{miss}} > 100$ GeV region. The observed 95% CL upper limit on the BSM cross section at the detector level is $\sigma_{\text{det}}^{95} = 0.4$ fb, for the $E_T^{\text{miss}} > 100$ GeV region, and its corresponding ϵ is chosen, conservatively, to be 0.6, according to Table 8. The particle-level 95% CL limit on the BSM cross section in the $E_T^{\text{miss}} > 100$ GeV region is therefore $\sigma_{\text{tru}}^{95} = 0.67$ fb, which would exclude the SUSY model considered here. The observed limit in the $E_T^{\text{miss}} > 100$ GeV region in the $H \rightarrow \gamma\gamma$ final state can be converted to a limit on the inclusive cross section for this SUSY model by taking into account the selection acceptance at the particle level and the $H \rightarrow \gamma\gamma$ branching ratio, and the resulting inclusive cross-section limit is 3.3 pb. This limit is of the same order of magnitude as the 2 pb upper limit in the dedicated search, but is 65% weaker.

Table 8: Range of ϵ values for all SRs. The detector efficiency ϵ is only calculated for processes where the reconstruction-level yield in a given signal region is greater than 0.1 events for 139 fb^{-1} of data.

SR	Relevant processes	Range of ϵ
Heavy flavour		
$\geq 3b$	$\tilde{b}\tilde{b}, \tilde{b} \rightarrow \tilde{\chi}_2^0 b, \tilde{\chi}_2^0 \rightarrow \tilde{\chi}_1^0 H, \tilde{t}_2 \tilde{t}_2, \tilde{t}_2 \rightarrow \tilde{t}_1 H, \tilde{t}_1 \rightarrow \tilde{\chi}_1^0 b q \bar{q} / b \ell \nu$	0.68–0.81
$\geq 4b$	$\tilde{b}\tilde{b}, \tilde{b} \rightarrow \tilde{\chi}_2^0 b, \tilde{\chi}_2^0 \rightarrow \tilde{\chi}_1^0 H, \tilde{t}_2 \tilde{t}_2, \tilde{t}_2 \rightarrow \tilde{t}_1 H, \tilde{t}_1 \rightarrow \tilde{\chi}_1^0 b q \bar{q} / b \ell \nu$	0.64–0.97
High jet activity		
$\geq 4j$	$\tilde{t}\tilde{t}H, \tilde{b}\tilde{b}, \tilde{b} \rightarrow \tilde{\chi}_2^0 b, \tilde{\chi}_2^0 \rightarrow \tilde{\chi}_1^0 H, \tilde{t}_2 \tilde{t}_2, \tilde{t}_2 \rightarrow \tilde{t}_1 H, \tilde{t}_1 \rightarrow \tilde{\chi}_1^0 b q \bar{q} / b \ell \nu, tWH$	0.60–0.70
$\geq 6j$	$\tilde{t}\tilde{t}H, \tilde{b}\tilde{b}, \tilde{b} \rightarrow \tilde{\chi}_2^0 b, \tilde{\chi}_2^0 \rightarrow \tilde{\chi}_1^0 H, \tilde{t}_2 \tilde{t}_2, \tilde{t}_2 \rightarrow \tilde{t}_1 H, \tilde{t}_1 \rightarrow \tilde{\chi}_1^0 b q \bar{q} / b \ell \nu, tWH$	0.64–0.80
$\geq 8j$	$\tilde{t}\tilde{t}H, \tilde{b}\tilde{b}, \tilde{b} \rightarrow \tilde{\chi}_2^0 b, \tilde{\chi}_2^0 \rightarrow \tilde{\chi}_1^0 H, \tilde{t}_2 \tilde{t}_2, \tilde{t}_2 \rightarrow \tilde{t}_1 H, \tilde{t}_1 \rightarrow \tilde{\chi}_1^0 b q \bar{q} / b \ell \nu$	0.65–0.90
$H_T > 500$ GeV	$\tilde{t}\tilde{t}H, \tilde{b}\tilde{b}, \tilde{b} \rightarrow \tilde{\chi}_2^0 b, \tilde{\chi}_2^0 \rightarrow \tilde{\chi}_1^0 H, \tilde{t}_2 \tilde{t}_2, \tilde{t}_2 \rightarrow \tilde{t}_1 H, \tilde{t}_1 \rightarrow \tilde{\chi}_1^0 b q \bar{q} / b \ell \nu, tWH$	0.52–0.66
$H_T > 1000$ GeV	$\tilde{t}\tilde{t}H, \tilde{b}\tilde{b}, \tilde{b} \rightarrow \tilde{\chi}_2^0 b, \tilde{\chi}_2^0 \rightarrow \tilde{\chi}_1^0 H, \tilde{t}_2 \tilde{t}_2, \tilde{t}_2 \rightarrow \tilde{t}_1 H, \tilde{t}_1 \rightarrow \tilde{\chi}_1^0 b q \bar{q} / b \ell \nu, tWH$	0.51–0.72
$H_T > 1500$ GeV	$\tilde{t}\tilde{t}H, \tilde{b}\tilde{b}, \tilde{b} \rightarrow \tilde{\chi}_2^0 b, \tilde{\chi}_2^0 \rightarrow \tilde{\chi}_1^0 H, \tilde{t}_2 \tilde{t}_2, \tilde{t}_2 \rightarrow \tilde{t}_1 H, \tilde{t}_1 \rightarrow \tilde{\chi}_1^0 b q \bar{q} / b \ell \nu$	0.41–0.73
E_T^{miss}		
$E_T^{\text{miss}} > 100$ GeV	$\tilde{t}\tilde{t}H, tWH, WH, ZH, \tilde{\chi}_1^\pm \tilde{\chi}_2^0 \rightarrow W/Z/H$	0.60–0.78
$E_T^{\text{miss}} > 200$ GeV	$\tilde{t}\tilde{t}H, tWH, WH, ZH, \tilde{\chi}_1^\pm \tilde{\chi}_2^0 \rightarrow W/Z/H$	0.60–0.79
$E_T^{\text{miss}} > 300$ GeV	$\tilde{t}\tilde{t}H, tWH, WH, ZH, \tilde{\chi}_1^\pm \tilde{\chi}_2^0 \rightarrow W/Z/H$	0.66–0.84
Lepton		
$\geq 1\ell$	$WH, \tilde{t}\tilde{t}H, tWH, \text{FCNC}, \tilde{\chi}_1^\pm \tilde{\chi}_2^0 \rightarrow W/Z/H$	0.40–0.48
2ℓ	$ZH, \tilde{t}\tilde{t}H, \tilde{t}_2 \tilde{t}_2, \tilde{t}_2 \rightarrow \tilde{t}_1 H, \tilde{t}_1 \rightarrow \tilde{\chi}_1^0 b q \bar{q} / b \ell \nu, \tilde{\chi}_1^\pm \tilde{\chi}_1^\mp \rightarrow H\ell^\pm H\ell^\pm, \tilde{\chi}_1^\pm \tilde{\chi}_1^0, \tilde{\chi}_1^\pm \rightarrow H\ell^\pm, \tilde{\chi}_1^0 \rightarrow W\ell/Z\nu/H\nu$	0.21–0.48
$2\ell-Z$	$\tilde{t}\tilde{t}H, \tilde{t}_2 \tilde{t}_2, \tilde{t}_2 \rightarrow \tilde{t}_1 H, \tilde{t}_1 \rightarrow \tilde{\chi}_1^0 b q \bar{q} / b \ell \nu, \tilde{\chi}_1^\pm \tilde{\chi}_1^\mp \rightarrow H\ell^\pm H\ell^\pm, \tilde{\chi}_1^\pm \tilde{\chi}_1^0, \tilde{\chi}_1^\pm \rightarrow H\ell^\pm, \tilde{\chi}_1^0 \rightarrow W\ell/Z\nu/H\nu$	0.20–0.46
$\geq 3\ell$	$\tilde{t}_2 \tilde{t}_2, \tilde{t}_2 \rightarrow \tilde{t}_1 H, \tilde{t}_1 \rightarrow \tilde{\chi}_1^0 b q \bar{q} / b \ell \nu, \tilde{\chi}_1^\pm \tilde{\chi}_1^\mp \rightarrow H\ell^\pm H\ell^\pm, \tilde{\chi}_1^\pm \tilde{\chi}_1^0, \tilde{\chi}_1^\pm \rightarrow H\ell^\pm, \tilde{\chi}_1^0 \rightarrow W\ell/Z\nu/H\nu$	0.18–0.33
$SS-2\ell$	$\tilde{t}_2 \tilde{t}_2, \tilde{t}_2 \rightarrow \tilde{t}_1 H, \tilde{t}_1 \rightarrow \tilde{\chi}_1^0 b q \bar{q} / b \ell \nu, \tilde{\chi}_1^\pm \tilde{\chi}_1^0, \tilde{\chi}_1^\pm \rightarrow H\ell^\pm, \tilde{\chi}_1^0 \rightarrow W\ell/Z\nu/H\nu$	0.29–0.49
$\geq 2\tau$	$ZH, \tilde{t}_2 \tilde{t}_2, \tilde{t}_2 \rightarrow \tilde{t}_1 H, \tilde{t}_1 \rightarrow \tilde{\chi}_1^0 b q \bar{q} / b \ell \nu, \tilde{b}\tilde{b}, \tilde{b} \rightarrow \tilde{\chi}_2^0 b, \tilde{\chi}_2^0 \rightarrow \tilde{\chi}_1^0 H, \tilde{\chi}_1^\pm \tilde{\chi}_1^\mp \rightarrow H\ell^\pm H\ell^\pm, \tilde{\chi}_1^\pm \tilde{\chi}_1^0, \tilde{\chi}_1^\pm \rightarrow H\ell^\pm, \tilde{\chi}_1^0 \rightarrow W\ell/Z\nu/H\nu$	0.04–0.09
Top quark		
t_{lep}	FCNC with semileptonically decaying top	0.32–0.36
t_{had}	FCNC with hadronically decaying top	0.29–0.30
tb	$\tilde{t}\tilde{t}H, tHj b, tWH, \text{FCNC}$ with semileptonically decaying top	0.41–0.52
Photon		
$1\gamma-m_{\gamma\gamma}^{12}$	$\tilde{t}_2 \tilde{t}_2, \tilde{t}_2 \rightarrow \tilde{t}_1 H, \tilde{t}_1 \rightarrow \tilde{\chi}_1^0 b q \bar{q} / b \ell \nu, \tilde{b}\tilde{b}, \tilde{b} \rightarrow \tilde{\chi}_2^0 b, \tilde{\chi}_2^0 \rightarrow \tilde{\chi}_1^0 H$	0.23–0.33
$1\gamma-m_{\gamma\gamma}^{23}$	$\tilde{t}_2 \tilde{t}_2, \tilde{t}_2 \rightarrow \tilde{t}_1 H, \tilde{t}_1 \rightarrow \tilde{\chi}_1^0 b q \bar{q} / b \ell \nu$	0.35–0.40

9 Conclusions

This paper reports a model-independent examination of the diphoton final states where a Higgs boson is produced, using a 139 fb^{-1} data sample of 13 TeV pp collisions collected by the ATLAS detector during Run 2 of the LHC. A total of 22 signal regions defined with various requirements on the additional reconstructed objects were examined, and no significant excess over the SM expectation was observed. Upper limits at 95% CL were set on the visible cross section of BSM Higgs boson production in each of these signal regions. To enable interpretation of the results as a constraint on other models, a set of detector efficiency factors is also reported.

Acknowledgements

We thank CERN for the very successful operation of the LHC, as well as the support staff from our institutions without whom ATLAS could not be operated efficiently.

We acknowledge the support of ANPCyT, Argentina; YerPhI, Armenia; ARC, Australia; BMWFW and FWF, Austria; ANAS, Azerbaijan; CNPq and FAPESP, Brazil; NSERC, NRC and CFI, Canada; CERN; ANID, Chile; CAS, MOST and NSFC, China; Minciencias, Colombia; MEYS CR, Czech Republic; DNRf and DNSRC, Denmark; IN2P3-CNRS and CEA-DRF/IRFU, France; SRNSFG, Georgia; BMBF, HGF and MPG, Germany; GSRI, Greece; RGC and Hong Kong SAR, China; ISF and Benozziyo Center, Israel; INFN, Italy; MEXT and JSPS, Japan; CNRST, Morocco; NWO, Netherlands; RCN, Norway; MEiN, Poland; FCT, Portugal; MNE/IFA, Romania; MESTD, Serbia; MSSR, Slovakia; ARRS and MIZŠ, Slovenia; DSI/NRF, South Africa; MICINN, Spain; SRC and Wallenberg Foundation, Sweden; SERI, SNSF and Cantons of Bern and Geneva, Switzerland; MOST, Taiwan; TENMAK, Türkiye; STFC, United Kingdom; DOE and NSF, United States of America. In addition, individual groups and members have received support from BCKDF, CANARIE, Compute Canada and CRC, Canada; PRIMUS 21/SCI/017 and UNCE SCI/013, Czech Republic; COST, ERC, ERDF, Horizon 2020 and Marie Skłodowska-Curie Actions, European Union; Investissements d’Avenir Labex, Investissements d’Avenir Idex and ANR, France; DFG and AvH Foundation, Germany; Herakleitos, Thales and Aristeia programmes co-financed by EU-ESF and the Greek NSRF, Greece; BSF-NSF and MINERVA, Israel; Norwegian Financial Mechanism 2014-2021, Norway; NCN and NAWA, Poland; La Caixa Banking Foundation, CERCA Programme Generalitat de Catalunya and PROMETEO and GenT Programmes Generalitat Valenciana, Spain; Göran Gustafssons Stiftelse, Sweden; The Royal Society and Leverhulme Trust, United Kingdom.

The crucial computing support from all WLCG partners is acknowledged gratefully, in particular from CERN, the ATLAS Tier-1 facilities at TRIUMF (Canada), NDGF (Denmark, Norway, Sweden), CC-IN2P3 (France), KIT/GridKA (Germany), INFN-CNAF (Italy), NL-T1 (Netherlands), PIC (Spain), ASGC (Taiwan), RAL (UK) and BNL (USA), the Tier-2 facilities worldwide and large non-WLCG resource providers. Major contributors of computing resources are listed in Ref. [107].

References

- [1] ATLAS Collaboration, *Observation of a new particle in the search for the Standard Model Higgs boson with the ATLAS detector at the LHC*, *Phys. Lett. B* **716** (2012) 1, arXiv: [1207.7214 \[hep-ex\]](#).
- [2] CMS Collaboration, *Observation of a new boson at a mass of 125 GeV with the CMS experiment at the LHC*, *Phys. Lett. B* **716** (2012) 30, arXiv: [1207.7235 \[hep-ex\]](#).
- [3] Y. Golfand and E. Likhtman, *Extension of the Algebra of Poincare Group Generators and Violation of P Invariance*, *JETP Lett.* **13** (1971) 323, [*Pisma Zh. Eksp. Teor. Fiz.* **13** (1971) 452].
- [4] D. Volkov and V. Akulov, *Is the neutrino a goldstone particle?*, *Phys. Lett. B* **46** (1973) 109.
- [5] J. Wess and B. Zumino, *Supergauge transformations in four dimensions*, *Nucl. Phys. B* **70** (1974) 39.
- [6] J. Wess and B. Zumino, *Supergauge invariant extension of quantum electrodynamics*, *Nucl. Phys. B* **78** (1974) 1.
- [7] S. Ferrara and B. Zumino, *Supergauge invariant Yang-Mills theories*, *Nucl. Phys. B* **79** (1974) 413.
- [8] A. Salam and J. Strathdee, *Super-symmetry and non-Abelian gauges*, *Phys. Lett. B* **51** (1974) 353.
- [9] J. A. Aguilar-Saavedra, *Effects of mixing with quark singlets*, *Phys. Rev. D* **67** (2003) 035003, arXiv: [hep-ph/0210112](#), Erratum: *Phys. Rev. D* **69** (2004) 099901.
- [10] S. Bejar, J. Guasch and J. Sola, *Loop induced flavor changing neutral decays of the top quark in a general two Higgs doublet model*, *Nucl. Phys. B* **600** (2001) 21, arXiv: [hep-ph/0011091](#).
- [11] J. Guasch and J. Sola, *FCNC top quark decays: A door to SUSY physics in high luminosity colliders?*, *Nucl. Phys. B* **562** (1999) 3, arXiv: [hep-ph/9906268](#).
- [12] J. J. Cao et al., *SUSY-induced FCNC top-quark processes at the large hadron collider*, *Phys. Rev. D* **75** (2007) 075021, arXiv: [hep-ph/0702264](#).
- [13] G. Eilam, A. Gemintern, T. Han, J. M. Yang and X. Zhang, *Top quark rare decay $t \rightarrow ch$ in R-parity violating SUSY*, *Phys. Lett. B* **510** (2001) 227, arXiv: [hep-ph/0102037](#).
- [14] F. del Aguila and M. J. Bowick, *The possibility of new fermions with $\Delta I = 0$ Mass*, *Nucl. Phys. B* **224** (1983) 107.
- [15] J. A. Aguilar-Saavedra, *Identifying top partners at LHC*, *JHEP* **11** (2009) 030, arXiv: [0907.3155 \[hep-ph\]](#).
- [16] ATLAS Collaboration, *A detailed map of Higgs boson interactions by the ATLAS experiment ten years after the discovery*, *Nature* **607** (2022) 52, arXiv: [2207.00092 \[hep-ex\]](#).
- [17] CMS Collaboration, *A portrait of the Higgs boson by the CMS experiment ten years after the discovery*, *Nature* **607** (2022) 60, arXiv: [2207.00043 \[hep-ex\]](#).

- [18] LHC Higgs Cross Section Working Group (D. de Florian et al.), *Handbook of LHC Higgs Cross Sections: 4. Deciphering the Nature of the Higgs Sector*, 2016, arXiv: [1610.07922 \[hep-ph\]](#).
- [19] ATLAS Collaboration, *Measurement of the properties of Higgs boson production at $\sqrt{s} = 13$ TeV in the $H \rightarrow \gamma\gamma$ channel using 139 fb^{-1} of pp collision data with the ATLAS experiment*, (2022), arXiv: [2207.00348 \[hep-ex\]](#).
- [20] ATLAS Collaboration, *Measurement of the total and differential Higgs boson production cross-sections at $\sqrt{s} = 13$ TeV with the ATLAS detector by combining the $H \rightarrow ZZ^* \rightarrow 4\ell$ and $H \rightarrow \gamma\gamma$ decay channels*, (2022), arXiv: [2207.08615 \[hep-ex\]](#).
- [21] ATLAS Collaboration, *The ATLAS Experiment at the CERN Large Hadron Collider*, [JINST 3 \(2008\) S08003](#).
- [22] ATLAS Collaboration, *ATLAS Insertable B-Layer Technical Design Report*, ATLAS-TDR-19, 2010, URL: <https://cds.cern.ch/record/1291633>, *ATLAS Insertable B-Layer Technical Design Report Addendum*, ATLAS-TDR-19-ADD-1, 2012, URL: <https://cds.cern.ch/record/1451888>.
- [23] B. Abbott et al., *Production and integration of the ATLAS Insertable B-Layer*, [JINST 13 \(2018\) T05008](#), arXiv: [1803.00844 \[physics.ins-det\]](#).
- [24] ATLAS Collaboration, *Performance of the ATLAS trigger system in 2015*, [Eur. Phys. J. C 77 \(2017\) 317](#), arXiv: [1611.09661 \[hep-ex\]](#).
- [25] ATLAS Collaboration, *The ATLAS Collaboration Software and Firmware*, ATL-SOFT-PUB-2021-001, 2021, URL: <https://cds.cern.ch/record/2767187>.
- [26] ATLAS Collaboration, *ATLAS data quality operations and performance for 2015–2018 data-taking*, [JINST 15 \(2020\) P04003](#), arXiv: [1911.04632 \[physics.ins-det\]](#).
- [27] ATLAS Collaboration, *Luminosity determination in pp collisions at $\sqrt{s} = 13$ TeV using the ATLAS detector at the LHC*, ATLAS-CONF-2019-021, 2019, URL: <https://cds.cern.ch/record/2677054>.
- [28] G. Avoni et al., *The new LUCID-2 detector for luminosity measurement and monitoring in ATLAS*, [JINST 13 \(2018\) P07017](#).
- [29] ATLAS Collaboration, *Performance of electron and photon triggers in ATLAS during LHC Run 2*, [Eur. Phys. J. C 80 \(2020\) 47](#), arXiv: [1909.00761 \[hep-ex\]](#).
- [30] K. Hamilton, P. Nason, E. Re and G. Zanderighi, *NNLOPS simulation of Higgs boson production*, [JHEP 10 \(2013\) 222](#), arXiv: [1309.0017 \[hep-ph\]](#).
- [31] P. Nason, *A New method for combining NLO QCD with shower Monte Carlo algorithms*, [JHEP 11 \(2004\) 040](#), arXiv: [hep-ph/0409146](#).
- [32] S. Frixione, P. Nason and C. Oleari, *Matching NLO QCD computations with parton shower simulations: the POWHEG method*, [JHEP 11 \(2007\) 070](#), arXiv: [0709.2092 \[hep-ph\]](#).
- [33] S. Alioli, P. Nason, C. Oleari and E. Re, *A general framework for implementing NLO calculations in shower Monte Carlo programs: the POWHEG BOX*, [JHEP 06 \(2010\) 043](#), arXiv: [1002.2581 \[hep-ph\]](#).

- [34] P. Nason and C. Oleari, *NLO Higgs boson production via vector-boson fusion matched with shower in POWHEG*, *JHEP* **02** (2010) 037, arXiv: [0911.5299 \[hep-ph\]](#).
- [35] K. Mimasu, V. Sanz and C. Williams, *Higher order QCD predictions for associated Higgs production with anomalous couplings to gauge bosons*, *JHEP* **08** (2016) 039, arXiv: [1512.02572 \[hep-ph\]](#).
- [36] J. M. Campbell et al., *NLO Higgs boson production plus one and two jets using the POWHEG BOX, MadGraph4 and MCFM*, *JHEP* **07** (2012) 092, arXiv: [1202.5475 \[hep-ph\]](#).
- [37] G. Luisoni, P. Nason, C. Oleari and F. Tramontano, *$HW^\pm/HZ + 0$ and 1 jet at NLO with the POWHEG BOX interfaced to GoSam and their merging within MinLO*, *JHEP* **10** (2013) 083, arXiv: [1306.2542 \[hep-ph\]](#).
- [38] H. B. Hartanto, B. Jäger, L. Reina and D. Wackerroth, *Higgs boson production in association with top quarks in the POWHEG BOX*, *Phys. Rev. D* **91** (2015) 094003, arXiv: [1501.04498 \[hep-ph\]](#).
- [39] J. Butterworth et al., *PDF4LHC recommendations for LHC Run II*, *J. Phys. G* **43** (2016) 023001, arXiv: [1510.03865 \[hep-ph\]](#).
- [40] T. Sjöstrand, S. Mrenna and P. Z. Skands, *A brief introduction to PYTHIA 8.1*, *Comput. Phys. Commun.* **178** (2008) 852, arXiv: [0710.3820 \[hep-ph\]](#).
- [41] T. Sjöstrand et al., *An introduction to PYTHIA 8.2*, *Comput. Phys. Commun.* **191** (2015) 159, arXiv: [1410.3012 \[hep-ph\]](#).
- [42] ATLAS Collaboration, *Measurement of the Z/γ^* boson transverse momentum distribution in pp collisions at $\sqrt{s} = 7$ TeV with the ATLAS detector*, *JHEP* **09** (2014) 145, arXiv: [1406.3660 \[hep-ex\]](#).
- [43] K. Hamilton, P. Nason and G. Zanderighi, *MINLO: multi-scale improved NLO*, *JHEP* **10** (2012) 155, arXiv: [1206.3572 \[hep-ph\]](#).
- [44] K. Hamilton, P. Nason, C. Oleari and G. Zanderighi, *Merging $H/W/Z + 0$ and 1 jet at NLO with no merging scale: a path to parton shower + NNLO matching*, *JHEP* **05** (2013) 082, arXiv: [1212.4504 \[hep-ph\]](#).
- [45] S. Catani and M. Grazzini, *Next-to-Next-to-Leading-Order Subtraction Formalism in Hadron Collisions and its Application to Higgs-boson Production at the Large Hadron Collider*, *Phys. Rev. Lett.* **98** (2007) 222002, arXiv: [hep-ph/0703012 \[hep-ph\]](#).
- [46] G. Bozzi, S. Catani, D. de Florian and M. Grazzini, *Transverse-momentum resummation and the spectrum of the Higgs boson at the LHC*, *Nucl. Phys. B* **737** (2006) 73, arXiv: [hep-ph/0508068 \[hep-ph\]](#).
- [47] D. de Florian, G. Ferrera, M. Grazzini and D. Tommasini, *Transverse-momentum resummation: Higgs boson production at the Tevatron and the LHC*, *JHEP* **11** (2011) 064, arXiv: [1109.2109 \[hep-ph\]](#).
- [48] S. Frixione, G. Ridolfi and P. Nason, *A positive-weight next-to-leading-order Monte Carlo for heavy flavour hadroproduction*, *JHEP* **09** (2007) 126, arXiv: [0707.3088 \[hep-ph\]](#).
- [49] The NNPDF Collaboration, R. D. Ball et al., *Parton distributions for the LHC run II*, *JHEP* **04** (2015) 040, arXiv: [1410.8849 \[hep-ph\]](#).

- [50] ATLAS Collaboration, *ATLAS Pythia 8 tunes to 7 TeV data*, ATL-PHYS-PUB-2014-021, 2014, URL: <https://cds.cern.ch/record/1966419>.
- [51] D. J. Lange, *The EvtGen particle decay simulation package*, *Nucl. Instrum. Meth. A* **462** (2001) 152.
- [52] E. Bothmann et al., *Event generation with Sherpa 2.2*, *SciPost Phys.* **7** (2019) 034, arXiv: [1905.09127](https://arxiv.org/abs/1905.09127) [[hep-ph](#)].
- [53] T. Gleisberg and S. Höche, *Comix, a new matrix element generator*, *JHEP* **12** (2008) 039, arXiv: [0808.3674](https://arxiv.org/abs/0808.3674) [[hep-ph](#)].
- [54] F. Buccioni et al., *OpenLoops 2*, *Eur. Phys. J. C* **79** (2019) 866, arXiv: [1907.13071](https://arxiv.org/abs/1907.13071) [[hep-ph](#)].
- [55] F. Cascioli, P. Maierhöfer and S. Pozzorini, *Scattering Amplitudes with Open Loops*, *Phys. Rev. Lett.* **108** (2012) 111601, arXiv: [1111.5206](https://arxiv.org/abs/1111.5206) [[hep-ph](#)].
- [56] A. Denner, S. Dittmaier and L. Hofer, *COLLIER: A fortran-based complex one-loop library in extended regularizations*, *Comput. Phys. Commun.* **212** (2017) 220, arXiv: [1604.06792](https://arxiv.org/abs/1604.06792) [[hep-ph](#)].
- [57] S. Schumann and F. Krauss, *A Parton shower algorithm based on Catani-Seymour dipole factorisation*, *JHEP* **03** (2008) 038, arXiv: [0709.1027](https://arxiv.org/abs/0709.1027) [[hep-ph](#)].
- [58] S. Höche, F. Krauss, M. Schönherr and F. Siegert, *A critical appraisal of NLO+PS matching methods*, *JHEP* **09** (2012) 049, arXiv: [1111.1220](https://arxiv.org/abs/1111.1220) [[hep-ph](#)].
- [59] S. Höche, F. Krauss, M. Schonherr and F. Siegert, *QCD matrix elements + parton showers: The NLO case*, *JHEP* **04** (2013) 027, arXiv: [1207.5030](https://arxiv.org/abs/1207.5030) [[hep-ph](#)].
- [60] S. Catani, F. Krauss, B. R. Webber and R. Kuhn, *QCD Matrix Elements + Parton Showers*, *JHEP* **11** (2001) 063, arXiv: [hep-ph/0109231](https://arxiv.org/abs/hep-ph/0109231).
- [61] S. Höche, F. Krauss, S. Schumann and F. Siegert, *QCD matrix elements and truncated showers*, *JHEP* **05** (2009) 053, arXiv: [0903.1219](https://arxiv.org/abs/0903.1219) [[hep-ph](#)].
- [62] F. Siegert, *A practical guide to event generation for prompt photon production with Sherpa*, *J. Phys. G* **44** (2017) 044007, arXiv: [1611.07226](https://arxiv.org/abs/1611.07226) [[hep-ph](#)].
- [63] S. Frixione, *Isolated photons in perturbative QCD*, *Phys. Lett. B* **429** (1998) 369, arXiv: [hep-ph/9801442](https://arxiv.org/abs/hep-ph/9801442).
- [64] NNPDF Collaboration, R. D. Ball et al., *Parton distributions with LHC data*, *Nucl. Phys. B* **867** (2013) 244, arXiv: [1207.1303](https://arxiv.org/abs/1207.1303) [[hep-ph](#)].
- [65] N. Arkani-Hamed, A. G. Cohen, E. Katz and A. E. Nelson, *The Littlest Higgs*, *JHEP* **07** (2002) 034, arXiv: [hep-ph/0206021](https://arxiv.org/abs/hep-ph/0206021).
- [66] K. Agashe, R. Contino and A. Pomarol, *The minimal composite Higgs model*, *Nucl. Phys. B* **719** (2005) 165, arXiv: [hep-ph/0412089](https://arxiv.org/abs/hep-ph/0412089).
- [67] L. Randall and R. Sundrum, *An Alternative to Compactification*, *Phys. Rev. Lett.* **83** (1999) 4690, arXiv: [hep-th/9906064](https://arxiv.org/abs/hep-th/9906064).
- [68] J. Alwall et al., *The automated computation of tree-level and next-to-leading order differential cross sections, and their matching to parton shower simulations*, *JHEP* **07** (2014) 079, arXiv: [1405.0301](https://arxiv.org/abs/1405.0301) [[hep-ph](#)].

- [69] ATLAS Collaboration, *Search for direct production of electroweakinos in final states with missing transverse momentum and a Higgs boson decaying into photons in pp collisions at $\sqrt{s} = 13$ TeV with the ATLAS detector*, [JHEP **10** \(2020\) 005](#), arXiv: [2004.10894 \[hep-ex\]](#).
- [70] ATLAS Collaboration, *Search for trilepton resonances from chargino and neutralino pair production in $\sqrt{s} = 13$ TeV pp collisions with the ATLAS detector*, [Phys. Rev. D **103** \(2020\) 112003](#), arXiv: [2011.10543 \[hep-ex\]](#).
- [71] ATLAS Collaboration, *Search for top squarks in events with a Higgs or Z boson using 139fb^{-1} of pp collision data at $\sqrt{s} = 13$ TeV with the ATLAS detector*, [Eur. Phys. J. C **80** \(2020\) 1080](#), arXiv: [2006.05880 \[hep-ex\]](#).
- [72] ATLAS Collaboration, *Search for bottom-squark pair production with the ATLAS detector in final states containing Higgs bosons, b-jets and missing transverse momentum*, [JHEP **12** \(2019\) 060](#), arXiv: [1908.03122 \[hep-ex\]](#).
- [73] ATLAS Collaboration, *Search for Heavy Resonances Decaying into a Photon and a Hadronically Decaying Higgs Boson in pp Collisions at $\sqrt{s} = 13$ TeV with the ATLAS Detector*, [Phys. Rev. Lett. **125** \(2020\) 251802](#), arXiv: [2008.05928 \[hep-ex\]](#).
- [74] ATLAS Collaboration, *Search for top quark decays $t \rightarrow qH$, with $H \rightarrow \gamma\gamma$, in $\sqrt{s} = 13$ TeV pp collisions using the ATLAS detector*, [JHEP **10** \(2017\) 129](#), arXiv: [1707.01404 \[hep-ex\]](#).
- [75] ATLAS Collaboration, *The Pythia 8 A3 tune description of ATLAS minimum bias and inelastic measurements incorporating the Donnachie–Landshoff diffractive model*, ATL-PHYS-PUB-2016-017, 2016, URL: <https://cds.cern.ch/record/2206965>.
- [76] S. Agostinelli et al., *GEANT4 – a simulation toolkit*, [Nucl. Instrum. Meth. A **506** \(2003\) 250](#).
- [77] ATLAS Collaboration, *The ATLAS Simulation Infrastructure*, [Eur. Phys. J. C **70** \(2010\) 823](#), arXiv: [1005.4568 \[physics.ins-det\]](#).
- [78] ATLAS Collaboration, *Measurement of Higgs boson production in the diphoton decay channel in pp collisions at center-of-mass energies of 7 and 8 TeV with the ATLAS detector*, [Phys. Rev. D **90** \(2014\) 112015](#), arXiv: [1408.7084 \[hep-ex\]](#).
- [79] ATLAS Collaboration, *Electron and photon performance measurements with the ATLAS detector using the 2015–2017 LHC proton–proton collision data*, [JINST **14** \(2019\) P12006](#), arXiv: [1908.00005 \[hep-ex\]](#).
- [80] M. Cacciari, G. P. Salam and G. Soyez, *The catchment area of jets*, [JHEP **04** \(2008\) 005](#), arXiv: [0802.1188 \[hep-ph\]](#).
- [81] M. Cacciari, G. P. Salam and S. Sapeta, *On the characterisation of the underlying event*, [JHEP **04** \(2010\) 065](#), arXiv: [0912.4926 \[hep-ph\]](#).
- [82] ATLAS Collaboration, *Measurement of the photon identification efficiencies with the ATLAS detector using LHC Run-1 data*, [Eur. Phys. J. C **76** \(2016\) 666](#), arXiv: [1606.01813 \[hep-ex\]](#).
- [83] ATLAS Collaboration, *Measurement of the inclusive isolated prompt photon cross section in pp collisions at $\sqrt{s} = 7$ TeV with the ATLAS detector*, [Phys. Rev. D **83** \(2011\) 052005](#), arXiv: [1012.4389 \[hep-ex\]](#).
- [84] ATLAS Collaboration, *Muon reconstruction performance of the ATLAS detector in proton–proton collision data at $\sqrt{s} = 13$ TeV*, [Eur. Phys. J. C **76** \(2016\) 292](#), arXiv: [1603.05598 \[hep-ex\]](#).

- [85] ATLAS Collaboration, *Jet reconstruction and performance using particle flow with the ATLAS Detector*, [Eur. Phys. J. C **77** \(2017\) 466](#), arXiv: [1703.10485 \[hep-ex\]](#).
- [86] M. Cacciari, G. P. Salam and G. Soyez, *The anti- k_t jet clustering algorithm*, [JHEP **04** \(2008\) 063](#), arXiv: [0802.1189 \[hep-ph\]](#).
- [87] M. Cacciari, G. P. Salam and G. Soyez, *FastJet user manual*, [Eur. Phys. J. C **72** \(2012\) 1896](#), arXiv: [1111.6097 \[hep-ph\]](#).
- [88] ATLAS Collaboration, *Topological cell clustering in the ATLAS calorimeters and its performance in LHC Run 1*, [Eur. Phys. J. C **77** \(2017\) 490](#), arXiv: [1603.02934 \[hep-ex\]](#).
- [89] ATLAS Collaboration, *Performance of pile-up mitigation techniques for jets in pp collisions at $\sqrt{s} = 8$ TeV using the ATLAS detector*, [Eur. Phys. J. C **76** \(2016\) 581](#), arXiv: [1510.03823 \[hep-ex\]](#).
- [90] ATLAS Collaboration, *Forward jet vertex tagging using the particle flow algorithm*, ATL-PHYS-PUB-2019-026, 2019, URL: <https://cds.cern.ch/record/2683100>.
- [91] ATLAS Collaboration, *ATLAS b-jet identification performance and efficiency measurement with $t\bar{t}$ events in pp collisions at $\sqrt{s} = 13$ TeV*, [Eur. Phys. J. C **79** \(2019\) 970](#), arXiv: [1907.05120 \[hep-ex\]](#).
- [92] ATLAS Collaboration, *Identification of hadronic tau lepton decays using neural networks in the ATLAS experiment*, ATL-PHYS-PUB-2019-033, 2019, URL: <https://cds.cern.ch/record/2688062>.
- [93] ATLAS Collaboration, *Performance of missing transverse momentum reconstruction with the ATLAS detector using proton-proton collisions at $\sqrt{s} = 13$ TeV*, [Eur. Phys. J. C **78** \(2018\) 903](#), arXiv: [1802.08168 \[hep-ex\]](#).
- [94] ATLAS Collaboration, *Study of the CP properties of the interaction of the Higgs boson with top quarks using top quark associated production of the Higgs boson and its decay into two photons with the ATLAS detector at the LHC*, [Phys. Rev. Lett. **125** \(2020\) 061802](#), arXiv: [2004.04545 \[hep-ex\]](#).
- [95] ATLAS Collaboration, *Measurements of the Higgs boson inclusive and differential fiducial cross-sections in the diphoton decay channel with pp collisions at $\sqrt{s} = 13$ TeV with the ATLAS detector*, [JHEP **08** \(2022\) 027](#), arXiv: [2202.00487 \[hep-ex\]](#).
- [96] M. Oreglia, *A Study of the Reactions $\psi' \rightarrow \gamma\gamma\psi$* , thesis [SLAC-0236](#) (1980).
- [97] ATLAS Collaboration, *Search for Scalar Diphoton Resonances in the Mass Range 65–600 GeV with the ATLAS Detector in pp Collision Data at $\sqrt{s} = 8$ TeV*, [Phys. Rev. Lett. **113** \(2014\) 171801](#), arXiv: [1407.6583 \[hep-ex\]](#).
- [98] ATLAS Collaboration, *Measurements of Higgs boson properties in the diphoton decay channel with 36fb^{-1} of pp collision data at $\sqrt{s} = 13$ TeV with the ATLAS detector*, [Phys. Rev. D **98** \(2018\) 052005](#), arXiv: [1802.04146 \[hep-ex\]](#).
- [99] ATLAS and CMS Collaborations, *Combined Measurement of the Higgs Boson Mass in pp Collisions at $\sqrt{s} = 7$ and 8 TeV with the ATLAS and CMS Experiments*, [Phys. Rev. Lett. **114** \(2015\) 191803](#), arXiv: [1503.07589 \[hep-ex\]](#).

- [100] ATLAS Collaboration, *Muon reconstruction and identification efficiency in ATLAS using the full Run 2 pp collision data set at $\sqrt{s} = 13$ TeV*, *Eur. Phys. J. C* **81** (2021) 578, arXiv: [2012.00578](https://arxiv.org/abs/2012.00578) [hep-ex].
- [101] ATLAS Collaboration, *Jet energy scale and resolution measured in proton-proton collisions at $\sqrt{s} = 13$ TeV with the ATLAS detector*, (2020), arXiv: [2007.02645](https://arxiv.org/abs/2007.02645) [hep-ex].
- [102] ATLAS Collaboration, *Measurement of the tau lepton reconstruction and identification performance in the ATLAS experiment using pp collisions at $\sqrt{s} = 13$ TeV*, ATLAS-CONF-2017-029, 2017, URL: <https://cds.cern.ch/record/2261772>.
- [103] ATLAS Collaboration, *Measurement of the Inelastic Proton-Proton Cross Section at $\sqrt{s} = 13$ TeV with the ATLAS Detector at the LHC*, *Phys. Rev. Lett.* **117** (2016) 182002, arXiv: [1606.02625](https://arxiv.org/abs/1606.02625) [hep-ex].
- [104] ATLAS Collaboration, *Formulae for Estimating Significance*, ATL-PHYS-PUB-2020-025, 2020, URL: <https://cds.cern.ch/record/2736148>.
- [105] A. L. Read, *Presentation of search results: the CL_s technique*, *J. Phys. G* **28** (2002) 2693.
- [106] ATLAS Collaboration, *Evaluating statistical uncertainties and correlations using the bootstrap method*, ATL-PHYS-PUB-2021-011, 2021, URL: <https://cds.cern.ch/record/2759945>.
- [107] ATLAS Collaboration, *ATLAS Computing Acknowledgements*, ATL-SOFT-PUB-2023-001, 2023, URL: <https://cds.cern.ch/record/2869272>.

The ATLAS Collaboration

G. Aad ¹⁰², B. Abbott ¹²⁰, K. Abeling ⁵⁵, S.H. Abidi ²⁹, A. Aboulhorma ^{35e},
H. Abramowicz ¹⁵¹, H. Abreu ¹⁵⁰, Y. Abulaiti ¹¹⁷, A.C. Abusleme Hoffman ^{137a},
B.S. Acharya ^{69a,69b,p}, C. Adam Bourdarios ⁴, L. Adamczyk ^{85a}, L. Adamek ¹⁵⁵,
S.V. Addepalli ²⁶, J. Adelman ¹¹⁵, A. Adiguzel ^{21c}, S. Adorni ⁵⁶, T. Adye ¹³⁴, A.A. Affolder ¹³⁶,
Y. Afik ³⁶, M.N. Agaras ¹³, J. Agarwala ^{73a,73b}, A. Aggarwal ¹⁰⁰, C. Agheorghiesei ^{27c},
J.A. Aguilar-Saavedra ^{130f}, A. Ahmad ³⁶, F. Ahmadov ^{38,aa}, W.S. Ahmed ¹⁰⁴, S. Ahuja ⁹⁵,
X. Ai ⁴⁸, G. Aielli ^{76a,76b}, M. Ait Tamlihat ^{35e}, B. Aitbenkikh ^{35a}, I. Aizenberg ¹⁶⁹,
M. Akbiyik ¹⁰⁰, T.P.A. Åkesson ⁹⁸, A.V. Akimov ³⁷, K. Al Houry ⁴¹, G.L. Alberghi ^{23b},
J. Albert ¹⁶⁵, P. Albicocco ⁵³, S. Alderweireldt ⁵², M. Aleksa ³⁶, I.N. Aleksandrov ³⁸,
C. Alexa ^{27b}, T. Alexopoulos ¹⁰, A. Alfonsi ¹¹⁴, F. Alfonsi ^{23b}, M. Alhroob ¹²⁰, B. Ali ¹³²,
S. Ali ¹⁴⁸, M. Aliev ³⁷, G. Alimonti ^{71a}, W. Alkakhki ⁵⁵, C. Allaire ⁶⁶, B.M.M. Allbrooke ¹⁴⁶,
C.A. Allendes Flores ^{137f}, P.P. Allport ²⁰, A. Aloisio ^{72a,72b}, F. Alonso ⁹⁰, C. Alpigliani ¹³⁸,
M. Alvarez Estevez ⁹⁹, A. Alvarez Fernandez ¹⁰⁰, M.G. Alviggi ^{72a,72b}, M. Aly ¹⁰¹,
Y. Amaral Coutinho ^{82b}, A. Ambler ¹⁰⁴, C. Amelung ³⁶, M. Amerl ¹⁰¹, C.G. Ames ¹⁰⁹,
D. Amidei ¹⁰⁶, S.P. Amor Dos Santos ^{130a}, K.R. Amos ¹⁶³, V. Ananiev ¹²⁵, C. Anastopoulos ¹³⁹,
T. Andeen ¹¹, J.K. Anders ³⁶, S.Y. Andrean ^{47a,47b}, A. Andreazza ^{71a,71b}, S. Angelidakis ⁹,
A. Angerami ^{41,ad}, A.V. Anisenkov ³⁷, A. Annovi ^{74a}, C. Antel ⁵⁶, M.T. Anthony ¹³⁹,
E. Antipov ¹⁴⁵, M. Antonelli ⁵³, D.J.A. Antrim ^{17a}, F. Anulli ^{75a}, M. Aoki ⁸³, T. Aoki ¹⁵³,
J.A. Aparisi Pozo ¹⁶³, M.A. Aparo ¹⁴⁶, L. Aperio Bella ⁴⁸, C. Appelt ¹⁸, N. Aranzabal ³⁶,
V. Araujo Ferraz ^{82a}, C. Arcangeletti ⁵³, A.T.H. Arce ⁵¹, E. Arena ⁹², J-F. Arguin ¹⁰⁸,
S. Argyropoulos ⁵⁴, J.-H. Arling ⁴⁸, A.J. Armbruster ³⁶, O. Arnaez ⁴, H. Arnold ¹¹⁴,
Z.P. Arrubarrena Tame ¹⁰⁹, G. Artoni ^{75a,75b}, H. Asada ¹¹¹, K. Asai ¹¹⁸, S. Asai ¹⁵³,
N.A. Asbah ⁶¹, J. Assahsah ^{35d}, K. Assamagan ²⁹, R. Astalos ^{28a}, R.J. Atkin ^{33a}, M. Atkinson ¹⁶²,
N.B. Atlay ¹⁸, H. Atmani ^{62b}, P.A. Atlasiddha ¹⁰⁶, K. Augsten ¹³², S. Auricchio ^{72a,72b},
A.D. Auriol ²⁰, V.A. Austrup ¹⁷¹, G. Avner ¹⁵⁰, G. Avolio ³⁶, K. Axiotis ⁵⁶, G. Azuelos ^{108,ah},
D. Babal ^{28a}, H. Bachacou ¹³⁵, K. Bachas ^{152,s}, A. Bachi ³⁴, F. Backman ^{47a,47b}, A. Badea ⁶¹,
P. Bagnaia ^{75a,75b}, M. Bahmani ¹⁸, A.J. Bailey ¹⁶³, V.R. Bailey ¹⁶², J.T. Baines ¹³⁴,
C. Bakalis ¹⁰, O.K. Baker ¹⁷², E. Bakos ¹⁵, D. Bakshi Gupta ⁸, R. Balasubramanian ¹¹⁴,
E.M. Baldin ³⁷, P. Balek ¹³³, E. Ballabene ^{71a,71b}, F. Balli ¹³⁵, L.M. Baltes ^{63a}, W.K. Balunas ³²,
J. Balz ¹⁰⁰, E. Banas ⁸⁶, M. Bandieramonte ¹²⁹, A. Bandyopadhyay ²⁴, S. Bansal ²⁴,
L. Barak ¹⁵¹, E.L. Barberio ¹⁰⁵, D. Barberis ^{57b,57a}, M. Barbero ¹⁰², G. Barbour ⁹⁶,
K.N. Barends ^{33a}, T. Barillari ¹¹⁰, M-S. Barisits ³⁶, T. Barklow ¹⁴³, P. Baron ¹²²,
D.A. Baron Moreno ¹⁰¹, A. Baroncelli ^{62a}, G. Barone ²⁹, A.J. Barr ¹²⁶,
L. Barranco Navarro ^{47a,47b}, F. Barreiro ⁹⁹, J. Barreiro Guimarães da Costa ^{14a}, U. Barron ¹⁵¹,
M.G. Barros Teixeira ^{130a}, S. Barsov ³⁷, F. Bartels ^{63a}, R. Bartoldus ¹⁴³, A.E. Barton ⁹¹,
P. Bartos ^{28a}, A. Basan ¹⁰⁰, M. Baselga ⁴⁹, I. Bashta ^{77a,77b}, A. Bassalat ^{66,b}, M.J. Basso ¹⁵⁵,
C.R. Basson ¹⁰¹, R.L. Bates ⁵⁹, S. Batlamous ^{35e}, J.R. Batley ³², B. Batool ¹⁴¹, M. Battaglia ¹³⁶,
D. Battulga ¹⁸, M. Bause ^{75a,75b}, P. Bauer ²⁴, J.B. Beacham ⁵¹, T. Beau ¹²⁷,
P.H. Beauchemin ¹⁵⁸, F. Becherer ⁵⁴, P. Bechtel ²⁴, H.P. Beck ^{19,r}, K. Becker ¹⁶⁷,
A.J. Beddall ^{21d}, V.A. Bednyakov ³⁸, C.P. Bee ¹⁴⁵, L.J. Beemster ¹⁵, T.A. Beermann ³⁶,
M. Begalli ^{82d}, M. Begel ²⁹, A. Behera ¹⁴⁵, J.K. Behr ⁴⁸, C. Beirao Da Cruz E Silva ³⁶,
J.F. Beirer ^{55,36}, F. Beisiegel ²⁴, M. Belfkir ¹⁵⁹, G. Bella ¹⁵¹, L. Bellagamba ^{23b}, A. Bellerive ³⁴,
P. Bellos ²⁰, K. Beloborodov ³⁷, N.L. Belyaev ³⁷, D. Bencheekroun ^{35a}, F. Bendebba ^{35a},
Y. Benhammou ¹⁵¹, M. Benoit ²⁹, J.R. Bensinger ²⁶, S. Bentvelsen ¹¹⁴, L. Beresford ³⁶,

M. Beretta [ID](#)⁵³, E. Bergeaas Kuutmann [ID](#)¹⁶¹, N. Berger [ID](#)⁴, B. Bergmann [ID](#)¹³², J. Beringer [ID](#)^{17a},
S. Berlendis [ID](#)⁷, G. Bernardi [ID](#)⁵, C. Bernius [ID](#)¹⁴³, F.U. Bernlochner [ID](#)²⁴, T. Berry [ID](#)⁹⁵, P. Berta [ID](#)¹³³,
A. Berthold [ID](#)⁵⁰, I.A. Bertram [ID](#)⁹¹, S. Bethke [ID](#)¹¹⁰, A. Betti [ID](#)^{75a,75b}, A.J. Bevan [ID](#)⁹⁴, M. Bhamjee [ID](#)^{33c},
S. Bhatta [ID](#)¹⁴⁵, D.S. Bhattacharya [ID](#)¹⁶⁶, P. Bhattarai [ID](#)²⁶, V.S. Bhopatkar [ID](#)¹²¹, R. Bi [ID](#)^{29,ak},
R.M. Bianchi [ID](#)¹²⁹, O. Biebel [ID](#)¹⁰⁹, R. Bielski [ID](#)¹²³, M. Biglietti [ID](#)^{77a}, T.R.V. Billoud [ID](#)¹³², M. Bindi [ID](#)⁵⁵,
A. Bingul [ID](#)^{21b}, C. Bini [ID](#)^{75a,75b}, A. Biondini [ID](#)⁹², C.J. Birch-sykes [ID](#)¹⁰¹, G.A. Bird [ID](#)^{20,134},
M. Birman [ID](#)¹⁶⁹, M. Biroš [ID](#)¹³³, T. Bisanz [ID](#)³⁶, E. Bisceglie [ID](#)^{43b,43a}, D. Biswas [ID](#)¹⁷⁰, A. Bitadze [ID](#)¹⁰¹,
K. Bjørke [ID](#)¹²⁵, I. Bloch [ID](#)⁴⁸, C. Blocker [ID](#)²⁶, A. Blue [ID](#)⁵⁹, U. Blumenschein [ID](#)⁹⁴, J. Blumenthal [ID](#)¹⁰⁰,
G.J. Bobbink [ID](#)¹¹⁴, V.S. Bobrovnikov [ID](#)³⁷, M. Boehler [ID](#)⁵⁴, D. Bogavac [ID](#)³⁶, A.G. Bogdanchikov [ID](#)³⁷,
C. Bohm [ID](#)^{47a}, V. Boisvert [ID](#)⁹⁵, P. Bokan [ID](#)⁴⁸, T. Bold [ID](#)^{85a}, M. Bomben [ID](#)⁵, M. Bona [ID](#)⁹⁴,
M. Boonekamp [ID](#)¹³⁵, C.D. Booth [ID](#)⁹⁵, A.G. Borbély [ID](#)⁵⁹, H.M. Borecka-Bielska [ID](#)¹⁰⁸, L.S. Borgna [ID](#)⁹⁶,
G. Borissov [ID](#)⁹¹, D. Bortoletto [ID](#)¹²⁶, D. Boscherini [ID](#)^{23b}, M. Bosman [ID](#)¹³, J.D. Bossio Sola [ID](#)³⁶,
K. Bouaouda [ID](#)^{35a}, N. Bouchhar [ID](#)¹⁶³, J. Boudreau [ID](#)¹²⁹, E.V. Bouhova-Thacker [ID](#)⁹¹, D. Boumediene [ID](#)⁴⁰,
R. Bouquet [ID](#)⁵, A. Boveia [ID](#)¹¹⁹, J. Boyd [ID](#)³⁶, D. Boye [ID](#)²⁹, I.R. Boyko [ID](#)³⁸, J. Bracinik [ID](#)²⁰,
N. Brahimi [ID](#)^{62d}, G. Brandt [ID](#)¹⁷¹, O. Brandt [ID](#)³², F. Braren [ID](#)⁴⁸, B. Brau [ID](#)¹⁰³, J.E. Brau [ID](#)¹²³,
K. Brendlinger [ID](#)⁴⁸, R. Brenner [ID](#)¹⁶⁹, L. Brenner [ID](#)¹¹⁴, R. Brenner [ID](#)¹⁶¹, S. Bressler [ID](#)¹⁶⁹, D. Britton [ID](#)⁵⁹,
D. Britzger [ID](#)¹¹⁰, I. Brock [ID](#)²⁴, G. Brooijmans [ID](#)⁴¹, W.K. Brooks [ID](#)^{137f}, E. Brost [ID](#)²⁹, L.M. Brown [ID](#)¹⁶⁵,
T.L. Bruckler [ID](#)¹²⁶, P.A. Bruckman de Renstrom [ID](#)⁸⁶, B. Brüers [ID](#)⁴⁸, D. Bruncko [ID](#)^{28b,*}, A. Bruni [ID](#)^{23b},
G. Bruni [ID](#)^{23b}, M. Bruschi [ID](#)^{23b}, N. Bruscino [ID](#)^{75a,75b}, T. Buanes [ID](#)¹⁶, Q. Buat [ID](#)¹³⁸, A.G. Buckley [ID](#)⁵⁹,
I.A. Budagov [ID](#)^{38,*}, M.K. Bugge [ID](#)¹²⁵, O. Bulekov [ID](#)³⁷, B.A. Bullard [ID](#)¹⁴³, S. Burdin [ID](#)⁹²,
C.D. Burgard [ID](#)⁴⁹, A.M. Burger [ID](#)⁴⁰, B. Burghgrave [ID](#)⁸, J.T.P. Burr [ID](#)³², C.D. Burton [ID](#)¹¹,
J.C. Burzynski [ID](#)¹⁴², E.L. Busch [ID](#)⁴¹, V. Büscher [ID](#)¹⁰⁰, P.J. Bussey [ID](#)⁵⁹, J.M. Butler [ID](#)²⁵, C.M. Buttar [ID](#)⁵⁹,
J.M. Butterworth [ID](#)⁹⁶, W. Buttinger [ID](#)¹³⁴, C.J. Buxo Vazquez [ID](#)¹⁰⁷, A.R. Buzykaev [ID](#)³⁷, G. Cabras [ID](#)^{23b},
S. Cabrera Urbán [ID](#)¹⁶³, D. Caforio [ID](#)⁵⁸, H. Cai [ID](#)¹²⁹, Y. Cai [ID](#)^{14a,14d}, V.M.M. Cairo [ID](#)³⁶, O. Cakir [ID](#)^{3a},
N. Calace [ID](#)³⁶, P. Calafiura [ID](#)^{17a}, G. Calderini [ID](#)¹²⁷, P. Calfayan [ID](#)⁶⁸, G. Callea [ID](#)⁵⁹, L.P. Caloba [ID](#)^{82b},
D. Calvet [ID](#)⁴⁰, S. Calvet [ID](#)⁴⁰, T.P. Calvet [ID](#)¹⁰², M. Calvetti [ID](#)^{74a,74b}, R. Camacho Toro [ID](#)¹²⁷,
S. Camarda [ID](#)³⁶, D. Camarero Munoz [ID](#)²⁶, P. Camarri [ID](#)^{76a,76b}, M.T. Camerlingo [ID](#)^{72a,72b},
D. Cameron [ID](#)¹²⁵, C. Camincher [ID](#)¹⁶⁵, M. Campanelli [ID](#)⁹⁶, A. Camplani [ID](#)⁴², V. Canale [ID](#)^{72a,72b},
A. Canesse [ID](#)¹⁰⁴, M. Cano Bret [ID](#)⁸⁰, J. Cantero [ID](#)¹⁶³, Y. Cao [ID](#)¹⁶², F. Capocasa [ID](#)²⁶, M. Capua [ID](#)^{43b,43a},
A. Carbone [ID](#)^{71a,71b}, R. Cardarelli [ID](#)^{76a}, J.C.J. Cardenas [ID](#)⁸, F. Cardillo [ID](#)¹⁶³, T. Carli [ID](#)³⁶,
G. Carlino [ID](#)^{72a}, J.I. Carlotto [ID](#)¹³, B.T. Carlson [ID](#)^{129,t}, E.M. Carlson [ID](#)^{165,156a}, L. Carminati [ID](#)^{71a,71b},
M. Carnesale [ID](#)^{75a,75b}, S. Caron [ID](#)¹¹³, E. Carquin [ID](#)^{137f}, S. Carrá [ID](#)^{71a,71b}, G. Carratta [ID](#)^{23b,23a},
F. Carrio Argos [ID](#)^{33g}, J.W.S. Carter [ID](#)¹⁵⁵, T.M. Carter [ID](#)⁵², M.P. Casado [ID](#)^{13,j}, A.F. Casha [ID](#)¹⁵⁵,
M. Caspar [ID](#)⁴⁸, E.G. Castiglia [ID](#)¹⁷², F.L. Castillo [ID](#)^{63a}, L. Castillo Garcia [ID](#)¹³, V. Castillo Gimenez [ID](#)¹⁶³,
N.F. Castro [ID](#)^{130a,130e}, A. Catinaccio [ID](#)³⁶, J.R. Catmore [ID](#)¹²⁵, V. Cavaliere [ID](#)²⁹, N. Cavalli [ID](#)^{23b,23a},
V. Cavasinni [ID](#)^{74a,74b}, E. Celebi [ID](#)^{21a}, F. Celli [ID](#)¹²⁶, M.S. Centonze [ID](#)^{70a,70b}, K. Cerny [ID](#)¹²²,
A.S. Cerqueira [ID](#)^{82a}, A. Cerri [ID](#)¹⁴⁶, L. Cerrito [ID](#)^{76a,76b}, F. Cerutti [ID](#)^{17a}, A. Cervelli [ID](#)^{23b}, G. Cesarini [ID](#)⁵³,
S.A. Cetin [ID](#)^{21d}, Z. Chadi [ID](#)^{35a}, D. Chakraborty [ID](#)¹¹⁵, M. Chala [ID](#)^{130f}, J. Chan [ID](#)¹⁷⁰, W.Y. Chan [ID](#)¹⁵³,
J.D. Chapman [ID](#)³², B. Chargeishvili [ID](#)^{149b}, D.G. Charlton [ID](#)²⁰, T.P. Charman [ID](#)⁹⁴, M. Chatterjee [ID](#)¹⁹,
S. Chekanov [ID](#)⁶, S.V. Chekulaev [ID](#)^{156a}, G.A. Chelkov [ID](#)^{38,a}, A. Chen [ID](#)¹⁰⁶, B. Chen [ID](#)¹⁵¹, B. Chen [ID](#)¹⁶⁵,
H. Chen [ID](#)^{14c}, H. Chen [ID](#)²⁹, J. Chen [ID](#)^{62c}, J. Chen [ID](#)¹⁴², S. Chen [ID](#)¹⁵³, S.J. Chen [ID](#)^{14c}, X. Chen [ID](#)^{62c},
X. Chen [ID](#)^{14b,ag}, Y. Chen [ID](#)^{62a}, C.L. Cheng [ID](#)¹⁷⁰, H.C. Cheng [ID](#)^{64a}, S. Cheong [ID](#)¹⁴³, A. Cheplakov [ID](#)³⁸,
E. Cheremushkina [ID](#)⁴⁸, E. Cherepanova [ID](#)¹¹⁴, R. Cherkaoui El Moursli [ID](#)^{35e}, E. Cheu [ID](#)⁷, K. Cheung [ID](#)⁶⁵,
L. Chevalier [ID](#)¹³⁵, V. Chiarella [ID](#)⁵³, G. Chiarelli [ID](#)^{74a}, N. Chiedde [ID](#)¹⁰², G. Chiodini [ID](#)^{70a},
A.S. Chisholm [ID](#)²⁰, A. Chitan [ID](#)^{27b}, M. Chitishvili [ID](#)¹⁶³, M.V. Chizhov [ID](#)³⁸, K. Choi [ID](#)¹¹,
A.R. Chomont [ID](#)^{75a,75b}, Y. Chou [ID](#)¹⁰³, E.Y.S. Chow [ID](#)¹¹⁴, T. Chowdhury [ID](#)^{33g}, L.D. Christopher [ID](#)^{33g},
K.L. Chu [ID](#)^{64a}, M.C. Chu [ID](#)^{64a}, X. Chu [ID](#)^{14a,14d}, J. Chudoba [ID](#)¹³¹, J.J. Chwastowski [ID](#)⁸⁶, D. Cieri [ID](#)¹¹⁰,

K.M. Ciesla ^{85a}, V. Cindro ⁹³, A. Ciocio ^{17a}, F. Cirotto ^{72a,72b}, Z.H. Citron ^{169,m},
 M. Citterio ^{71a}, D.A. Ciubotaru ^{27b}, B.M. Ciungu ¹⁵⁵, A. Clark ⁵⁶, P.J. Clark ⁵²,
 J.M. Clavijo Columbie ⁴⁸, S.E. Clawson ¹⁰¹, C. Clement ^{47a,47b}, J. Clercx ⁴⁸, L. Clissa ^{23b,23a},
 Y. Coadou ¹⁰², M. Cobal ^{69a,69c}, A. Coccaro ^{57b}, R.F. Coelho Barrue ^{130a},
 R. Coelho Lopes De Sa ¹⁰³, S. Coelli ^{71a}, H. Cohen ¹⁵¹, A.E.C. Coimbra ^{71a,71b}, B. Cole ⁴¹,
 J. Collot ⁶⁰, P. Conde Muiño ^{130a,130g}, M.P. Connell ^{33c}, S.H. Connell ^{33c}, I.A. Connelly ⁵⁹,
 E.I. Conroy ¹²⁶, F. Conventi ^{72a,ai}, H.G. Cooke ²⁰, A.M. Cooper-Sarkar ¹²⁶, F. Cormier ¹⁶⁴,
 L.D. Corpe ³⁶, M. Corradi ^{75a,75b}, F. Corriveau ^{104,y}, A. Cortes-Gonzalez ¹⁸, M.J. Costa ¹⁶³,
 F. Costanza ⁴, D. Costanzo ¹³⁹, B.M. Cote ¹¹⁹, G. Cowan ⁹⁵, J.W. Cowley ³², K. Cranmer ¹¹⁷,
 S. Crépe-Renaudin ⁶⁰, F. Crescioli ¹²⁷, M. Cristinziani ¹⁴¹, M. Cristoforetti ^{78a,78b,d}, V. Croft ¹¹⁴,
 G. Crosetti ^{43b,43a}, A. Cueto ³⁶, T. Cuhadar Donszelmann ¹⁶⁰, H. Cui ^{14a,14d}, Z. Cui ⁷,
 W.R. Cunningham ⁵⁹, F. Curcio ^{43b,43a}, P. Czodrowski ³⁶, M.M. Czurylo ^{63b},
 M.J. Da Cunha Sargedas De Sousa ^{62a}, J.V. Da Fonseca Pinto ^{82b}, C. Da Via ¹⁰¹, W. Dabrowski ^{85a},
 T. Dado ⁴⁹, S. Dahbi ^{33g}, T. Dai ¹⁰⁶, C. Dallapiccola ¹⁰³, M. Dam ⁴², G. D'amen ²⁹,
 V. D'Amico ¹⁰⁹, J. Damp ¹⁰⁰, J.R. Dandoy ¹²⁸, M.F. Daneri ³⁰, M. Danninger ¹⁴², V. Dao ³⁶,
 G. Darbo ^{57b}, S. Darmora ⁶, S.J. Das ^{29,ak}, S. D'Auria ^{71a,71b}, C. David ^{156b}, T. Davidek ¹³³,
 B. Davis-Purcell ³⁴, I. Dawson ⁹⁴, K. De ⁸, R. De Asmundis ^{72a}, N. De Biase ⁴⁸,
 S. De Castro ^{23b,23a}, N. De Groot ¹¹³, P. de Jong ¹¹⁴, H. De la Torre ¹⁰⁷, A. De Maria ^{14c},
 A. De Salvo ^{75a}, U. De Sanctis ^{76a,76b}, A. De Santo ¹⁴⁶, J.B. De Vivie De Regie ⁶⁰, D.V. Dedovich ³⁸,
 J. Degens ¹¹⁴, A.M. Deiana ⁴⁴, F. Del Corso ^{23b,23a}, J. Del Peso ⁹⁹, F. Del Rio ^{63a}, F. Deliot ¹³⁵,
 C.M. Delitzsch ⁴⁹, M. Della Pietra ^{72a,72b}, D. Della Volpe ⁵⁶, A. Dell'Acqua ³⁶,
 L. Dell'Asta ^{71a,71b}, M. Delmastro ⁴, P.A. Delsart ⁶⁰, S. Demers ¹⁷², M. Demichev ³⁸,
 S.P. Denisov ³⁷, L. D'Eramo ¹¹⁵, D. Derendarz ⁸⁶, F. Derue ¹²⁷, P. Dervan ⁹², K. Desch ²⁴,
 K. Dette ¹⁵⁵, C. Deutsch ²⁴, F.A. Di Bello ^{57b,57a}, A. Di Ciaccio ^{76a,76b}, L. Di Ciaccio ⁴,
 A. Di Domenico ^{75a,75b}, C. Di Donato ^{72a,72b}, A. Di Girolamo ³⁶, G. Di Gregorio ⁵,
 A. Di Luca ^{78a,78b}, B. Di Micco ^{77a,77b}, R. Di Nardo ^{77a,77b}, C. Diaconu ¹⁰², F.A. Dias ¹¹⁴,
 T. Dias Do Vale ¹⁴², M.A. Diaz ^{137a,137b}, F.G. Diaz Capriles ²⁴, M. Didenko ¹⁶³, E.B. Diehl ¹⁰⁶,
 L. Diehl ⁵⁴, S. Díez Cornell ⁴⁸, C. Díez Pardos ¹⁴¹, C. Dimitriadi ^{24,161}, A. Dimitrievska ^{17a},
 J. Dingfelder ²⁴, I-M. Dinu ^{27b}, S.J. Dittmeier ^{63b}, F. Dittus ³⁶, F. Djama ¹⁰², T. Djobava ^{149b},
 J.I. Djuvsland ¹⁶, C. Doglioni ^{101,98}, J. Dolejsi ¹³³, Z. Dolezal ¹³³, M. Donadelli ^{82c},
 B. Dong ¹⁰⁷, J. Donini ⁴⁰, A. D'Onofrio ^{77a,77b}, M. D'Onofrio ⁹², J. Dopke ¹³⁴, A. Doria ^{72a},
 M.T. Dova ⁹⁰, A.T. Doyle ⁵⁹, M.A. Draguet ¹²⁶, E. Drechsler ¹⁴², E. Dreyer ¹⁶⁹,
 I. Drivas-koulouris ¹⁰, A.S. Drobac ¹⁵⁸, M. Drozdova ⁵⁶, D. Du ^{62a}, T.A. du Pree ¹¹⁴,
 F. Dubinin ³⁷, M. Dubovsky ^{28a}, E. Duchovni ¹⁶⁹, G. Duckeck ¹⁰⁹, O.A. Ducu ^{27b}, D. Duda ¹¹⁰,
 A. Dudarev ³⁶, E.R. Duden ²⁶, M. D'uffizi ¹⁰¹, L. Duflot ⁶⁶, M. Dührssen ³⁶, C. Dülßen ¹⁷¹,
 A.E. Dumitriu ^{27b}, M. Dunford ^{63a}, S. Dungs ⁴⁹, K. Dunne ^{47a,47b}, A. Duperrin ¹⁰²,
 H. Duran Yildiz ^{3a}, M. Düren ⁵⁸, A. Durglishvili ^{149b}, B.L. Dwyer ¹¹⁵, G.I. Dyckes ^{17a},
 M. Dyndal ^{85a}, S. Dysch ¹⁰¹, B.S. Dziedzic ⁸⁶, Z.O. Earnshaw ¹⁴⁶, B. Eckerova ^{28a},
 S. Eggebrecht ⁵⁵, M.G. Eggleston ⁵¹, E. Egidio Purcino De Souza ¹²⁷, L.F. Ehrke ⁵⁶, G. Eigen ¹⁶,
 K. Einsweiler ^{17a}, T. Ekelof ¹⁶¹, P.A. Ekman ⁹⁸, Y. El Ghazali ^{35b}, H. El Jarrari ^{35e,148},
 A. El Moussaouy ^{35a}, V. Ellajosyula ¹⁶¹, M. Ellert ¹⁶¹, F. Ellinghaus ¹⁷¹, A.A. Elliot ⁹⁴,
 N. Ellis ³⁶, J. Elmsheuser ²⁹, M. Elsing ³⁶, D. Emelianov ¹³⁴, Y. Enari ¹⁵³, I. Ene ^{17a},
 S. Epari ¹³, J. Erdmann ⁴⁹, P.A. Erland ⁸⁶, M. Errenst ¹⁷¹, M. Escalier ⁶⁶, C. Escobar ¹⁶³,
 E. Etzion ¹⁵¹, G. Evans ^{130a}, H. Evans ⁶⁸, M.O. Evans ¹⁴⁶, A. Ezhilov ³⁷, S. Ezzarqtouni ^{35a},
 F. Fabbri ⁵⁹, L. Fabbri ^{23b,23a}, G. Facini ⁹⁶, V. Fadeyev ¹³⁶, R.M. Fakhrutdinov ³⁷,
 S. Falciano ^{75a}, L.F. Falda Ulhoa Coelho ³⁶, P.J. Falke ²⁴, S. Falke ³⁶, J. Faltova ¹³³, Y. Fan ^{14a},
 Y. Fang ^{14a,14d}, M. Fanti ^{71a,71b}, M. Faraj ^{69a,69b}, Z. Farazpay ⁹⁷, A. Farbin ⁸, A. Farilla ^{77a},

T. Farooque ¹⁰⁷, S.M. Farrington ⁵², F. Fassi ^{35e}, D. Fassouliotis ⁹, M. Faucci Giannelli ^{76a,76b}, W.J. Fawcett ³², L. Fayard ⁶⁶, P. Federic ¹³³, P. Federicova ¹³¹, O.L. Fedin ^{37,a}, G. Fedotov ³⁷, M. Feickert ¹⁷⁰, L. Feligioni ¹⁰², A. Fell ¹³⁹, D.E. Fellers ¹²³, C. Feng ^{62b}, M. Feng ^{14b}, Z. Feng ¹¹⁴, M.J. Fenton ¹⁶⁰, A.B. Fenyuk ³⁷, L. Ferencz ⁴⁸, R.A.M. Ferguson ⁹¹, S.I. Fernandez Luengo ^{137f}, J. Ferrando ⁴⁸, A. Ferrari ¹⁶¹, P. Ferrari ^{114,113}, R. Ferrari ^{73a}, D. Ferrere ⁵⁶, C. Ferretti ¹⁰⁶, F. Fiedler ¹⁰⁰, A. Filipčič ⁹³, E.K. Filmer ¹, F. Filthaut ¹¹³, M.C.N. Fiolhais ^{130a,130c,c}, L. Fiorini ¹⁶³, F. Fischer ¹⁴¹, W.C. Fisher ¹⁰⁷, T. Fitschen ¹⁰¹, I. Fleck ¹⁴¹, P. Fleischmann ¹⁰⁶, T. Flick ¹⁷¹, L. Flores ¹²⁸, M. Flores ^{33d,ae}, L.R. Flores Castillo ^{64a}, F.M. Follega ^{78a,78b}, N. Fomin ¹⁶, J.H. Foo ¹⁵⁵, B.C. Forland ⁶⁸, A. Formica ¹³⁵, A.C. Forti ¹⁰¹, E. Fortin ¹⁰², A.W. Fortman ⁶¹, M.G. Foti ^{17a}, L. Fountas ^{9,k}, D. Fournier ⁶⁶, H. Fox ⁹¹, P. Francavilla ^{74a,74b}, S. Francescato ⁶¹, S. Franchellucci ⁵⁶, M. Franchini ^{23b,23a}, S. Franchino ^{63a}, D. Francis ³⁶, L. Franco ¹¹³, L. Franconi ¹⁹, M. Franklin ⁶¹, G. Frattari ²⁶, A.C. Freegard ⁹⁴, W.S. Freund ^{82b}, Y.Y. Frid ¹⁵¹, N. Fritzsche ⁵⁰, A. Froch ⁵⁴, D. Froidevaux ³⁶, J.A. Frost ¹²⁶, Y. Fu ^{62a}, M. Fujimoto ¹¹⁸, E. Fullana Torregrosa ^{163,*}, J. Fuster ¹⁶³, A. Gabrielli ^{23b,23a}, A. Gabrielli ¹⁵⁵, P. Gadow ⁴⁸, G. Gagliardi ^{57b,57a}, L.G. Gagnon ^{17a}, G.E. Gallardo ¹²⁶, E.J. Gallas ¹²⁶, B.J. Gallop ¹³⁴, R. Gamboa Goni ⁹⁴, K.K. Gan ¹¹⁹, S. Ganguly ¹⁵³, J. Gao ^{62a}, Y. Gao ⁵², F.M. Garay Walls ^{137a,137b}, B. Garcia ^{29,ak}, C. García ¹⁶³, J.E. García Navarro ¹⁶³, M. Garcia-Sciveres ^{17a}, R.W. Gardner ³⁹, D. Garg ⁸⁰, R.B. Garg ^{143,q}, C.A. Garner ¹⁵⁵, S.J. Gasiorowski ¹³⁸, P. Gaspar ^{82b}, G. Gaudio ^{73a}, V. Gautam ¹³, P. Gauzzi ^{75a,75b}, I.L. Gavrilenko ³⁷, A. Gavrilyuk ³⁷, C. Gay ¹⁶⁴, G. Gaycken ⁴⁸, E.N. Gazis ¹⁰, A.A. Geanta ^{27b,27e}, C.M. Gee ¹³⁶, C. Gemme ^{57b}, M.H. Genest ⁶⁰, S. Gentile ^{75a,75b}, S. George ⁹⁵, W.F. George ²⁰, T. Gerialis ⁴⁶, L.O. Gerlach ⁵⁵, P. Gessinger-Befurt ³⁶, M.E. Geyik ¹⁷¹, M. Ghneimat ¹⁴¹, K. Ghorbanian ⁹⁴, A. Ghosal ¹⁴¹, A. Ghosh ¹⁶⁰, A. Ghosh ⁷, B. Giacobbe ^{23b}, S. Giagu ^{75a,75b}, P. Giannetti ^{74a}, A. Giannini ^{62a}, S.M. Gibson ⁹⁵, M. Gignac ¹³⁶, D.T. Gil ^{85b}, A.K. Gilbert ^{85a}, B.J. Gilbert ⁴¹, D. Gillberg ³⁴, G. Gilles ¹¹⁴, N.E.K. Gillwald ⁴⁸, L. Ginabat ¹²⁷, D.M. Gingrich ^{2,ah}, M.P. Giordani ^{69a,69c}, P.F. Giraud ¹³⁵, G. Giugliarelli ^{69a,69c}, D. Giugni ^{71a}, F. Giuli ³⁶, I. Gkialas ^{9,k}, L.K. Gladilin ³⁷, C. Glasman ⁹⁹, G.R. Gledhill ¹²³, M. Glisic ¹²³, I. Gnesi ^{43b,g}, Y. Go ^{29,ak}, M. Goblirsch-Kolb ²⁶, B. Gocke ⁴⁹, D. Godin ¹⁰⁸, B. Gokturk ^{21a}, S. Goldfarb ¹⁰⁵, T. Golling ⁵⁶, M.G.D. Gololo ^{33g}, D. Golubkov ³⁷, J.P. Gombas ¹⁰⁷, A. Gomes ^{130a,130b}, G. Gomes Da Silva ¹⁴¹, A.J. Gomez Delegido ¹⁶³, R. Gonçalves ^{130a,130c}, G. Gonella ¹²³, L. Gonella ²⁰, A. Gongadze ³⁸, F. Gonnella ²⁰, J.L. Gonski ⁴¹, R.Y. González Andana ⁵², S. González de la Hoz ¹⁶³, S. Gonzalez Fernandez ¹³, R. Gonzalez Lopez ⁹², C. Gonzalez Renteria ^{17a}, R. Gonzalez Suarez ¹⁶¹, S. Gonzalez-Sevilla ⁵⁶, G.R. Gonzalvo Rodriguez ¹⁶³, L. Goossens ³⁶, P.A. Gorbounov ³⁷, B. Gorini ³⁶, E. Gorini ^{70a,70b}, A. Gorišek ⁹³, A.T. Goshaw ⁵¹, M.I. Gostkin ³⁸, S. Goswami ¹²¹, C.A. Gottardo ³⁶, M. Goughri ^{35b}, V. Goumarre ⁴⁸, A.G. Goussiou ¹³⁸, N. Govender ^{33c}, I. Grabowska-Bold ^{85a}, K. Graham ³⁴, E. Gramstad ¹²⁵, S. Grancagnolo ¹⁸, M. Grandi ¹⁴⁶, V. Gratchev ^{37,*}, P.M. Gravila ^{27f}, F.G. Gravili ^{70a,70b}, H.M. Gray ^{17a}, M. Greco ^{70a,70b}, C. Grefe ²⁴, I.M. Gregor ⁴⁸, P. Grenier ¹⁴³, C. Grieco ¹³, A.A. Grillo ¹³⁶, K. Grimm ^{31,n}, S. Grinstein ^{13,v}, J.-F. Grivaz ⁶⁶, E. Gross ¹⁶⁹, J. Grosse-Knetter ⁵⁵, C. Grud ¹⁰⁶, J.C. Grundy ¹²⁶, L. Guan ¹⁰⁶, W. Guan ¹⁷⁰, C. Gubbels ¹⁶⁴, J.G.R. Guerrero Rojas ¹⁶³, G. Guerrieri ^{69a,69b}, F. Guescini ¹¹⁰, R. Gugel ¹⁰⁰, J.A.M. Guhit ¹⁰⁶, A. Guida ⁴⁸, T. Guillemin ⁴, E. Guilloton ^{167,134}, S. Guindon ³⁶, F. Guo ^{14a,14d}, J. Guo ^{62c}, L. Guo ⁶⁶, Y. Guo ¹⁰⁶, R. Gupta ⁴⁸, S. Gurbuz ²⁴, S.S. Gurdasani ⁵⁴, G. Gustavino ³⁶, M. Guth ⁵⁶, P. Gutierrez ¹²⁰, L.F. Gutierrez Zagazeta ¹²⁸, C. Gutschow ⁹⁶, C. Gwenlan ¹²⁶, C.B. Gwilliam ⁹², E.S. Haaland ¹²⁵, A. Haas ¹¹⁷, M. Habedank ⁴⁸, C. Haber ^{17a}, H.K. Hadavand ⁸, A. Hadeef ¹⁰⁰, S. Hadzic ¹¹⁰, E.H. Haines ⁹⁶, M. Haleem ¹⁶⁶, J. Haley ¹²¹, J.J. Hall ¹³⁹, G.D. Hallewell ¹⁰², L. Halser ¹⁹, K. Hamano ¹⁶⁵, H. Hamdaoui ^{35e},

M. Hamer ^{id24}, G.N. Hamity ^{id52}, E.J. Hampshire ^{id95}, J. Han ^{id62b}, K. Han ^{id62a}, L. Han ^{id14c},
L. Han ^{id62a}, S. Han ^{id17a}, Y.F. Han ^{id155}, K. Hanagaki ^{id83}, M. Hance ^{id136}, D.A. Hangal ^{id41,ad},
H. Hanif ^{id142}, M.D. Hank ^{id128}, R. Hankache ^{id101}, J.B. Hansen ^{id42}, J.D. Hansen ^{id42}, P.H. Hansen ^{id42},
K. Hara ^{id157}, D. Harada ^{id56}, T. Harenberg ^{id171}, S. Harkusha ^{id37}, Y.T. Harris ^{id126}, N.M. Harrison ^{id119},
P.F. Harrison ^{id167}, N.M. Hartman ^{id143}, N.M. Hartmann ^{id109}, Y. Hasegawa ^{id140}, A. Hasib ^{id52},
S. Haug ^{id19}, R. Hauser ^{id107}, M. Havranek ^{id132}, C.M. Hawkes ^{id20}, R.J. Hawkings ^{id36},
S. Hayashida ^{id111}, D. Hayden ^{id107}, C. Hayes ^{id106}, R.L. Hayes ^{id114}, C.P. Hays ^{id126}, J.M. Hays ^{id94},
H.S. Hayward ^{id92}, F. He ^{id62a}, Y. He ^{id154}, Y. He ^{id127}, N.B. Heatley ^{id94}, V. Hedberg ^{id98},
A.L. Heggelund ^{id125}, N.D. Hehir ^{id94}, C. Heidegger ^{id54}, K.K. Heidegger ^{id54}, W.D. Heidorn ^{id81},
J. Heilman ^{id34}, S. Heim ^{id48}, T. Heim ^{id17a}, J.G. Heinlein ^{id128}, J.J. Heinrich ^{id123}, L. Heinrich ^{id110,af},
J. Hejbal ^{id131}, L. Helary ^{id48}, A. Held ^{id170}, S. Hellesund ^{id125}, C.M. Helling ^{id164}, S. Hellman ^{id47a,47b},
C. Hensens ^{id36}, R.C.W. Henderson ^{id91}, L. Henkelmann ^{id32}, A.M. Henriques Correia ^{id36}, H. Herde ^{id98},
Y. Hernández Jiménez ^{id145}, L.M. Herrmann ^{id24}, T. Herrmann ^{id50}, G. Herten ^{id54}, R. Hertenberger ^{id109},
L. Hervas ^{id36}, N.P. Hessey ^{id156a}, H. Hibi ^{id84}, S.J. Hillier ^{id20}, F. Hinterkeuser ^{id24}, M. Hirose ^{id124},
S. Hirose ^{id157}, D. Hirschbuehl ^{id171}, T.G. Hitchings ^{id101}, B. Hiti ^{id93}, J. Hobbs ^{id145}, R. Hobincu ^{id27e},
N. Hod ^{id169}, M.C. Hodgkinson ^{id139}, B.H. Hodgkinson ^{id32}, A. Hoecker ^{id36}, J. Hofer ^{id48}, T. Holm ^{id24},
M. Holzbock ^{id110}, L.B.A.H. Hommels ^{id32}, B.P. Honan ^{id101}, J. Hong ^{id62c}, T.M. Hong ^{id129},
J.C. Honig ^{id54}, B.H. Hooberman ^{id162}, W.H. Hopkins ^{id6}, Y. Horii ^{id111}, S. Hou ^{id148}, A.S. Howard ^{id93},
J. Howarth ^{id59}, J. Hoya ^{id6}, M. Hrabovsky ^{id122}, A. Hrynevich ^{id48}, T. Hryn'ova ^{id4}, P.J. Hsu ^{id65},
S.-C. Hsu ^{id138}, Q. Hu ^{id41}, Y.F. Hu ^{id14a,14d,aj}, D.P. Huang ^{id96}, S. Huang ^{id64b}, X. Huang ^{id14c},
Y. Huang ^{id62a}, Y. Huang ^{id14a}, Z. Huang ^{id101}, Z. Hubacek ^{id132}, M. Huebner ^{id24}, F. Huegging ^{id24},
T.B. Huffman ^{id126}, M. Huhtinen ^{id36}, S.K. Huiberts ^{id16}, R. Hulsken ^{id104}, N. Huseynov ^{id12,a},
J. Huston ^{id107}, J. Huth ^{id61}, R. Hyneman ^{id143}, G. Iacobucci ^{id56}, G. Iakovidis ^{id29}, I. Ibragimov ^{id141},
L. Iconomidou-Fayard ^{id66}, P. Iengo ^{id72a,72b}, R. Iguchi ^{id153}, T. Iizawa ^{id56}, Y. Ikegami ^{id83}, A. Ilg ^{id19},
N. Ilic ^{id155}, H. Imam ^{id35a}, T. Ingebretsen Carlson ^{id47a,47b}, G. Introzzi ^{id73a,73b}, M. Iodice ^{id77a},
V. Ippolito ^{id75a,75b}, M. Ishino ^{id153}, W. Islam ^{id170}, C. Issever ^{id18,48}, S. Istin ^{id21a,am}, H. Ito ^{id168},
J.M. Iturbe Ponce ^{id64a}, R. Iuppa ^{id78a,78b}, A. Ivina ^{id169}, J.M. Izen ^{id45}, V. Izzo ^{id72a}, P. Jacka ^{id131,132},
P. Jackson ^{id1}, R.M. Jacobs ^{id48}, B.P. Jaeger ^{id142}, C.S. Jagfeld ^{id109}, P. Jain ^{id54}, G. Jäkel ^{id171},
K. Jakobs ^{id54}, T. Jakoubek ^{id169}, J. Jamieson ^{id59}, K.W. Janas ^{id85a}, A.E. Jaspan ^{id92}, M. Javurkova ^{id103},
F. Jeanneau ^{id135}, L. Jeanty ^{id123}, J. Jejelava ^{id149a,ab}, P. Jenni ^{id54,h}, C.E. Jessiman ^{id34}, S. Jézéquel ^{id4},
C. Jia ^{id62b}, J. Jia ^{id145}, X. Jia ^{id61}, X. Jia ^{id14a,14d}, Z. Jia ^{id14c}, Y. Jiang ^{id62a}, S. Jiggins ^{id48},
J. Jimenez Pena ^{id110}, S. Jin ^{id14c}, A. Jinaru ^{id27b}, O. Jinnouchi ^{id154}, P. Johansson ^{id139}, K.A. Johns ^{id7},
J.W. Johnson ^{id136}, D.M. Jones ^{id32}, E. Jones ^{id167}, P. Jones ^{id32}, R.W.L. Jones ^{id91}, T.J. Jones ^{id92},
R. Joshi ^{id119}, J. Jovicevic ^{id15}, X. Ju ^{id17a}, J.J. Jungburth ^{id36}, T. Junkermann ^{id63a},
A. Juste Rozas ^{id13,v}, S. Kabana ^{id137e}, A. Kaczmarzka ^{id86}, M. Kado ^{id110}, H. Kagan ^{id119},
M. Kagan ^{id143}, A. Kahn ^{id41}, A. Kahn ^{id128}, C. Kahra ^{id100}, T. Kaji ^{id168}, E. Kajomovitz ^{id150},
N. Kakati ^{id169}, C.W. Kalderon ^{id29}, A. Kamenshchikov ^{id155}, S. Kanayama ^{id154}, N.J. Kang ^{id136},
D. Kar ^{id33g}, K. Karava ^{id126}, M.J. Kareem ^{id156b}, E. Karentzos ^{id54}, I. Karkanias ^{id152,f},
S.N. Karpov ^{id38}, Z.M. Karpova ^{id38}, V. Kartvelishvili ^{id91}, A.N. Karyukhin ^{id37}, E. Kasimi ^{id152,f},
J. Katzy ^{id48}, S. Kaur ^{id34}, K. Kawade ^{id140}, T. Kawamoto ^{id135}, G. Kawamura ^{id55}, E.F. Kay ^{id165},
F.I. Kaya ^{id158}, S. Kazakos ^{id13}, V.F. Kazanin ^{id37}, Y. Ke ^{id145}, J.M. Keaveney ^{id33a}, R. Keeler ^{id165},
G.V. Kehris ^{id61}, J.S. Keller ^{id34}, A.S. Kelly ^{id96}, D. Kelsey ^{id146}, J.J. Kempster ^{id146}, K.E. Kennedy ^{id41},
P.D. Kennedy ^{id100}, O. Kepka ^{id131}, B.P. Kerridge ^{id167}, S. Kersten ^{id171}, B.P. Kerševan ^{id93},
S. Keshri ^{id66}, L. Keszeghova ^{id28a}, S. Ketabchi Haghightat ^{id155}, M. Khandoga ^{id127}, A. Khanov ^{id121},
A.G. Kharlamov ^{id37}, T. Kharlamova ^{id37}, E.E. Khoda ^{id138}, T.J. Khoo ^{id18}, G. Khoriauli ^{id166},
J. Khubua ^{id149b}, Y.A.R. Khwaira ^{id66}, M. Kiehn ^{id36}, A. Kilgallon ^{id123}, D.W. Kim ^{id47a,47b},
E. Kim ^{id154}, Y.K. Kim ^{id39}, N. Kimura ^{id96}, A. Kirchhoff ^{id55}, C. Kirfel ^{id24}, J. Kirk ^{id134},

A.E. Kiryunin ¹¹⁰, T. Kishimoto ¹⁵³, D.P. Kisiuk ¹⁵⁵, C. Kitsaki ¹⁰, O. Kivernyk ²⁴,
 M. Klassen ^{63a}, C. Klein ³⁴, L. Klein ¹⁶⁶, M.H. Klein ¹⁰⁶, M. Klein ⁹², S.B. Klein ⁵⁶,
 U. Klein ⁹², P. Klimek ³⁶, A. Klimentov ²⁹, F. Klimpel ¹¹⁰, T. Klioutchnikova ³⁶, P. Kluit ¹¹⁴,
 S. Kluth ¹¹⁰, E. Kneringer ⁷⁹, T.M. Knight ¹⁵⁵, A. Knue ⁵⁴, R. Kobayashi ⁸⁷, M. Kocian ¹⁴³,
 P. Kodyš ¹³³, D.M. Koeck ¹⁴⁶, P.T. Koenig ²⁴, T. Koffas ³⁴, M. Kolb ¹³⁵, I. Koletsou ⁴,
 T. Komarek ¹²², K. Köneke ⁵⁴, A.X.Y. Kong ¹, T. Kono ¹¹⁸, N. Konstantinidis ⁹⁶, B. Konya ⁹⁸,
 R. Kopeliansky ⁶⁸, S. Koperny ^{85a}, K. Korcyl ⁸⁶, K. Kordas ^{152,f}, G. Koren ¹⁵¹, A. Korn ⁹⁶,
 S. Korn ⁵⁵, I. Korolkov ¹³, N. Korotkova ³⁷, B. Kortman ¹¹⁴, O. Kortner ¹¹⁰, S. Kortner ¹¹⁰,
 W.H. Kostecka ¹¹⁵, V.V. Kostyukhin ¹⁴¹, A. Kotsokechagia ¹³⁵, A. Kotwal ⁵¹, A. Koulouris ³⁶,
 A. Kourkoumeli-Charalampidi ^{73a,73b}, C. Kourkoumelis ⁹, E. Kourlitis ⁶, O. Kovanda ¹⁴⁶,
 R. Kowalewski ¹⁶⁵, W. Kozanecki ¹³⁵, A.S. Kozhin ³⁷, V.A. Kramarenko ³⁷, G. Kramberger ⁹³,
 P. Kramer ¹⁰⁰, M.W. Krasny ¹²⁷, A. Krasznahorkay ³⁶, J.A. Kremer ¹⁰⁰, T. Kresse ⁵⁰,
 J. Kretschmar ⁹², K. Kreul ¹⁸, P. Krieger ¹⁵⁵, S. Krishnamurthy ¹⁰³, M. Krivos ¹³³,
 K. Krizka ²⁰, K. Kroeninger ⁴⁹, H. Kroha ¹¹⁰, J. Kroll ¹³¹, J. Kroll ¹²⁸, K.S. Krowpman ¹⁰⁷,
 U. Kruchonak ³⁸, H. Krüger ²⁴, N. Krumnack ⁸¹, M.C. Kruse ⁵¹, J.A. Krzysiak ⁸⁶,
 O. Kuchinskaia ³⁷, S. Kuday ^{3a}, S. Kuehn ³⁶, R. Kuesters ⁵⁴, T. Kuhl ⁴⁸, V. Kukhtin ³⁸,
 Y. Kulchitsky ^{37,a}, S. Kuleshov ^{137d,137b}, M. Kumar ^{33g}, N. Kumari ¹⁰², A. Kupco ¹³¹, T. Kupfer ⁴⁹,
 A. Kupich ³⁷, O. Kuprash ⁵⁴, H. Kurashige ⁸⁴, L.L. Kurchaninov ^{156a}, Y.A. Kurochkin ³⁷,
 A. Kurova ³⁷, M. Kuze ¹⁵⁴, A.K. Kvam ¹⁰³, J. Kvita ¹²², T. Kwan ¹⁰⁴, N.G. Kyriacou ¹⁰⁶,
 L.A.O. Laatu ¹⁰², C. Lacasta ¹⁶³, F. Lacava ^{75a,75b}, H. Lacker ¹⁸, D. Lacour ¹²⁷, N.N. Lad ⁹⁶,
 E. Ladygin ³⁸, B. Laforge ¹²⁷, T. Lagouri ^{137e}, S. Lai ⁵⁵, I.K. Lakomic ^{85a}, N. Lalloue ⁶⁰,
 J.E. Lambert ¹²⁰, S. Lammers ⁶⁸, W. Lampl ⁷, C. Lampoudis ^{152,f}, A.N. Lancaster ¹¹⁵,
 E. Lançon ²⁹, U. Landgraf ⁵⁴, M.P.J. Landon ⁹⁴, V.S. Lang ⁵⁴, R.J. Langenberg ¹⁰³,
 A.J. Lankford ¹⁶⁰, F. Lanni ³⁶, K. Lantzsch ²⁴, A. Lanza ^{73a}, A. Lapertosa ^{57b,57a},
 J.F. Laporte ¹³⁵, T. Lari ^{71a}, F. Lasagni Manghi ^{23b}, M. Lassnig ³⁶, V. Latonova ¹³¹,
 A. Laudrain ¹⁰⁰, A. Laurier ¹⁵⁰, S.D. Lawlor ⁹⁵, Z. Lawrence ¹⁰¹, M. Lazzaroni ^{71a,71b}, B. Le ¹⁰¹,
 E.M. Le Boulicaut ⁵¹, B. Leban ⁹³, A. Lebedev ⁸¹, M. LeBlanc ³⁶, F. Ledroit-Guillon ⁶⁰,
 A.C.A. Lee ⁹⁶, G.R. Lee ¹⁶, S.C. Lee ¹⁴⁸, S. Lee ^{47a,47b}, T.F. Lee ⁹², L.L. Leeuw ^{33c},
 H.P. Lefebvre ⁹⁵, M. Lefebvre ¹⁶⁵, C. Leggett ^{17a}, K. Lehmann ¹⁴², G. Lehmann Miotto ³⁶,
 M. Leigh ⁵⁶, W.A. Leight ¹⁰³, A. Leisos ^{152,u}, M.A.L. Leite ^{82c}, C.E. Leitgeb ⁴⁸, R. Leitner ¹³³,
 K.J.C. Leney ⁴⁴, T. Lenz ²⁴, S. Leone ^{74a}, C. Leonidopoulos ⁵², A. Leopold ¹⁴⁴, C. Leroy ¹⁰⁸,
 R. Les ¹⁰⁷, C.G. Lester ³², M. Levchenko ³⁷, J. Levêque ⁴, D. Levin ¹⁰⁶, L.J. Levinson ¹⁶⁹,
 M.P. Lewicki ⁸⁶, D.J. Lewis ⁴, A. Li ⁵, B. Li ^{62b}, C. Li ^{62a}, C-Q. Li ^{62c}, H. Li ^{62a}, H. Li ^{62b},
 H. Li ^{14c}, H. Li ^{62b}, J. Li ^{62c}, K. Li ¹³⁸, L. Li ^{62c}, M. Li ^{14a,14d}, Q.Y. Li ^{62a}, S. Li ^{14a,14d},
 S. Li ^{62d,62c,e}, T. Li ^{62b}, X. Li ¹⁰⁴, Z. Li ^{62b}, Z. Li ¹²⁶, Z. Li ¹⁰⁴, Z. Li ⁹², Z. Li ^{14a,14d},
 Z. Liang ^{14a}, M. Liberatore ⁴⁸, B. Liberti ^{76a}, K. Lie ^{64c}, J. Lieber Marin ^{82b}, H. Lien ⁶⁸,
 K. Lin ¹⁰⁷, R.A. Linck ⁶⁸, R.E. Lindley ⁷, J.H. Lindon ², A. Linss ⁴⁸, E. Lipeles ¹²⁸,
 A. Lipniacka ¹⁶, A. Lister ¹⁶⁴, J.D. Little ⁴, B. Liu ^{14a}, B.X. Liu ¹⁴², D. Liu ^{62d,62c},
 J.B. Liu ^{62a}, J.K.K. Liu ³², K. Liu ^{62d,62c}, M. Liu ^{62a}, M.Y. Liu ^{62a}, P. Liu ^{14a},
 Q. Liu ^{62d,138,62c}, X. Liu ^{62a}, Y. Liu ^{14c,14d}, Y.L. Liu ¹⁰⁶, Y.W. Liu ^{62a}, J. Llorente Merino ¹⁴²,
 S.L. Lloyd ⁹⁴, E.M. Lobodzinska ⁴⁸, P. Loch ⁷, S. Loffredo ^{76a,76b}, T. Lohse ¹⁸,
 K. Lohwasser ¹³⁹, E. Loiacono ⁴⁸, M. Lokajicek ^{131,*}, J.D. Long ¹⁶², I. Longarini ¹⁶⁰,
 L. Longo ^{70a,70b}, R. Longo ¹⁶², I. Lopez Paz ⁶⁷, A. Lopez Solis ⁴⁸, J. Lorenz ¹⁰⁹,
 N. Lorenzo Martinez ⁴, A.M. Lory ¹⁰⁹, X. Lou ^{47a,47b}, X. Lou ^{14a,14d}, A. Lounis ⁶⁶, J. Love ⁶,
 P.A. Love ⁹¹, G. Lu ^{14a,14d}, M. Lu ⁸⁰, S. Lu ¹²⁸, Y.J. Lu ⁶⁵, H.J. Lubatti ¹³⁸, C. Luci ^{75a,75b},
 F.L. Lucio Alves ^{14c}, A. Lucotte ⁶⁰, F. Luehring ⁶⁸, I. Luise ¹⁴⁵, O. Lukianchuk ⁶⁶,
 O. Lundberg ¹⁴⁴, B. Lund-Jensen ¹⁴⁴, N.A. Luongo ¹²³, M.S. Lutz ¹⁵¹, D. Lynn ²⁹, H. Lyons ⁹²,














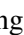
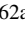


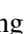
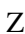
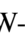
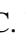





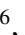





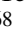





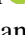

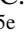
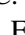
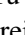


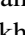
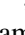
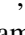
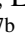
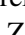


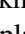
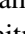





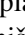
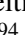



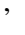




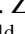
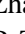


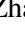


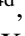
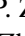




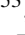
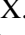



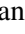

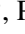
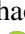



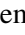

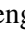




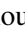
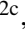




R. Lysak ¹³¹, E. Lytken ⁹⁸, V. Lyubushkin ³⁸, T. Lyubushkina ³⁸, M.M. Lyukova ¹⁴⁵, H. Ma ²⁹, L.L. Ma ^{62b}, Y. Ma ⁹⁶, D.M. Mac Donell ¹⁶⁵, G. Maccarrone ⁵³, J.C. MacDonald ¹³⁹, R. Madar ⁴⁰, W.F. Mader ⁵⁰, J. Maeda ⁸⁴, T. Maeno ²⁹, M. Maerker ⁵⁰, H. Maguire ¹³⁹, A. Maio ^{130a,130b,130d}, K. Maj ^{85a}, O. Majersky ⁴⁸, S. Majewski ¹²³, N. Makovec ⁶⁶, V. Maksimovic ¹⁵, B. Malaescu ¹²⁷, Pa. Malecki ⁸⁶, V.P. Maleev ³⁷, F. Malek ⁶⁰, D. Malito ^{43b,43a}, U. Mallik ⁸⁰, C. Malone ³², S. Maltezos ¹⁰, S. Malyukov ³⁸, J. Mamuzic ¹³, G. Mancini ⁵³, G. Manco ^{73a,73b}, J.P. Mandalia ⁹⁴, I. Mandić ⁹³, L. Manhaes de Andrade Filho ^{82a}, I.M. Maniatis ¹⁶⁹, J. Manjarres Ramos ^{102,ac}, D.C. Mankad ¹⁶⁹, A. Mann ¹⁰⁹, B. Mansoulie ¹³⁵, S. Manzoni ³⁶, A. Marantis ^{152,u}, G. Marchiori ⁵, M. Marcisovsky ¹³¹, C. Marcon ^{71a,71b}, M. Marinescu ²⁰, M. Marjanovic ¹²⁰, E.J. Marshall ⁹¹, Z. Marshall ^{17a}, S. Marti-Garcia ¹⁶³, T.A. Martin ¹⁶⁷, V.J. Martin ⁵², B. Martin dit Latour ¹⁶, L. Martinelli ^{75a,75b}, M. Martinez ^{13,v}, P. Martinez Agullo ¹⁶³, V.I. Martinez Outschoorn ¹⁰³, P. Martinez Suarez ¹³, S. Martin-Haugh ¹³⁴, V.S. Martoiu ^{27b}, A.C. Martyniuk ⁹⁶, A. Marzin ³⁶, S.R. Maschek ¹¹⁰, D. Mascione ^{78a,78b}, L. Masetti ¹⁰⁰, T. Mashimo ¹⁵³, J. Masik ¹⁰¹, A.L. Maslennikov ³⁷, L. Massa ^{23b}, P. Massarotti ^{72a,72b}, P. Mastrandrea ^{74a,74b}, A. Mastroberardino ^{43b,43a}, T. Masubuchi ¹⁵³, T. Mathisen ¹⁶¹, N. Matsuzawa ¹⁵³, J. Maurer ^{27b}, B. Maček ⁹³, D.A. Maximov ³⁷, R. Mazini ¹⁴⁸, I. Maznas ^{152,f}, M. Mazza ¹⁰⁷, S.M. Mazza ¹³⁶, C. Mc Ginn ²⁹, J.P. Mc Gowan ¹⁰⁴, S.P. Mc Kee ¹⁰⁶, E.F. McDonald ¹⁰⁵, A.E. McDougall ¹¹⁴, J.A. Mcfayden ¹⁴⁶, G. Mchedlidze ^{149b}, R.P. Mckenzie ^{33g}, T.C. Mclachlan ⁴⁸, D.J. Mclaughlin ⁹⁶, K.D. McLean ¹⁶⁵, S.J. McMahon ¹³⁴, P.C. McNamara ¹⁰⁵, C.M. Mcpartland ⁹², R.A. McPherson ^{165,y}, T. Megy ⁴⁰, S. Mehlhase ¹⁰⁹, A. Mehta ⁹², D. Melini ¹⁵⁰, B.R. Mellado Garcia ^{33g}, A.H. Melo ⁵⁵, F. Meloni ⁴⁸, A.M. Mendes Jacques Da Costa ¹⁰¹, H.Y. Meng ¹⁵⁵, L. Meng ⁹¹, S. Menke ¹¹⁰, M. Mentink ³⁶, E. Meoni ^{43b,43a}, C. Merlassino ¹²⁶, L. Merola ^{72a,72b}, C. Meroni ^{71a}, G. Merz ¹⁰⁶, O. Meshkov ³⁷, J. Metcalfe ⁶, A.S. Mete ⁶, C. Meyer ⁶⁸, J-P. Meyer ¹³⁵, R.P. Middleton ¹³⁴, L. Mijović ⁵², G. Mikenberg ¹⁶⁹, M. Mikesstikova ¹³¹, M. Mikuž ⁹³, H. Mildner ¹³⁹, A. Milic ³⁶, C.D. Milke ⁴⁴, D.W. Miller ³⁹, L.S. Miller ³⁴, A. Milov ¹⁶⁹, D.A. Milstead ^{47a,47b}, T. Min ^{14c}, A.A. Minaenko ³⁷, I.A. Minashvili ^{149b}, L. Mince ⁵⁹, A.I. Mincer ¹¹⁷, B. Mindur ^{85a}, M. Mineev ³⁸, Y. Mino ⁸⁷, L.M. Mir ¹³, M. Miralles Lopez ¹⁶³, M. Mironova ¹²⁶, M.C. Missio ¹¹³, T. Mitani ¹⁶⁸, A. Mitra ¹⁶⁷, V.A. Mitsou ¹⁶³, O. Miu ¹⁵⁵, P.S. Miyagawa ⁹⁴, Y. Miyazaki ⁸⁹, A. Mizukami ⁸³, T. Mkrtychyan ^{63a}, M. Mlinarevic ⁹⁶, T. Mlinarevic ⁹⁶, M. Mlynarikova ³⁶, S. Mobius ⁵⁵, K. Mochizuki ¹⁰⁸, P. Moder ⁴⁸, P. Mogg ¹⁰⁹, A.F. Mohammed ^{14a,14d}, S. Mohapatra ⁴¹, G. Mokgatitwane ^{33g}, B. Mondal ¹⁴¹, S. Mondal ¹³², K. Mönig ⁴⁸, E. Monnier ¹⁰², L. Monsonis Romero ¹⁶³, J. Montejo Berlingen ⁸³, M. Montella ¹¹⁹, F. Monticelli ⁹⁰, N. Morange ⁶⁶, A.L. Moreira De Carvalho ^{130a}, M. Moreno Llácer ¹⁶³, C. Moreno Martinez ⁵⁶, P. Morettini ^{57b}, S. Morgenstern ¹⁶⁷, M. Morii ⁶¹, M. Morinaga ¹⁵³, A.K. Morley ³⁶, F. Morodei ^{75a,75b}, L. Morvaj ³⁶, P. Moschovakos ³⁶, B. Moser ³⁶, M. Mosidze ^{149b}, T. Moskalets ⁵⁴, P. Moskvitina ¹¹³, J. Moss ^{31,o}, E.J.W. Moyse ¹⁰³, O. Mtintsilana ^{33g}, S. Muanza ¹⁰², J. Mueller ¹²⁹, D. Muenstermann ⁹¹, R. Müller ¹⁹, G.A. Mullier ¹⁶¹, J.J. Mullin ¹²⁸, D.P. Mungo ¹⁵⁵, J.L. Munoz Martinez ¹³, D. Munoz Perez ¹⁶³, F.J. Munoz Sanchez ¹⁰¹, M. Murin ¹⁰¹, W.J. Murray ^{167,134}, A. Murrone ^{71a,71b}, J.M. Muse ¹²⁰, M. Muškinja ^{17a}, C. Mwewa ²⁹, A.G. Myagkov ^{37,a}, A.J. Myers ⁸, A.A. Myers ¹²⁹, G. Myers ⁶⁸, M. Myska ¹³², B.P. Nachman ^{17a}, O. Nackenhorst ⁴⁹, A. Nag ⁵⁰, K. Nagai ¹²⁶, K. Nagano ⁸³, J.L. Nagle ^{29,ak}, E. Nagy ¹⁰², A.M. Nairz ³⁶, Y. Nakahama ⁸³, K. Nakamura ⁸³, H. Nanjo ¹²⁴, R. Narayan ⁴⁴, E.A. Narayanan ¹¹², I. Naryshkin ³⁷, M. Naseri ³⁴, C. Nass ²⁴, G. Navarro ^{22a}, J. Navarro-Gonzalez ¹⁶³, R. Nayak ¹⁵¹, A. Nayaz ¹⁸, P.Y. Nechaeva ³⁷, F. Nechansky ⁴⁸, L. Nedic ¹²⁶, T.J. Neep ²⁰, A. Negri ^{73a,73b}, M. Negrini ^{23b}, C. Nellist ¹¹⁴, C. Nelson ¹⁰⁴, K. Nelson ¹⁰⁶, S. Nemecek ¹³¹, M. Nessi ^{36,i}, M.S. Neubauer ¹⁶², F. Neuhaus ¹⁰⁰,

J. Neundorff ⁴⁸, R. Newhouse ¹⁶⁴, P.R. Newman ²⁰, C.W. Ng ¹²⁹, Y.W.Y. Ng ⁴⁸, B. Ngair ^{35e}, H.D.N. Nguyen ¹⁰⁸, R.B. Nickerson ¹²⁶, R. Nicolaidou ¹³⁵, J. Nielsen ¹³⁶, M. Niemeyer ⁵⁵, N. Nikiforou ³⁶, V. Nikolaenko ^{37,a}, I. Nikolic-Audit ¹²⁷, K. Nikolopoulos ²⁰, P. Nilsson ²⁹, I. Ninca ⁴⁸, H.R. Nindhito ⁵⁶, G. Ninio ¹⁵¹, A. Nisati ^{75a}, N. Nishu ², R. Nisius ¹¹⁰, J-E. Nitschke ⁵⁰, E.K. Nkadimeng ^{33g}, S.J. Noacco Rosende ⁹⁰, T. Nobe ¹⁵³, D.L. Noel ³², Y. Noguchi ⁸⁷, T. Nommensen ¹⁴⁷, M.A. Nomura ²⁹, M.B. Norfolk ¹³⁹, R.R.B. Norisam ⁹⁶, B.J. Norman ³⁴, J. Novak ⁹³, T. Novak ⁴⁸, L. Novotny ¹³², R. Novotny ¹¹², L. Nozka ¹²², K. Ntekas ¹⁶⁰, N.M.J. Nunes De Moura Junior ^{82b}, E. Nurse ⁹⁶, J. Ocariz ¹²⁷, A. Ochi ⁸⁴, I. Ochoa ^{130a}, S. Oerdek ¹⁶¹, J.T. Offermann ³⁹, A. Ogrodnik ^{85a}, A. Oh ¹⁰¹, C.C. Ohm ¹⁴⁴, H. Oide ⁸³, R. Oishi ¹⁵³, M.L. Ojeda ⁴⁸, Y. Okazaki ⁸⁷, M.W. O'Keefe ⁹², Y. Okumura ¹⁵³, L.F. Oleiro Seabra ^{130a}, S.A. Olivares Pino ^{137d}, D. Oliveira Damazio ²⁹, D. Oliveira Goncalves ^{82a}, J.L. Oliver ¹⁶⁰, M.J.R. Olsson ¹⁶⁰, A. Olszewski ⁸⁶, J. Olszowska ^{86,*}, Ö.O. Öncel ⁵⁴, D.C. O'Neil ¹⁴², A.P. O'Neill ¹⁹, A. Onofre ^{130a,130e}, P.U.E. Onyisi ¹¹, M.J. Oreglia ³⁹, G.E. Orellana ⁹⁰, D. Orestano ^{77a,77b}, N. Orlando ¹³, R.S. Orr ¹⁵⁵, V. O'Shea ⁵⁹, R. Ospanov ^{62a}, G. Otero y Garzon ³⁰, H. Otono ⁸⁹, P.S. Ott ^{63a}, G.J. Ottino ^{17a}, M. Ouchrif ^{35d}, J. Ouellette ²⁹, F. Ould-Saada ¹²⁵, M. Owen ⁵⁹, R.E. Owen ¹³⁴, K.Y. Oyulmaz ^{21a}, V.E. Ozcan ^{21a}, N. Ozturk ⁸, S. Ozturk ^{21d}, H.A. Pacey ³², K. Pachal ⁵¹, A. Pacheco Pages ¹³, C. Padilla Aranda ¹³, G. Padovano ^{75a,75b}, S. Pagan Griso ^{17a}, G. Palacino ⁶⁸, A. Palazzo ^{70a,70b}, S. Palestini ³⁶, J. Pan ¹⁷², T. Pan ^{64a}, D.K. Panchal ¹¹, C.E. Pandini ¹¹⁴, J.G. Panduro Vazquez ⁹⁵, H. Pang ^{14b}, P. Pani ⁴⁸, G. Panizzo ^{69a,69c}, L. Paolozzi ⁵⁶, C. Papadatos ¹⁰⁸, S. Parajuli ⁴⁴, A. Paramonov ⁶, C. Paraskevopoulos ¹⁰, D. Paredes Hernandez ^{64b}, T.H. Park ¹⁵⁵, M.A. Parker ³², F. Parodi ^{57b,57a}, E.W. Parrish ¹¹⁵, V.A. Parrish ⁵², J.A. Parsons ⁴¹, U. Parzefall ⁵⁴, B. Pascual Dias ¹⁰⁸, L. Pascual Dominguez ¹⁵¹, F. Pasquali ¹¹⁴, E. Pasqualucci ^{75a}, S. Passaggio ^{57b}, F. Pastore ⁹⁵, P. Pasuwan ^{47a,47b}, P. Patel ⁸⁶, U.M. Patel ⁵¹, J.R. Pater ¹⁰¹, T. Pauly ³⁶, J. Pearkes ¹⁴³, M. Pedersen ¹²⁵, R. Pedro ^{130a}, S.V. Peleganchuk ³⁷, O. Penc ³⁶, E.A. Pender ⁵², H. Peng ^{62a}, K.E. Pensi ¹⁰⁹, M. Penzin ³⁷, B.S. Peralva ^{82d}, A.P. Pereira Peixoto ⁶⁰, L. Pereira Sanchez ^{47a,47b}, D.V. Perepelitsa ^{29,ak}, E. Perez Codina ^{156a}, M. Perganti ¹⁰, L. Perini ^{71a,71b,*}, H. Pernegger ³⁶, S. Perrella ³⁶, A. Perrevoort ¹¹³, O. Perrin ⁴⁰, K. Peters ⁴⁸, R.F.Y. Peters ¹⁰¹, B.A. Petersen ³⁶, T.C. Petersen ⁴², E. Petit ¹⁰², V. Petousis ¹³², C. Petridou ^{152,f}, A. Petrukhin ¹⁴¹, M. Pettee ^{17a}, N.E. Pettersson ³⁶, A. Petukhov ³⁷, K. Petukhova ¹³³, A. Peyaud ¹³⁵, R. Pezoa ^{137f}, L. Pezzotti ³⁶, G. Pezzullo ¹⁷², T.M. Pham ¹⁷⁰, T. Pham ¹⁰⁵, P.W. Phillips ¹³⁴, M.W. Phipps ¹⁶², G. Piacquadio ¹⁴⁵, E. Pianori ^{17a}, F. Piazza ^{71a,71b}, R. Piegaia ³⁰, D. Pietreanu ^{27b}, A.D. Pilkington ¹⁰¹, M. Pinamonti ^{69a,69c}, J.L. Pinfeld ², B.C. Pinheiro Pereira ^{130a}, C. Pitman Donaldson ⁹⁶, D.A. Pizzi ³⁴, L. Pizzimento ^{76a,76b}, A. Pizzini ¹¹⁴, M.-A. Pleier ²⁹, V. Plesanovs ⁵⁴, V. Pleskot ¹³³, E. Plotnikova ³⁸, G. Poddar ⁴, R. Poettgen ⁹⁸, L. Poggioli ¹²⁷, D. Pohl ²⁴, I. Pokharel ⁵⁵, S. Polacek ¹³³, G. Polesello ^{73a}, A. Poley ^{142,156a}, R. Polifka ¹³², A. Polini ^{23b}, C.S. Pollard ¹⁶⁷, Z.B. Pollock ¹¹⁹, V. Polychronakos ²⁹, E. Pompa Pacchi ^{75a,75b}, D. Ponomarenko ¹¹³, L. Pontecorvo ³⁶, S. Popa ^{27a}, G.A. Popeneciu ^{27d}, D.M. Portillo Quintero ^{156a}, S. Pospisil ¹³², P. Postolache ^{27c}, K. Potamianos ¹²⁶, P.P. Potepa ^{85a}, I.N. Potrap ³⁸, C.J. Potter ³², H. Potti ¹, T. Poulsen ⁴⁸, J. Poveda ¹⁶³, M.E. Pozo Astigarraga ³⁶, A. Prades Ibanez ¹⁶³, M.M. Prapa ⁴⁶, J. Pretel ⁵⁴, D. Price ¹⁰¹, M. Primavera ^{70a}, M.A. Principe Martin ⁹⁹, R. Privara ¹²², M.L. Proffitt ¹³⁸, N. Proklova ¹²⁸, K. Prokofiev ^{64c}, G. Proto ^{76a,76b}, S. Protopopescu ²⁹, J. Proudfoot ⁶, M. Przybycien ^{85a}, W.W. Przygoda ^{85b}, J.E. Puddefoot ¹³⁹, D. Pudzha ³⁷, D. Pyatiizbyantseva ³⁷, J. Qian ¹⁰⁶, D. Qichen ¹⁰¹, Y. Qin ¹⁰¹, S. Qiu ^{17a}, T. Qiu ⁵², A. Quadt ⁵⁵, M. Queitsch-Maitland ¹⁰¹, G. Quetant ⁵⁶, G. Rabanal Bolanos ⁶¹, D. Rafanoharana ⁵⁴, F. Ragusa ^{71a,71b}, J.L. Rainbolt ³⁹, J.A. Raine ⁵⁶, S. Rajagopalan ²⁹, E. Ramakoti ³⁷, K. Ran ^{48,14d}, N.P. Rapheeha ^{33g}, V. Raskina ¹²⁷,

D.F. Rassloff ^{63a}, S. Rave ¹⁰⁰, B. Ravina ⁵⁵, I. Ravinovich ¹⁶⁹, M. Raymond ³⁶, A.L. Read ¹²⁵,
 N.P. Readioff ¹³⁹, D.M. Rebuzzi ^{73a,73b}, G. Redlinger ²⁹, K. Reeves ⁴⁵, J.A. Reidelsturz ¹⁷¹,
 D. Reikher ¹⁵¹, A. Rej ¹⁴¹, C. Rembser ³⁶, A. Renardi ⁴⁸, M. Renda ^{27b}, M.B. Rendel ¹¹⁰,
 F. Renner ⁴⁸, A.G. Rennie ⁵⁹, S. Resconi ^{71a}, M. Ressegotti ^{57b,57a}, E.D. Resseguie ^{17a},
 S. Rettie ³⁶, J.G. Reyes Rivera ¹⁰⁷, B. Reynolds ¹¹⁹, E. Reynolds ^{17a}, M. Rezaei Estabragh ¹⁷¹,
 O.L. Rezanova ³⁷, P. Reznicek ¹³³, N. Ribaric ⁹¹, E. Ricci ^{78a,78b}, R. Richter ¹¹⁰,
 S. Richter ^{47a,47b}, E. Richter-Was ^{85b}, M. Ridel ¹²⁷, S. Ridouani ^{35d}, P. Rieck ¹¹⁷, P. Riedler ³⁶,
 M. Rijssenbeek ¹⁴⁵, A. Rimoldi ^{73a,73b}, M. Rimoldi ⁴⁸, L. Rinaldi ^{23b,23a}, T.T. Rinn ²⁹,
 M.P. Rinnagel ¹⁰⁹, G. Ripellino ¹⁶¹, I. Riu ¹³, P. Rivadeneira ⁴⁸, J.C. Rivera Vergara ¹⁶⁵,
 F. Rizatdinova ¹²¹, E. Rizvi ⁹⁴, C. Rizzi ⁵⁶, B.A. Roberts ¹⁶⁷, B.R. Roberts ^{17a},
 S.H. Robertson ^{104,y}, M. Robin ⁴⁸, D. Robinson ³², C.M. Robles Gajardo ^{137f},
 M. Robles Manzano ¹⁰⁰, A. Robson ⁵⁹, A. Rocchi ^{76a,76b}, C. Roda ^{74a,74b}, S. Rodriguez Bosca ^{63a},
 Y. Rodriguez Garcia ^{22a}, A. Rodriguez Rodriguez ⁵⁴, A.M. Rodríguez Vera ^{156b}, S. Roe ³⁶,
 J.T. Roemer ¹⁶⁰, A.R. Roepe-Gier ¹³⁶, J. Roggel ¹⁷¹, O. Røhne ¹²⁵, R.A. Rojas ¹⁰³,
 B. Roland ⁵⁴, C.P.A. Roland ⁶⁸, J. Roloff ²⁹, A. Romaniouk ³⁷, E. Romano ^{73a,73b},
 M. Romano ^{23b}, A.C. Romero Hernandez ¹⁶², N. Rompotis ⁹², L. Roos ¹²⁷, S. Rosati ^{75a},
 B.J. Rosser ³⁹, E. Rossi ⁴, E. Rossi ^{72a,72b}, L.P. Rossi ^{57b}, L. Rossini ⁴⁸, R. Rosten ¹¹⁹,
 M. Rotaru ^{27b}, B. Rottler ⁵⁴, C. Rougier ^{102,ac}, D. Rousseau ⁶⁶, D. Rousso ³², G. Rovelli ^{73a,73b},
 A. Roy ¹⁶², S. Roy-Garand ¹⁵⁵, A. Rozanov ¹⁰², Y. Rozen ¹⁵⁰, X. Ruan ^{33g},
 A. Rubio Jimenez ¹⁶³, A.J. Ruby ⁹², V.H. Ruelas Rivera ¹⁸, T.A. Ruggeri ¹, F. Rühr ⁵⁴,
 A. Ruiz-Martinez ¹⁶³, A. Rummler ³⁶, Z. Rurikova ⁵⁴, N.A. Rusakovich ³⁸, H.L. Russell ¹⁶⁵,
 J.P. Rutherford ⁷, K. Rybacki ⁹¹, M. Rybar ¹³³, E.B. Rye ¹²⁵, A. Ryzhov ³⁷,
 J.A. Sabater Iglesias ⁵⁶, P. Sabatini ¹⁶³, L. Sabetta ^{75a,75b}, H.F-W. Sadrozinski ¹³⁶,
 F. Safai Tehrani ^{75a}, B. Safarzadeh Samani ¹⁴⁶, M. Safdari ¹⁴³, S. Saha ¹⁰⁴, M. Sahinsoy ¹¹⁰,
 M. Saimpert ¹³⁵, M. Saito ¹⁵³, T. Saito ¹⁵³, D. Salamani ³⁶, A. Salnikov ¹⁴³, J. Salt ¹⁶³,
 A. Salvador Salas ¹³, D. Salvatore ^{43b,43a}, F. Salvatore ¹⁴⁶, A. Salzburger ³⁶, D. Sammel ⁵⁴,
 D. Sampsonidis ^{152,f}, D. Sampsonidou ^{62d,62c}, J. Sánchez ¹⁶³, A. Sanchez Pineda ⁴,
 V. Sanchez Sebastian ¹⁶³, H. Sandaker ¹²⁵, C.O. Sander ⁴⁸, J.A. Sandesara ¹⁰³, M. Sandhoff ¹⁷¹,
 C. Sandoval ^{22b}, D.P.C. Sankey ¹³⁴, T. Sano ⁸⁷, A. Sansoni ⁵³, L. Santi ^{75a,75b}, C. Santoni ⁴⁰,
 H. Santos ^{130a,130b}, S.N. Santpur ^{17a}, A. Santra ¹⁶⁹, K.A. Saoucha ¹³⁹, J.G. Saraiva ^{130a,130d},
 J. Sardain ⁷, O. Sasaki ⁸³, K. Sato ¹⁵⁷, C. Sauer ^{63b}, F. Sauerburger ⁵⁴, E. Sauvan ⁴,
 P. Savard ^{155,ah}, R. Sawada ¹⁵³, C. Sawyer ¹³⁴, L. Sawyer ⁹⁷, I. Sayago Galvan ¹⁶³, C. Sbarra ^{23b},
 A. Sbrizzi ^{23b,23a}, T. Scanlon ⁹⁶, J. Schaarschmidt ¹³⁸, P. Schacht ¹¹⁰, D. Schaefer ³⁹,
 U. Schäfer ¹⁰⁰, A.C. Schaffer ^{66,44}, D. Schaile ¹⁰⁹, R.D. Schamberger ¹⁴⁵, E. Schanet ¹⁰⁹,
 C. Scharf ¹⁸, M.M. Schefer ¹⁹, V.A. Schegelsky ³⁷, D. Scheirich ¹³³, F. Schenck ¹⁸,
 M. Schernau ¹⁶⁰, C. Scheulen ⁵⁵, C. Schiavi ^{57b,57a}, Z.M. Schillaci ²⁶, E.J. Schioppa ^{70a,70b},
 M. Schioppa ^{43b,43a}, B. Schlag ¹⁰⁰, K.E. Schleicher ⁵⁴, S. Schlenker ³⁶, J. Schmeing ¹⁷¹,
 M.A. Schmidt ¹⁷¹, K. Schmieden ¹⁰⁰, C. Schmitt ¹⁰⁰, S. Schmitt ⁴⁸, L. Schoeffel ¹³⁵,
 A. Schoening ^{63b}, P.G. Scholer ⁵⁴, E. Schopf ¹²⁶, M. Schott ¹⁰⁰, J. Schovancova ³⁶,
 S. Schramm ⁵⁶, F. Schroeder ¹⁷¹, H-C. Schultz-Coulon ^{63a}, M. Schumacher ⁵⁴, B.A. Schumm ¹³⁶,
 Ph. Schune ¹³⁵, H.R. Schwartz ¹³⁶, A. Schwartzman ¹⁴³, T.A. Schwarz ¹⁰⁶, Ph. Schwemling ¹³⁵,
 R. Schwienhorst ¹⁰⁷, A. Sciandra ¹³⁶, G. Sciolla ²⁶, F. Scuri ^{74a}, F. Scutti ¹⁰⁵, C.D. Sebastiani ⁹²,
 K. Sedlaczek ⁴⁹, P. Seema ¹⁸, S.C. Seidel ¹¹², A. Seiden ¹³⁶, B.D. Seidlitz ⁴¹, C. Seitz ⁴⁸,
 J.M. Seixas ^{82b}, G. Sekhniaidze ^{72a}, S.J. Sekula ⁴⁴, L. Selem ⁴, N. Semprini-Cesari ^{23b,23a},
 S. Sen ⁵¹, D. Sengupta ⁵⁶, V. Senthilkumar ¹⁶³, L. Serin ⁶⁶, L. Serkin ^{69a,69b}, M. Sessa ^{77a,77b},
 H. Severini ¹²⁰, F. Sforza ^{57b,57a}, A. Sfyrta ⁵⁶, E. Shabalina ⁵⁵, R. Shaheen ¹⁴⁴,
 J.D. Shahinian ¹²⁸, D. Shaked Renous ¹⁶⁹, L.Y. Shan ^{14a}, M. Shapiro ^{17a}, A. Sharma ³⁶,

A.S. Sharma ¹⁶⁴, P. Sharma ⁸⁰, S. Sharma ⁴⁸, P.B. Shatalov ³⁷, K. Shaw ¹⁴⁶, S.M. Shaw ¹⁰¹,
 Q. Shen ^{62c,5}, P. Sherwood ⁹⁶, L. Shi ⁹⁶, C.O. Shimmin ¹⁷², Y. Shimogama ¹⁶⁸, J.D. Shinner ⁹⁵,
 I.P.J. Shipsey ¹²⁶, S. Shirabe ⁶⁰, M. Shiyakova ³⁸, J. Shlomi ¹⁶⁹, M.J. Shochet ³⁹, J. Shojaii ¹⁰⁵,
 D.R. Shope ¹²⁵, S. Shrestha ^{119,al}, E.M. Shrif ^{33g}, M.J. Shroff ¹⁶⁵, P. Sicho ¹³¹,
 A.M. Sickles ¹⁶², E. Sideras Haddad ^{33g}, A. Sidoti ^{23b}, F. Siegert ⁵⁰, Dj. Sijacki ¹⁵,
 R. Sikora ^{85a}, F. Sili ⁹⁰, J.M. Silva ²⁰, M.V. Silva Oliveira ³⁶, S.B. Silverstein ^{47a}, S. Simion ⁶⁶,
 R. Simoniello ³⁶, E.L. Simpson ⁵⁹, H. Simpson ¹⁴⁶, L.R. Simpson ¹⁰⁶, N.D. Simpson ⁹⁸,
 S. Simsek ^{21d}, S. Sindhu ⁵⁵, P. Sinervo ¹⁵⁵, S. Singh ¹⁴², S. Singh ¹⁵⁵, S. Sinha ⁴⁸,
 S. Sinha ^{33g}, M. Sioli ^{23b,23a}, I. Siral ³⁶, S. Yu. Sivoklov ^{37,*}, J. Sjölin ^{47a,47b}, A. Skaf ⁵⁵,
 E. Skorda ⁹⁸, P. Skubic ¹²⁰, M. Slawinska ⁸⁶, V. Smakhtin ¹⁶⁹, B.H. Smart ¹³⁴, J. Smiesko ³⁶,
 S. Yu. Smirnov ³⁷, Y. Smirnov ³⁷, L.N. Smirnova ^{37,a}, O. Smirnova ⁹⁸, A.C. Smith ⁴¹,
 E.A. Smith ³⁹, H.A. Smith ¹²⁶, J.L. Smith ⁹², R. Smith ¹⁴³, M. Smizanska ⁹¹, K. Smolek ¹³²,
 A. Smykiewicz ⁸⁶, A.A. Snesarev ³⁷, H.L. Snoek ¹¹⁴, S. Snyder ²⁹, R. Sobie ^{165,y}, A. Soffer ¹⁵¹,
 C.A. Solans Sanchez ³⁶, E. Yu. Soldatov ³⁷, U. Soldevila ¹⁶³, A.A. Solodkov ³⁷, S. Solomon ⁵⁴,
 A. Soloshenko ³⁸, K. Solovieva ⁵⁴, O.V. Solovyanov ⁴⁰, V. Solovyev ³⁷, P. Sommer ³⁶,
 A. Sonay ¹³, W.Y. Song ^{156b}, J.M. Sonneveld ¹¹⁴, A. Sopczak ¹³², A.L. Sopio ⁹⁶,
 F. Sopkova ^{28b}, V. Sothilingam ^{63a}, S. Sottocornola ⁶⁸, R. Soualah ^{116b}, Z. Soumami ^{35e},
 D. South ⁴⁸, S. Spagnolo ^{70a,70b}, M. Spalla ¹¹⁰, D. Sperlich ⁵⁴, G. Spigo ³⁶, M. Spina ¹⁴⁶,
 S. Spinali ⁹¹, D.P. Spiteri ⁵⁹, M. Spousta ¹³³, E.J. Staats ³⁴, A. Stabile ^{71a,71b}, R. Stamen ^{63a},
 M. Stamenkovic ¹¹⁴, A. Stampekis ²⁰, M. Standke ²⁴, E. Stanecka ⁸⁶, M.V. Stange ⁵⁰,
 B. Stanislaus ^{17a}, M.M. Stanitzki ⁴⁸, M. Stankaityte ¹²⁶, B. Stapf ⁴⁸, E.A. Starchenko ³⁷,
 G.H. Stark ¹³⁶, J. Stark ^{102,ac}, D.M. Starke ^{156b}, P. Staroba ¹³¹, P. Starovoitov ^{63a}, S. Stärz ¹⁰⁴,
 R. Staszewski ⁸⁶, G. Stavropoulos ⁴⁶, J. Steentoft ¹⁶¹, P. Steinberg ²⁹, B. Stelzer ^{142,156a},
 H.J. Stelzer ¹²⁹, O. Stelzer-Chilton ^{156a}, H. Stenzel ⁵⁸, T.J. Stevenson ¹⁴⁶, G.A. Stewart ³⁶,
 J.R. Stewart ¹²¹, M.C. Stockton ³⁶, G. Stoica ^{27b}, M. Stolarski ^{130a}, S. Stonjek ¹¹⁰,
 A. Straessner ⁵⁰, J. Strandberg ¹⁴⁴, S. Strandberg ^{47a,47b}, M. Strauss ¹²⁰, T. Strebler ¹⁰²,
 P. Strizenc ^{28b}, R. Ströhmer ¹⁶⁶, D.M. Strom ¹²³, L.R. Strom ⁴⁸, R. Stroynowski ⁴⁴,
 A. Strubig ^{47a,47b}, S.A. Stucci ²⁹, B. Stugu ¹⁶, J. Stupak ¹²⁰, N.A. Styles ⁴⁸, D. Su ¹⁴³,
 S. Su ^{62a}, W. Su ^{62d,138,62c}, X. Su ^{62a,66}, K. Sugizaki ¹⁵³, V.V. Sulim ³⁷, M.J. Sullivan ⁹²,
 D.M.S. Sultan ^{78a,78b}, L. Sultanaliyeva ³⁷, S. Sultansoy ^{3b}, T. Sumida ⁸⁷, S. Sun ¹⁰⁶, S. Sun ¹⁷⁰,
 O. Sunneborn Gudnadottir ¹⁶¹, M.R. Sutton ¹⁴⁶, M. Svatos ¹³¹, M. Swiatlowski ^{156a},
 T. Swirski ¹⁶⁶, I. Sykora ^{28a}, M. Sykora ¹³³, T. Sykora ¹³³, D. Ta ¹⁰⁰, K. Tackmann ^{48,w},
 A. Taffard ¹⁶⁰, R. Tafirout ^{156a}, J.S. Tafoya Vargas ⁶⁶, R.H.M. Taibah ¹²⁷, R. Takashima ⁸⁸,
 E.P. Takeva ⁵², Y. Takubo ⁸³, M. Talby ¹⁰², A.A. Talyshev ³⁷, K.C. Tam ^{64b}, N.M. Tamir ¹⁵¹,
 A. Tanaka ¹⁵³, J. Tanaka ¹⁵³, R. Tanaka ⁶⁶, M. Tanasini ^{57b,57a}, J. Tang ^{62c}, Z. Tao ¹⁶⁴,
 S. Tapia Araya ^{137f}, S. Tapprogge ¹⁰⁰, A. Tarek Abouelfadl Mohamed ¹⁰⁷, S. Tarem ¹⁵⁰,
 K. Tariq ^{62b}, G. Tarna ^{102,27b}, G.F. Tartarelli ^{71a}, P. Tas ¹³³, M. Tasevsky ¹³¹, E. Tassi ^{43b,43a},
 A.C. Tate ¹⁶², G. Tateno ¹⁵³, Y. Tayalati ^{35e,x}, G.N. Taylor ¹⁰⁵, W. Taylor ^{156b}, H. Teagle ⁹²,
 A.S. Tee ¹⁷⁰, R. Teixeira De Lima ¹⁴³, P. Teixeira-Dias ⁹⁵, J.J. Teoh ¹⁵⁵, K. Terashi ¹⁵³,
 J. Terron ⁹⁹, S. Terzo ¹³, M. Testa ⁵³, R.J. Teuscher ^{155,y}, A. Thaler ⁷⁹, O. Theiner ⁵⁶,
 N. Themistokleous ⁵², T. Thevenaux-Pelzer ¹⁰², O. Thielmann ¹⁷¹, D.W. Thomas ⁹⁵,
 J.P. Thomas ²⁰, E.A. Thompson ^{17a}, P.D. Thompson ²⁰, E. Thomson ¹²⁸, E.J. Thorpe ⁹⁴,
 Y. Tian ⁵⁵, V. Tikhomirov ^{37,a}, Yu.A. Tikhonov ³⁷, S. Timoshenko ³⁷, E.X.L. Ting ¹, P. Tipton ¹⁷²,
 S.H. Tlou ^{33g}, A. Tnourji ⁴⁰, K. Todome ^{23b,23a}, S. Todorova-Nova ¹³³, S. Todt ⁵⁰, M. Togawa ⁸³,
 J. Tojo ⁸⁹, S. Tokár ^{28a}, K. Tokushuku ⁸³, O. Toldaiev ⁶⁸, R. Tombs ³², M. Tomoto ^{83,111},
 L. Tompkins ^{143,q}, K.W. Topolnicki ^{85b}, P. Tornambe ¹⁰³, E. Torrence ¹²³, H. Torres ⁵⁰,
 E. Torró Pastor ¹⁶³, M. Toscani ³⁰, C. Toscirri ³⁹, M. Tost ¹¹, D.R. Tovey ¹³⁹, A. Traeet ¹⁶,

I.S. Trandafir ^{27b}, T. Trefzger ¹⁶⁶, A. Tricoli ²⁹, I.M. Trigger ^{156a}, S. Trincaz-Duvoid ¹²⁷,
 D.A. Trischuk ²⁶, B. Trocmé ⁶⁰, C. Troncon ^{71a}, L. Truong ^{33c}, M. Trzebinski ⁸⁶, A. Trzupek ⁸⁶,
 F. Tsai ¹⁴⁵, M. Tsai ¹⁰⁶, A. Tsiamis ^{152,f}, P.V. Tsiarehka ³⁷, S. Tsigaridas ^{156a}, A. Tsigiridis ^{152,u},
 V. Tsiskaridze ¹⁴⁵, E.G. Tskhadadze ^{149a}, M. Tsopoulou ^{152,f}, Y. Tsujikawa ⁸⁷, I.I. Tsukerman ³⁷,
 V. Tsulaia ^{17a}, S. Tsuno ⁸³, O. Tsur ¹⁵⁰, D. Tsybychev ¹⁴⁵, Y. Tu ^{64b}, A. Tudorache ^{27b},
 V. Tudorache ^{27b}, A.N. Tuna ³⁶, S. Turchikhin ³⁸, I. Turk Cakir ^{3a}, R. Turra ^{71a},
 T. Turtuvshin ^{38,z}, P.M. Tuts ⁴¹, S. Tzamarias ^{152,f}, P. Tzanis ¹⁰, E. Tzovara ¹⁰⁰, K. Uchida ¹⁵³,
 F. Ukegawa ¹⁵⁷, P.A. Ulloa Poblete ^{137c}, E.N. Umaka ²⁹, G. Unal ³⁶, M. Unal ¹¹, A. Undrus ²⁹,
 G. Unel ¹⁶⁰, J. Urban ^{28b}, P. Urquijo ¹⁰⁵, G. Usai ⁸, R. Ushioda ¹⁵⁴, M. Usman ¹⁰⁸,
 Z. Uysal ^{21b}, L. Vacavant ¹⁰², V. Vacek ¹³², B. Vachon ¹⁰⁴, K.O.H. Vadla ¹²⁵, T. Vafeiadis ³⁶,
 A. Vaitkus ⁹⁶, C. Valderanis ¹⁰⁹, E. Valdes Santurio ^{47a,47b}, M. Valente ^{156a}, S. Valentinetti ^{23b,23a},
 A. Valero ¹⁶³, A. Vallier ^{102,ac}, J.A. Valls Ferrer ¹⁶³, D.R. Van Arneeman ¹¹⁴, T.R. Van Daalen ¹³⁸,
 P. Van Gemmeren ⁶, M. Van Rijnbach ^{125,36}, S. Van Stroud ⁹⁶, I. Van Vulpen ¹¹⁴,
 M. Vanadia ^{76a,76b}, W. Vandelli ³⁶, M. Vandenbroucke ¹³⁵, E.R. Vandewall ¹²¹, D. Vannicola ¹⁵¹,
 L. Vannoli ^{57b,57a}, R. Vari ^{75a}, E.W. Varnes ⁷, C. Varni ^{17a}, T. Varol ¹⁴⁸, D. Varouchas ⁶⁶,
 L. Varriale ¹⁶³, K.E. Varvell ¹⁴⁷, M.E. Vasile ^{27b}, L. Vaslin ⁴⁰, G.A. Vasquez ¹⁶⁵, F. Vazeille ⁴⁰,
 T. Vazquez Schroeder ³⁶, J. Veatch ³¹, V. Vecchio ¹⁰¹, M.J. Veen ¹⁰³, I. Veliscek ¹²⁶,
 L.M. Veloce ¹⁵⁵, F. Veloso ^{130a,130c}, S. Veneziano ^{75a}, A. Ventura ^{70a,70b}, A. Verbytskyi ¹¹⁰,
 M. Verducci ^{74a,74b}, C. Vergis ²⁴, M. Verissimo De Araujo ^{82b}, W. Verkerke ¹¹⁴,
 J.C. Vermeulen ¹¹⁴, C. Vernieri ¹⁴³, P.J. Verschuuren ⁹⁵, M. Vessella ¹⁰³, M.C. Vetterli ^{142,ah},
 A. Vgenopoulos ^{152,f}, N. Viaux Maira ^{137f}, T. Vickey ¹³⁹, O.E. Vickey Boeriu ¹³⁹,
 G.H.A. Viehhauser ¹²⁶, L. Vigani ^{63b}, M. Villa ^{23b,23a}, M. Villaplana Perez ¹⁶³, E.M. Villhauer ⁵²,
 E. Vilucchi ⁵³, M.G. Vincter ³⁴, G.S. Virdee ²⁰, A. Vishwakarma ⁵², C. Vittori ³⁶,
 I. Vivarelli ¹⁴⁶, V. Vladimirov ¹⁶⁷, E. Voevodina ¹¹⁰, F. Vogel ¹⁰⁹, P. Vokac ¹³², J. Von Ahnen ⁴⁸,
 E. Von Toerne ²⁴, B. Vormwald ³⁶, V. Vorobel ¹³³, K. Vorobev ³⁷, M. Vos ¹⁶³, K. Voss ¹⁴¹,
 J.H. Vossebeld ⁹², M. Vozak ¹¹⁴, L. Vozdecky ⁹⁴, N. Vranjes ¹⁵, M. Vranjes Milosavljevic ¹⁵,
 M. Vreeswijk ¹¹⁴, R. Vuillermet ³⁶, O. Vujinovic ¹⁰⁰, I. Vukotic ³⁹, S. Wada ¹⁵⁷, C. Wagner ¹⁰³,
 J.M. Wagner ^{17a}, W. Wagner ¹⁷¹, S. Wahdan ¹⁷¹, H. Wahlberg ⁹⁰, R. Wakasa ¹⁵⁷,
 M. Wakida ¹¹¹, J. Walder ¹³⁴, R. Walker ¹⁰⁹, W. Walkowiak ¹⁴¹, A.M. Wang ⁶¹, A.Z. Wang ¹⁷⁰,
 C. Wang ¹⁰⁰, C. Wang ^{62c}, H. Wang ^{17a}, J. Wang ^{64a}, R.-J. Wang ¹⁰⁰, R. Wang ⁶¹, R. Wang ⁶,
 S.M. Wang ¹⁴⁸, S. Wang ^{62b}, T. Wang ^{62a}, W.T. Wang ⁸⁰, X. Wang ^{14c}, X. Wang ¹⁶²,
 X. Wang ^{62c}, Y. Wang ^{62d}, Y. Wang ^{14c}, Z. Wang ¹⁰⁶, Z. Wang ^{62d,51,62c}, Z. Wang ¹⁰⁶,
 A. Warburton ¹⁰⁴, R.J. Ward ²⁰, N. Warrack ⁵⁹, A.T. Watson ²⁰, H. Watson ⁵⁹, M.F. Watson ²⁰,
 G. Watts ¹³⁸, B.M. Waugh ⁹⁶, C. Weber ²⁹, H.A. Weber ¹⁸, M.S. Weber ¹⁹, S.M. Weber ^{63a},
 C. Wei ^{62a}, Y. Wei ¹²⁶, A.R. Weidberg ¹²⁶, E.J. Weik ¹¹⁷, J. Weingarten ⁴⁹, M. Weirich ¹⁰⁰,
 C. Weiser ⁵⁴, C.J. Wells ⁴⁸, T. Wenaus ²⁹, B. Wendland ⁴⁹, T. Wengler ³⁶, N.S. Wenke ¹¹⁰,
 N. Wermes ²⁴, M. Wessels ^{63a}, K. Whalen ¹²³, A.M. Wharton ⁹¹, A.S. White ⁶¹, A. White ⁸,
 M.J. White ¹, D. Whiteson ¹⁶⁰, L. Wickremasinghe ¹²⁴, W. Wiedenmann ¹⁷⁰, C. Wiel ⁵⁰,
 M. Wielers ¹³⁴, C. Wigglesworth ⁴², L.A.M. Wiik-Fuchs ⁵⁴, D.J. Wilbern ¹²⁰, H.G. Wilkens ³⁶,
 D.M. Williams ⁴¹, H.H. Williams ¹²⁸, S. Williams ³², S. Willocq ¹⁰³, B.J. Wilson ¹⁰¹,
 P.J. Windischhofer ³⁹, F. Winklmeier ¹²³, B.T. Winter ⁵⁴, J.K. Winter ¹⁰¹, M. Wittgen ¹⁴³,
 M. Wobisch ⁹⁷, R. Wölker ¹²⁶, J. Wollrath ¹⁶⁰, M.W. Wolter ⁸⁶, H. Wolters ^{130a,130c},
 V.W.S. Wong ¹⁶⁴, A.F. Wongel ⁴⁸, S.D. Worm ⁴⁸, B.K. Wosiek ⁸⁶, K.W. Woźniak ⁸⁶,
 K. Wraight ⁵⁹, J. Wu ^{14a,14d}, M. Wu ^{64a}, M. Wu ¹¹³, S.L. Wu ¹⁷⁰, X. Wu ⁵⁶, Y. Wu ^{62a},
 Z. Wu ^{135,62a}, J. Wuerzinger ¹¹⁰, T.R. Wyatt ¹⁰¹, B.M. Wynne ⁵², S. Xella ⁴², L. Xia ^{14c},
 M. Xia ^{14b}, J. Xiang ^{64c}, X. Xiao ¹⁰⁶, M. Xie ^{62a}, X. Xie ^{62a}, S. Xin ^{14a,14d}, J. Xiong ^{17a},
 I. Xiotidis ¹⁴⁶, D. Xu ^{14a}, H. Xu ^{62a}, H. Xu ^{62a}, L. Xu ^{62a}, R. Xu ¹²⁸, T. Xu ¹⁰⁶, Y. Xu ^{14b},

Z. Xu , Z. Xu , B. Yabsley , S. Yacoob , N. Yamaguchi , Y. Yamaguchi , H. Yamauchi , T. Yamazaki , Y. Yamazaki , J. Yan , S. Yan , Z. Yan , H.J. Yang , H.T. Yang , S. Yang , T. Yang , X. Yang , X. Yang , Y. Yang , Y. Yang , Z. Yang , W.-M. Yao , Y.C. Yap , H. Ye , H. Ye , J. Ye , S. Ye , X. Ye , Y. Yeh , I. Yeletsikh , B.K. Yeo , M.R. Yexley , P. Yin , K. Yorita , S. Younas , C.J.S. Young , C. Young , Y. Yu , M. Yuan , R. Yuan , L. Yue , M. Zaazoua , B. Zabinski , E. Zaid , T. Zakareishvili , N. Zakharchuk , S. Zambito , J.A. Zamora Saa , J. Zang , D. Zanzi , O. Zaplatilek , C. Zeitnitz , H. Zeng , J.C. Zeng , D.T. Zenger Jr , O. Zenin , T. Ženiš , S. Zenz , S. Zerradi , D. Zerwas , M. Zhai , B. Zhang , D.F. Zhang , J. Zhang , J. Zhang , K. Zhang , L. Zhang , P. Zhang , R. Zhang , S. Zhang , T. Zhang , X. Zhang , X. Zhang , Y. Zhang , Z. Zhang , Z. Zhang , H. Zhao , P. Zhao , T. Zhao , Y. Zhao , Z. Zhao , A. Zhemchugov , X. Zheng , Z. Zheng , D. Zhong , B. Zhou , C. Zhou , H. Zhou , N. Zhou , Y. Zhou , C.G. Zhu , H.L. Zhu , J. Zhu , Y. Zhu , Y. Zhu , X. Zhuang , K. Zhukov , V. Zhulanov , N.I. Zimine , J. Zinsser , M. Ziolkowski , L. Živković , A. Zoccoli , K. Zoch , T.G. Zorbas , O. Zormpa , W. Zou , L. Zwalinski .

¹Department of Physics, University of Adelaide, Adelaide; Australia.

²Department of Physics, University of Alberta, Edmonton AB; Canada.

³(^a)Department of Physics, Ankara University, Ankara; (^b)Division of Physics, TOBB University of Economics and Technology, Ankara; Türkiye.

⁴LAPP, Université Savoie Mont Blanc, CNRS/IN2P3, Annecy; France.

⁵APC, Université Paris Cité, CNRS/IN2P3, Paris; France.

⁶High Energy Physics Division, Argonne National Laboratory, Argonne IL; United States of America.

⁷Department of Physics, University of Arizona, Tucson AZ; United States of America.

⁸Department of Physics, University of Texas at Arlington, Arlington TX; United States of America.

⁹Physics Department, National and Kapodistrian University of Athens, Athens; Greece.

¹⁰Physics Department, National Technical University of Athens, Zografou; Greece.

¹¹Department of Physics, University of Texas at Austin, Austin TX; United States of America.

¹²Institute of Physics, Azerbaijan Academy of Sciences, Baku; Azerbaijan.

¹³Institut de Física d'Altes Energies (IFAE), Barcelona Institute of Science and Technology, Barcelona; Spain.

¹⁴(^a)Institute of High Energy Physics, Chinese Academy of Sciences, Beijing; (^b)Physics Department, Tsinghua University, Beijing; (^c)Department of Physics, Nanjing University, Nanjing; (^d)University of Chinese Academy of Science (UCAS), Beijing; China.

¹⁵Institute of Physics, University of Belgrade, Belgrade; Serbia.

¹⁶Department for Physics and Technology, University of Bergen, Bergen; Norway.

¹⁷(^a)Physics Division, Lawrence Berkeley National Laboratory, Berkeley CA; (^b)University of California, Berkeley CA; United States of America.

¹⁸Institut für Physik, Humboldt Universität zu Berlin, Berlin; Germany.

¹⁹Albert Einstein Center for Fundamental Physics and Laboratory for High Energy Physics, University of Bern, Bern; Switzerland.

²⁰School of Physics and Astronomy, University of Birmingham, Birmingham; United Kingdom.

²¹(^a)Department of Physics, Bogazici University, Istanbul; (^b)Department of Physics Engineering, Gaziantep University, Gaziantep; (^c)Department of Physics, Istanbul University, Istanbul; (^d)Istinye

University, Sariyer, Istanbul; Türkiye.

^{22(a)}Facultad de Ciencias y Centro de Investigaciones, Universidad Antonio Nariño, Bogotá;^(b)Departamento de Física, Universidad Nacional de Colombia, Bogotá; Colombia.

^{23(a)}Dipartimento di Fisica e Astronomia A. Righi, Università di Bologna, Bologna;^(b)INFN Sezione di Bologna; Italy.

²⁴Physikalisches Institut, Universität Bonn, Bonn; Germany.

²⁵Department of Physics, Boston University, Boston MA; United States of America.

²⁶Department of Physics, Brandeis University, Waltham MA; United States of America.

^{27(a)}Transilvania University of Brasov, Brasov;^(b)Horia Hulubei National Institute of Physics and Nuclear Engineering, Bucharest;^(c)Department of Physics, Alexandru Ioan Cuza University of Iasi, Iasi;^(d)National Institute for Research and Development of Isotopic and Molecular Technologies, Physics Department, Cluj-Napoca;^(e)University Politehnica Bucharest, Bucharest;^(f)West University in Timisoara, Timisoara;^(g)Faculty of Physics, University of Bucharest, Bucharest; Romania.

^{28(a)}Faculty of Mathematics, Physics and Informatics, Comenius University, Bratislava;^(b)Department of Subnuclear Physics, Institute of Experimental Physics of the Slovak Academy of Sciences, Kosice; Slovak Republic.

²⁹Physics Department, Brookhaven National Laboratory, Upton NY; United States of America.

³⁰Universidad de Buenos Aires, Facultad de Ciencias Exactas y Naturales, Departamento de Física, y CONICET, Instituto de Física de Buenos Aires (IFIBA), Buenos Aires; Argentina.

³¹California State University, CA; United States of America.

³²Cavendish Laboratory, University of Cambridge, Cambridge; United Kingdom.

^{33(a)}Department of Physics, University of Cape Town, Cape Town;^(b)iThemba Labs, Western Cape;^(c)Department of Mechanical Engineering Science, University of Johannesburg, Johannesburg;^(d)National Institute of Physics, University of the Philippines Diliman (Philippines);^(e)University of South Africa, Department of Physics, Pretoria;^(f)University of Zululand, KwaDlangezwa;^(g)School of Physics, University of the Witwatersrand, Johannesburg; South Africa.

³⁴Department of Physics, Carleton University, Ottawa ON; Canada.

^{35(a)}Faculté des Sciences Ain Chock, Réseau Universitaire de Physique des Hautes Energies - Université Hassan II, Casablanca;^(b)Faculté des Sciences, Université Ibn-Tofail, Kénitra;^(c)Faculté des Sciences Semlalia, Université Cadi Ayyad, LPHEA-Marrakech;^(d)LPMR, Faculté des Sciences, Université Mohamed Premier, Oujda;^(e)Faculté des sciences, Université Mohammed V, Rabat;^(f)Institute of Applied Physics, Mohammed VI Polytechnic University, Ben Guerir; Morocco.

³⁶CERN, Geneva; Switzerland.

³⁷Affiliated with an institute covered by a cooperation agreement with CERN.

³⁸Affiliated with an international laboratory covered by a cooperation agreement with CERN.

³⁹Enrico Fermi Institute, University of Chicago, Chicago IL; United States of America.

⁴⁰LPC, Université Clermont Auvergne, CNRS/IN2P3, Clermont-Ferrand; France.

⁴¹Nevis Laboratory, Columbia University, Irvington NY; United States of America.

⁴²Niels Bohr Institute, University of Copenhagen, Copenhagen; Denmark.

^{43(a)}Dipartimento di Fisica, Università della Calabria, Rende;^(b)INFN Gruppo Collegato di Cosenza, Laboratori Nazionali di Frascati; Italy.

⁴⁴Physics Department, Southern Methodist University, Dallas TX; United States of America.

⁴⁵Physics Department, University of Texas at Dallas, Richardson TX; United States of America.

⁴⁶National Centre for Scientific Research "Demokritos", Agia Paraskevi; Greece.

^{47(a)}Department of Physics, Stockholm University;^(b)Oskar Klein Centre, Stockholm; Sweden.

⁴⁸Deutsches Elektronen-Synchrotron DESY, Hamburg and Zeuthen; Germany.

⁴⁹Fakultät Physik, Technische Universität Dortmund, Dortmund; Germany.

- ⁵⁰Institut für Kern- und Teilchenphysik, Technische Universität Dresden, Dresden; Germany.
- ⁵¹Department of Physics, Duke University, Durham NC; United States of America.
- ⁵²SUPA - School of Physics and Astronomy, University of Edinburgh, Edinburgh; United Kingdom.
- ⁵³INFN e Laboratori Nazionali di Frascati, Frascati; Italy.
- ⁵⁴Physikalisches Institut, Albert-Ludwigs-Universität Freiburg, Freiburg; Germany.
- ⁵⁵II. Physikalisches Institut, Georg-August-Universität Göttingen, Göttingen; Germany.
- ⁵⁶Département de Physique Nucléaire et Corpusculaire, Université de Genève, Genève; Switzerland.
- ⁵⁷(^a)Dipartimento di Fisica, Università di Genova, Genova;(^b)INFN Sezione di Genova; Italy.
- ⁵⁸II. Physikalisches Institut, Justus-Liebig-Universität Giessen, Giessen; Germany.
- ⁵⁹SUPA - School of Physics and Astronomy, University of Glasgow, Glasgow; United Kingdom.
- ⁶⁰LPSC, Université Grenoble Alpes, CNRS/IN2P3, Grenoble INP, Grenoble; France.
- ⁶¹Laboratory for Particle Physics and Cosmology, Harvard University, Cambridge MA; United States of America.
- ⁶²(^a)Department of Modern Physics and State Key Laboratory of Particle Detection and Electronics, University of Science and Technology of China, Hefei;(^b)Institute of Frontier and Interdisciplinary Science and Key Laboratory of Particle Physics and Particle Irradiation (MOE), Shandong University, Qingdao;(^c)School of Physics and Astronomy, Shanghai Jiao Tong University, Key Laboratory for Particle Astrophysics and Cosmology (MOE), SKLPPC, Shanghai;(^d)Tsun-Dao Lee Institute, Shanghai; China.
- ⁶³(^a)Kirchhoff-Institut für Physik, Ruprecht-Karls-Universität Heidelberg, Heidelberg;(^b)Physikalisches Institut, Ruprecht-Karls-Universität Heidelberg, Heidelberg; Germany.
- ⁶⁴(^a)Department of Physics, Chinese University of Hong Kong, Shatin, N.T., Hong Kong;(^b)Department of Physics, University of Hong Kong, Hong Kong;(^c)Department of Physics and Institute for Advanced Study, Hong Kong University of Science and Technology, Clear Water Bay, Kowloon, Hong Kong; China.
- ⁶⁵Department of Physics, National Tsing Hua University, Hsinchu; Taiwan.
- ⁶⁶IJCLab, Université Paris-Saclay, CNRS/IN2P3, 91405, Orsay; France.
- ⁶⁷Centro Nacional de Microelectrónica (IMB-CNM-CSIC), Barcelona; Spain.
- ⁶⁸Department of Physics, Indiana University, Bloomington IN; United States of America.
- ⁶⁹(^a)INFN Gruppo Collegato di Udine, Sezione di Trieste, Udine;(^b)ICTP, Trieste;(^c)Dipartimento Politecnico di Ingegneria e Architettura, Università di Udine, Udine; Italy.
- ⁷⁰(^a)INFN Sezione di Lecce;(^b)Dipartimento di Matematica e Fisica, Università del Salento, Lecce; Italy.
- ⁷¹(^a)INFN Sezione di Milano;(^b)Dipartimento di Fisica, Università di Milano, Milano; Italy.
- ⁷²(^a)INFN Sezione di Napoli;(^b)Dipartimento di Fisica, Università di Napoli, Napoli; Italy.
- ⁷³(^a)INFN Sezione di Pavia;(^b)Dipartimento di Fisica, Università di Pavia, Pavia; Italy.
- ⁷⁴(^a)INFN Sezione di Pisa;(^b)Dipartimento di Fisica E. Fermi, Università di Pisa, Pisa; Italy.
- ⁷⁵(^a)INFN Sezione di Roma;(^b)Dipartimento di Fisica, Sapienza Università di Roma, Roma; Italy.
- ⁷⁶(^a)INFN Sezione di Roma Tor Vergata;(^b)Dipartimento di Fisica, Università di Roma Tor Vergata, Roma; Italy.
- ⁷⁷(^a)INFN Sezione di Roma Tre;(^b)Dipartimento di Matematica e Fisica, Università Roma Tre, Roma; Italy.
- ⁷⁸(^a)INFN-TIFPA;(^b)Università degli Studi di Trento, Trento; Italy.
- ⁷⁹Universität Innsbruck, Department of Astro and Particle Physics, Innsbruck; Austria.
- ⁸⁰University of Iowa, Iowa City IA; United States of America.
- ⁸¹Department of Physics and Astronomy, Iowa State University, Ames IA; United States of America.
- ⁸²(^a)Departamento de Engenharia Elétrica, Universidade Federal de Juiz de Fora (UFJF), Juiz de Fora;(^b)Universidade Federal do Rio De Janeiro COPPE/EE/IF, Rio de Janeiro;(^c)Instituto de Física, Universidade de São Paulo, São Paulo;(^d)Rio de Janeiro State University, Rio de Janeiro; Brazil.
- ⁸³KEK, High Energy Accelerator Research Organization, Tsukuba; Japan.

- ⁸⁴Graduate School of Science, Kobe University, Kobe; Japan.
- ⁸⁵(^a) AGH University of Science and Technology, Faculty of Physics and Applied Computer Science, Krakow; (^b) Marian Smoluchowski Institute of Physics, Jagiellonian University, Krakow; Poland.
- ⁸⁶Institute of Nuclear Physics Polish Academy of Sciences, Krakow; Poland.
- ⁸⁷Faculty of Science, Kyoto University, Kyoto; Japan.
- ⁸⁸Kyoto University of Education, Kyoto; Japan.
- ⁸⁹Research Center for Advanced Particle Physics and Department of Physics, Kyushu University, Fukuoka ; Japan.
- ⁹⁰Instituto de Física La Plata, Universidad Nacional de La Plata and CONICET, La Plata; Argentina.
- ⁹¹Physics Department, Lancaster University, Lancaster; United Kingdom.
- ⁹²Oliver Lodge Laboratory, University of Liverpool, Liverpool; United Kingdom.
- ⁹³Department of Experimental Particle Physics, Jožef Stefan Institute and Department of Physics, University of Ljubljana, Ljubljana; Slovenia.
- ⁹⁴School of Physics and Astronomy, Queen Mary University of London, London; United Kingdom.
- ⁹⁵Department of Physics, Royal Holloway University of London, Egham; United Kingdom.
- ⁹⁶Department of Physics and Astronomy, University College London, London; United Kingdom.
- ⁹⁷Louisiana Tech University, Ruston LA; United States of America.
- ⁹⁸Fysiska institutionen, Lunds universitet, Lund; Sweden.
- ⁹⁹Departamento de Física Teórica C-15 and CIAFF, Universidad Autónoma de Madrid, Madrid; Spain.
- ¹⁰⁰Institut für Physik, Universität Mainz, Mainz; Germany.
- ¹⁰¹School of Physics and Astronomy, University of Manchester, Manchester; United Kingdom.
- ¹⁰²CPPM, Aix-Marseille Université, CNRS/IN2P3, Marseille; France.
- ¹⁰³Department of Physics, University of Massachusetts, Amherst MA; United States of America.
- ¹⁰⁴Department of Physics, McGill University, Montreal QC; Canada.
- ¹⁰⁵School of Physics, University of Melbourne, Victoria; Australia.
- ¹⁰⁶Department of Physics, University of Michigan, Ann Arbor MI; United States of America.
- ¹⁰⁷Department of Physics and Astronomy, Michigan State University, East Lansing MI; United States of America.
- ¹⁰⁸Group of Particle Physics, University of Montreal, Montreal QC; Canada.
- ¹⁰⁹Fakultät für Physik, Ludwig-Maximilians-Universität München, München; Germany.
- ¹¹⁰Max-Planck-Institut für Physik (Werner-Heisenberg-Institut), München; Germany.
- ¹¹¹Graduate School of Science and Kobayashi-Maskawa Institute, Nagoya University, Nagoya; Japan.
- ¹¹²Department of Physics and Astronomy, University of New Mexico, Albuquerque NM; United States of America.
- ¹¹³Institute for Mathematics, Astrophysics and Particle Physics, Radboud University/Nikhef, Nijmegen; Netherlands.
- ¹¹⁴Nikhef National Institute for Subatomic Physics and University of Amsterdam, Amsterdam; Netherlands.
- ¹¹⁵Department of Physics, Northern Illinois University, DeKalb IL; United States of America.
- ¹¹⁶(^a) New York University Abu Dhabi, Abu Dhabi; (^b) University of Sharjah, Sharjah; United Arab Emirates.
- ¹¹⁷Department of Physics, New York University, New York NY; United States of America.
- ¹¹⁸Ochanomizu University, Otsuka, Bunkyo-ku, Tokyo; Japan.
- ¹¹⁹Ohio State University, Columbus OH; United States of America.
- ¹²⁰Homer L. Dodge Department of Physics and Astronomy, University of Oklahoma, Norman OK; United States of America.
- ¹²¹Department of Physics, Oklahoma State University, Stillwater OK; United States of America.

- ¹²²Palacký University, Joint Laboratory of Optics, Olomouc; Czech Republic.
- ¹²³Institute for Fundamental Science, University of Oregon, Eugene, OR; United States of America.
- ¹²⁴Graduate School of Science, Osaka University, Osaka; Japan.
- ¹²⁵Department of Physics, University of Oslo, Oslo; Norway.
- ¹²⁶Department of Physics, Oxford University, Oxford; United Kingdom.
- ¹²⁷LPNHE, Sorbonne Université, Université Paris Cité, CNRS/IN2P3, Paris; France.
- ¹²⁸Department of Physics, University of Pennsylvania, Philadelphia PA; United States of America.
- ¹²⁹Department of Physics and Astronomy, University of Pittsburgh, Pittsburgh PA; United States of America.
- ¹³⁰(^a)Laboratório de Instrumentação e Física Experimental de Partículas - LIP, Lisboa;(b)Departamento de Física, Faculdade de Ciências, Universidade de Lisboa, Lisboa;(c)Departamento de Física, Universidade de Coimbra, Coimbra;(d)Centro de Física Nuclear da Universidade de Lisboa, Lisboa;(e)Departamento de Física, Universidade do Minho, Braga;(f)Departamento de Física Teórica y del Cosmos, Universidad de Granada, Granada (Spain);(g)Departamento de Física, Instituto Superior Técnico, Universidade de Lisboa, Lisboa; Portugal.
- ¹³¹Institute of Physics of the Czech Academy of Sciences, Prague; Czech Republic.
- ¹³²Czech Technical University in Prague, Prague; Czech Republic.
- ¹³³Charles University, Faculty of Mathematics and Physics, Prague; Czech Republic.
- ¹³⁴Particle Physics Department, Rutherford Appleton Laboratory, Didcot; United Kingdom.
- ¹³⁵IRFU, CEA, Université Paris-Saclay, Gif-sur-Yvette; France.
- ¹³⁶Santa Cruz Institute for Particle Physics, University of California Santa Cruz, Santa Cruz CA; United States of America.
- ¹³⁷(^a)Departamento de Física, Pontificia Universidad Católica de Chile, Santiago;(b)Millennium Institute for Subatomic physics at high energy frontier (SAPHIR), Santiago;(c)Instituto de Investigación Multidisciplinario en Ciencia y Tecnología, y Departamento de Física, Universidad de La Serena;(d)Universidad Andres Bello, Department of Physics, Santiago;(e)Instituto de Alta Investigación, Universidad de Tarapacá, Arica;(f)Departamento de Física, Universidad Técnica Federico Santa María, Valparaíso; Chile.
- ¹³⁸Department of Physics, University of Washington, Seattle WA; United States of America.
- ¹³⁹Department of Physics and Astronomy, University of Sheffield, Sheffield; United Kingdom.
- ¹⁴⁰Department of Physics, Shinshu University, Nagano; Japan.
- ¹⁴¹Department Physik, Universität Siegen, Siegen; Germany.
- ¹⁴²Department of Physics, Simon Fraser University, Burnaby BC; Canada.
- ¹⁴³SLAC National Accelerator Laboratory, Stanford CA; United States of America.
- ¹⁴⁴Department of Physics, Royal Institute of Technology, Stockholm; Sweden.
- ¹⁴⁵Departments of Physics and Astronomy, Stony Brook University, Stony Brook NY; United States of America.
- ¹⁴⁶Department of Physics and Astronomy, University of Sussex, Brighton; United Kingdom.
- ¹⁴⁷School of Physics, University of Sydney, Sydney; Australia.
- ¹⁴⁸Institute of Physics, Academia Sinica, Taipei; Taiwan.
- ¹⁴⁹(^a)E. Andronikashvili Institute of Physics, Iv. Javakhishvili Tbilisi State University, Tbilisi;(b)High Energy Physics Institute, Tbilisi State University, Tbilisi;(c)University of Georgia, Tbilisi; Georgia.
- ¹⁵⁰Department of Physics, Technion, Israel Institute of Technology, Haifa; Israel.
- ¹⁵¹Raymond and Beverly Sackler School of Physics and Astronomy, Tel Aviv University, Tel Aviv; Israel.
- ¹⁵²Department of Physics, Aristotle University of Thessaloniki, Thessaloniki; Greece.
- ¹⁵³International Center for Elementary Particle Physics and Department of Physics, University of Tokyo, Tokyo; Japan.

- ¹⁵⁴Department of Physics, Tokyo Institute of Technology, Tokyo; Japan.
- ¹⁵⁵Department of Physics, University of Toronto, Toronto ON; Canada.
- ¹⁵⁶(^a)TRIUMF, Vancouver BC; (^b)Department of Physics and Astronomy, York University, Toronto ON; Canada.
- ¹⁵⁷Division of Physics and Tomonaga Center for the History of the Universe, Faculty of Pure and Applied Sciences, University of Tsukuba, Tsukuba; Japan.
- ¹⁵⁸Department of Physics and Astronomy, Tufts University, Medford MA; United States of America.
- ¹⁵⁹United Arab Emirates University, Al Ain; United Arab Emirates.
- ¹⁶⁰Department of Physics and Astronomy, University of California Irvine, Irvine CA; United States of America.
- ¹⁶¹Department of Physics and Astronomy, University of Uppsala, Uppsala; Sweden.
- ¹⁶²Department of Physics, University of Illinois, Urbana IL; United States of America.
- ¹⁶³Instituto de Física Corpuscular (IFIC), Centro Mixto Universidad de Valencia - CSIC, Valencia; Spain.
- ¹⁶⁴Department of Physics, University of British Columbia, Vancouver BC; Canada.
- ¹⁶⁵Department of Physics and Astronomy, University of Victoria, Victoria BC; Canada.
- ¹⁶⁶Fakultät für Physik und Astronomie, Julius-Maximilians-Universität Würzburg, Würzburg; Germany.
- ¹⁶⁷Department of Physics, University of Warwick, Coventry; United Kingdom.
- ¹⁶⁸Waseda University, Tokyo; Japan.
- ¹⁶⁹Department of Particle Physics and Astrophysics, Weizmann Institute of Science, Rehovot; Israel.
- ¹⁷⁰Department of Physics, University of Wisconsin, Madison WI; United States of America.
- ¹⁷¹Fakultät für Mathematik und Naturwissenschaften, Fachgruppe Physik, Bergische Universität Wuppertal, Wuppertal; Germany.
- ¹⁷²Department of Physics, Yale University, New Haven CT; United States of America.
- ^a Also Affiliated with an institute covered by a cooperation agreement with CERN.
- ^b Also at An-Najah National University, Nablus; Palestine.
- ^c Also at Borough of Manhattan Community College, City University of New York, New York NY; United States of America.
- ^d Also at Bruno Kessler Foundation, Trento; Italy.
- ^e Also at Center for High Energy Physics, Peking University; China.
- ^f Also at Center for Interdisciplinary Research and Innovation (CIRI-AUTH), Thessaloniki ; Greece.
- ^g Also at Centro Studi e Ricerche Enrico Fermi; Italy.
- ^h Also at CERN, Geneva; Switzerland.
- ⁱ Also at Département de Physique Nucléaire et Corpusculaire, Université de Genève, Genève; Switzerland.
- ^j Also at Departament de Física de la Universitat Autònoma de Barcelona, Barcelona; Spain.
- ^k Also at Department of Financial and Management Engineering, University of the Aegean, Chios; Greece.
- ^l Also at Department of Physics and Astronomy, Michigan State University, East Lansing MI; United States of America.
- ^m Also at Department of Physics, Ben Gurion University of the Negev, Beer Sheva; Israel.
- ⁿ Also at Department of Physics, California State University, East Bay; United States of America.
- ^o Also at Department of Physics, California State University, Sacramento; United States of America.
- ^p Also at Department of Physics, King's College London, London; United Kingdom.
- ^q Also at Department of Physics, Stanford University, Stanford CA; United States of America.
- ^r Also at Department of Physics, University of Fribourg, Fribourg; Switzerland.
- ^s Also at Department of Physics, University of Thessaly; Greece.
- ^t Also at Department of Physics, Westmont College, Santa Barbara; United States of America.
- ^u Also at Hellenic Open University, Patras; Greece.
- ^v Also at Institutio Catalana de Recerca i Estudis Avancats, ICREA, Barcelona; Spain.

- ^w Also at Institut für Experimentalphysik, Universität Hamburg, Hamburg; Germany.
- ^x Also at Institute of Applied Physics, Mohammed VI Polytechnic University, Ben Guerir; Morocco.
- ^y Also at Institute of Particle Physics (IPP); Canada.
- ^z Also at Institute of Physics and Technology, Ulaanbaatar; Mongolia.
- ^{aa} Also at Institute of Physics, Azerbaijan Academy of Sciences, Baku; Azerbaijan.
- ^{ab} Also at Institute of Theoretical Physics, Ilia State University, Tbilisi; Georgia.
- ^{ac} Also at L2IT, Université de Toulouse, CNRS/IN2P3, UPS, Toulouse; France.
- ^{ad} Also at Lawrence Livermore National Laboratory, Livermore; United States of America.
- ^{ae} Also at National Institute of Physics, University of the Philippines Diliman (Philippines); Philippines.
- ^{af} Also at Technical University of Munich, Munich; Germany.
- ^{ag} Also at The Collaborative Innovation Center of Quantum Matter (CICQM), Beijing; China.
- ^{ah} Also at TRIUMF, Vancouver BC; Canada.
- ^{ai} Also at Università di Napoli Parthenope, Napoli; Italy.
- ^{aj} Also at University of Chinese Academy of Sciences (UCAS), Beijing; China.
- ^{ak} Also at University of Colorado Boulder, Department of Physics, Colorado; United States of America.
- ^{al} Also at Washington College, Maryland; United States of America.
- ^{am} Also at Yeditepe University, Physics Department, Istanbul; Türkiye.
- * Deceased